GEOLOGY AND GEOPHYSICS

© F.A.Kadirov, M.Floyd, R.Reilinger, Ak.A.Alizadeh, I.S.Guliyev, S.G.Mammadov, R.T.Safarov, 2015

ACTIVE GEODYNAMICS OF THE CAUCASUS REGION: IMPLICATIONS FOR EARTHQUAKE HAZARDS IN AZERBAIJAN

F.A.Kadirov[1], M.Floyd[2], R.Reilinger[2], Ak.A.Alizadeh[1], I.S.Guliyev[1], S.G.Mammadov[1], R.T.Safarov[1]

1 – *Institute of Geology and Geophysics, Azerbaijan National Academy of Sciences, 119, H.Javid ave., Baku, AZ1143*

2 – *Massachusetts Institute of Technology, Cambridge, USA*

In this paper we present GPS observations of crustal deformation in the Africa-Arabia-Eurasia zone of plate interaction, and use these observations to constrain broad-scale tectonic processes within the collision zone of the Arabian and Eurasian plates. Within this plate tectonics context, we examine deformation of the Caucasus system (Lesser and Greater Caucasus and intervening Caucasian Isthmus) and show that most crustal shortening in the collision zone is accommodated by the Greater Caucasus Fold-and-Thrust Belt (GCFTB) along the southern edge of the Greater Caucasus Mountains. The eastern GCFTB appears to bifurcate west of Baku, with one branch following the accurate geometry of the Greater Caucasus, turning towards the south and traversing the Neftchala Peninsula. A second branch (or branches) may extend directly into the Caspian Sea south of Baku, likely connecting to the Central Caspian Seismic Zone (CCSZ). We model deformation in terms of a locked thrust fault that coincides in general with the main surface trace of the GCFTB. We consider two end-member models, each of which tests the likelihood of one or other of the branches being the dominant cause of observed deformation. Our models indicate that strain is actively accumulating on the fault along the ~200 km segment of the fault west of Baku (approximately between longitudes 47-49°E). Parts of this segment of the fault broke in major earthquakes historically (1191, 1859, 1902) suggesting that significant future earthquakes (M~6-7) are likely on the central and western segment of the fault. We observe a similar deformation pattern across the eastern end of the GCFTB along a profile crossing the Kur Depression and Greater Caucasus Mountains in the vicinity of Baku. Along this eastern segment, a branch of the fault changes from a NW-SE striking thrust to an ~ N-S oriented strike-slip fault (or in multiple splays). The similar deformation pattern along the eastern and central GCFTB segments raises the possibility that major earthquakes may also occur in eastern Azerbaijan. However, the eastern segment of the GCFTB has no record of large historic earthquakes, and is characterized by thick, highly saturated and over-pressured sediments within the Kur Depression and adjacent Caspian Basin that may inhibit elastic strain accumulation in favour of fault creep, and/or distributed faulting and folding. Thus, while our analyses suggest that large earthquakes are likely in central and western Azerbaijan, it is still uncertain whether significant earthquakes are also likely along the eastern segment, and on which structure. Ongoing and future focused studies of active deformation promise to shed further light on the tectonics and earthquake hazards in this highly populated and developed part of Azerbaijan.

Introduction and Background

The Geology and Geophysics Institute of the Azerbaijan National Academy of Sciences and the Department of Earth, Atmospheric, and Planetary Sciences at Massachusetts Institute of Technology have been using the Global Positioning System (GPS) to monitor crustal deformation in the territory of Azerbaijan since 1998 (Kadirov et al., 2008). These studies, coordinated and integrated with GPS studies in neighboring parts of the Arabia-Eurasia collision zone, provide new constraints on the fundamental geodynamic processes that are actively deforming the collision zone (e.g. Reilinger et al., 2006; Kadirov et al., 2012; Forte et al., 2012). These geodynamic processes produced and maintain the high elevation of the Turkish-Iranian Plateau (Figure 1) and are the cause of the volcanic and earthquake activity that characterize this region.

The question of earthquake hazards has played a central role in our research because of the increasing vulnerability of the growing population and rapid infrastructure development in Azerbaijan, particularly in the Baku-Absheron region. Azerbaijan has suffered earthquakes historically,

including highly destructive earthquakes in 1191, 1859 and 1902 in the Shamakhi region. The 1191 and 1859 earthquakes devastated the then capital city of Shirvan, instigating a relocation of the capital to its present location in Baku (Mushketov, Orlov, 1893; Kondorskaya, Shebalin, 1982). Our GPS studies are part of the Geology and Geophysics Institute's mission that includes understanding the hazards associated with earthquakes: where they are most likely to occur, their expected maximum magnitude, and their likelihood of occurrence. This information is necessary in order to take appropriate preparedness and mitigation measures to reduce the risk to the population and infrastructure, including the vulnerable facilities associated with the petroleum industry that are critical to the economy of Azerbaijan.

In this paper we use GPS observations to constrain Arabia-Eurasia relative plate motions, and the character of inter-plate deformations in the Arabia-Eurasia collision zone. Within this broader context, we focus on earthquake hazards in the Azerbaijan Caucasus and SW Caspian Basin.

Tectonic setting of the Caucasus Mountains

In the broadest context, the Lesser and Greater Caucasus Mountains lie within the zone of plate interaction where the African and Arabian plates are actively converging with the Eurasian Plate (Figure 1). McKenzie et al. (1970), McKenzie (1970, 1972), and Jackson and McKenzie (1984, 1988) provided a plate tectonic description of the region, recognizing active continental collision in eastern Turkey, the Caucasus, and the Zagros; lateral transport of Anatolia (Turkey) towards the west; subduction of African oceanic lithosphere (i.e., Neotethys) along the Hellenic and Cyprus trenches; N-S extension in the Aegean and western Turkey; and ocean rifting along the Red Sea and Gulf of Aden. Convergence of Arabia and Africa with Eurasia has been occurring for > 100 Ma as the intervening Neotethys Ocean lithosphere has been subducting beneath Eurasia. While ocean subduction continues at present along the Hellenic and Cyprus trenches, complete ocean closure north of the Arabian plate occurred ~27 Ma (e.g., McQuarrie, van Hindsbergan, 2013).

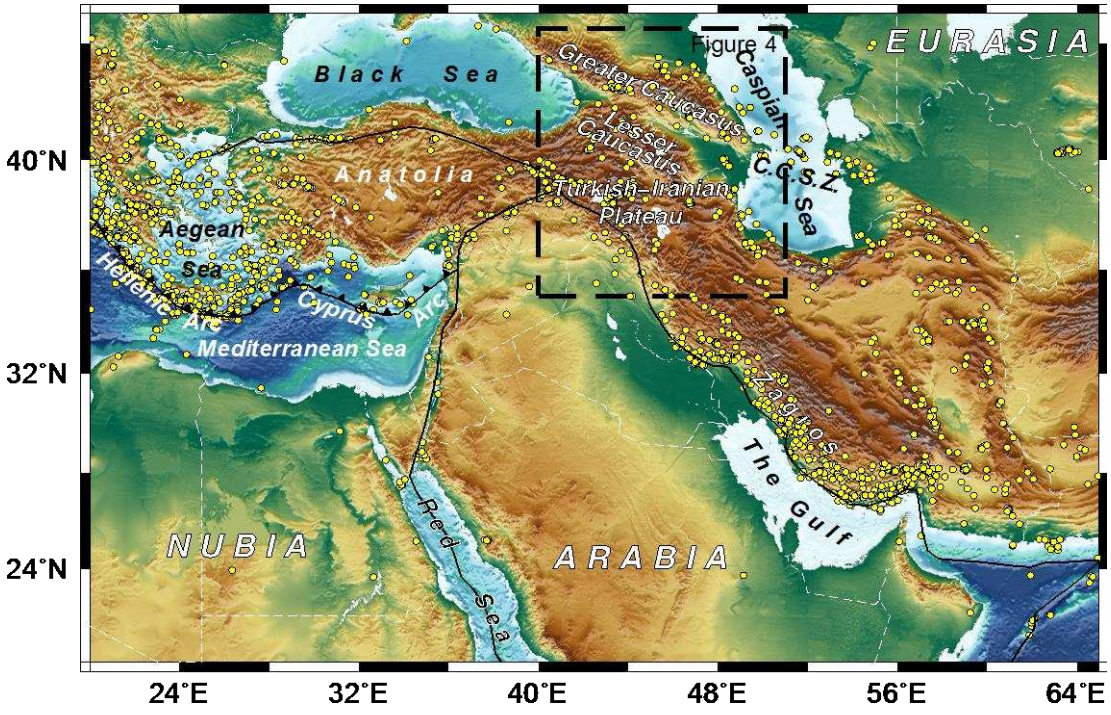


Figure 1. Tectonic overview of the Arabia-Eurasia Collision Zone. Yellow dots are earthquakes from the EHB catalogue (Engdahl et al., 1998) and updates thereof to 2008, plus ISC locations from 2009 onwards. Major plate boundaries are from Bird (2003)

Subsequent seismological, geophysical and geological studies added important refinements to this plate tectonic characterization, including the westward "extrusion" of Anatolia accommodated by the North and East Anatolian faults (Sengor et al., 1985), partitioning of crustal deformation in the eastern Turkey/Caucasus continental collision zone (Jackson, 1992; Allen et al., 2004; Copley and Jackson, 2006), the influence of slab detachment on uplift and volcanism of the Turkish Iranian Plateau (e.g., Sengor et al., 2004; Barazangi et al., 2006), and early subduction of the S Caspian oceanic basin beneath the N Caspian Eurasian continental lithosphere along the central Caspian Seismic Zone (e.g., Jackson et al., 2002).

The Greater Caucasus Mountains are thought to have formed by tectonic inversion of a former back-arc ocean that opened during north-dipping subduction of the Neotethys (e.g. Zonenshain and Le Pichon, 1986; Forte et al., 2012), where the eastern Black Sea, Kur Depression in Azerbaijan and southern Caspian Sea are the remaining remnants of the back-arc basin. Both the timing and spatial evolution of shortening and exhumation remain uncertain with preferred estimates of the timing being Late Miocene to Early Pliocene (e.g. Kopp and Shcherba, 1985; Philip et al., 1989; Vincent et al., 2007). Total shortening across the Greater Caucasus is also uncertain with estimates ranging from 150-400 km (e.g., McQuarrie and van Hindbergen, 2013), and an increase in total shortening from west to east (e.g., Král and Gurbanov, 1996; Avdeev, Niemi, 2008; Forte et al., 2012).

Global Positioning System

During the past ~20 years, the active tectonics of the Africa-Arabia-Eurasia plate system have been measured directly by geodetic observations, most importantly the Global Positioning System (GPS) (Hager et al., 1991; Dixon, 1991). GPS consists of a system of 32 satellites 20000 km above the earth's surface that complete 2 orbits of the earth each 24 hrs (*http://tycho.usno.navy.mil/gpscurr.html).* The satellites are operated by the US Department of Defence in cooperation with the Interagency GPS Executive Board. Other Global Navigation Satellite Systems (GNSS) have been developed by Russia (GLONASS), a European consortium (Galileo), Japan (QZSS), and China (Beidou), but these systems are not used in the results we report.

There are three components to using the GPS system for precise positioning, the satellite constellation, a global network of GPS tracking stations (Mueller, Beutler, 1992), and data processing involving applying physical models and parameter estimation. Most important for this chapter, positions are determined with an accuracy of ~2 mm in horizontal coordinates and 3-10 mm in heights by recording data over a 24-hour period. These precisions are possible because of highly accurate timing provided by atomic clocks on the GPS satellites, precise orbital positions for the satellites provided by the International GNSS Service *(http://igs.org/)* (determined from the global network of observing stations) and processing software that uses advanced mathematical models to account for the Earth's rotation, solid-Earth and ocean tides, and the ionospheric and atmospheric delays of the GPS signal, among other factors that influence position estimates (e.g. Herring et al., 2010).

Estimating surface motions from GPS observations

The GPS measurements presented in this chapter include recording stations (cGPS) that remain in place indefinitely (Figure 2A), and survey-mode (sGPS) observations where the GPS antenna is positioned temporarily over a survey marker (Figure 2B). By repeating these GPS measurements episodically, we are able to estimate how the position has changed during the observation period. cGPS observations allow estimation of position on a daily basis, or more frequently. However, reliable estimates of long-term, secular site velocities require a minimum of 2.5 years of observations even for continuously recording stations because annual and semi-annual systematic errors can bias estimates of steady state motion (Blewitt, Lavellee, 2002).

While the precision of our site velocities varies with observation period, the GPS horizontal velocities we determine using the GAMIT-GLOBK processing software (Herring et al., 2010) have 1-sigma uncertainties in the range of 0.2-0.9 mm/yr, with most sites <0.5 mm/yr. Because deformation rates across the Greater Caucasus Mountains vary from 2-14 mm/yr from northwest to southeast, these precisions allow us to investigate details of the mountain building processes and associated earthquake hazards.

Velocity estimates are determined in a global reference frame; that is, with respect to the global network of tracking stations. The reference frame is determined and maintained (updated) by the International Terrestrial Reference Frame (ITRF) Ser-

vice (Altamimi et al., 2007) using well-positioned stations, with a long history of well-behaved observations, located around the globe and accounting for motions of the Earth's tectonic plates. We determine site velocities within the ITRF (2008), but we present them in a reference frame fixed to the Eurasian Plate. It is important to bear in mind that the relative motion between measurement sites (i.e., deformation or strain rate) is invariant to changes in reference frame.



Figure 2. A – GPS continuously recording station located in Sheki, Azerbaijan. B – GPS survey site in the Greater Caucasus. The antenna is precisely located above the mark that is cemented into the bedrock

Present-day Arabia-Eurasia continental collision

Figure 3 shows the velocities of GPS sites in the zone of interaction of the African, Arabian, and Eurasian plates (Reilinger et al., 2006 and updates thereof for sites in Azerbaijan). Virtually all major active tectonic processes are well resolved and quantified by the GPS observations, including the northward motion and counter clockwise (CCW) rotation of the Arabian Plate and active opening of the Red Sea (e.g. ArRajehi et al., 2010), crustal shortening of the Zagros fold and thrust zone in Iran (e.g., Djamour et al., 2010), the CCW rotation of the Turkish region accommodated by the North Anatolian Fault (McClusky et al., 2000; Reilinger et al., 2006), northwest motion of the African Plate with respect to Eurasia (McClusky et al., 2003), and the change from NNW motion of Arabia to NNE motion of the Caucasus system (Reilinger et al., 2006; Vernant and Chery, 2006).

Reilinger et al. (2006) used the GPS velocity field to estimate how AR-EU convergence is partitioned between lateral "extrusion" of crustal blocks and crustal shortening. They found that a large majority (~70%) of the convergence is accommodated by lateral transport and ~15% by shortening along the GCFTB, with the remainder being accommodated by other structures or distributed strain. The only slightly thickened crust in the Lesser Caucasus-E Turkey Plateau (Gok et al., 2003; Barazangi et al., 2006), in spite of 150-400 km of continental convergence (McQuarrie, van Hindbergen, 2013), indicates that the geodetic results reflect long-term, tectonic deformation processes in the collision zone (i.e., if not for lateral transport, the crust would be expected to be much thicker). The utility of geodetic studies for constraining long-term geodynamic processes finds further support from comparison between present-day, geodetically derived Arabia-Eurasia convergence rates and longer-term plate convergence rates derived from plate tectonic reconstructions (e.g., McQuarrie et al., 2003) that indicate that these plate motions have been remarkably constant (±10-15%) since the onset of continental collision in the Early Miocene (e.g., ArRajehi et al., 2010).

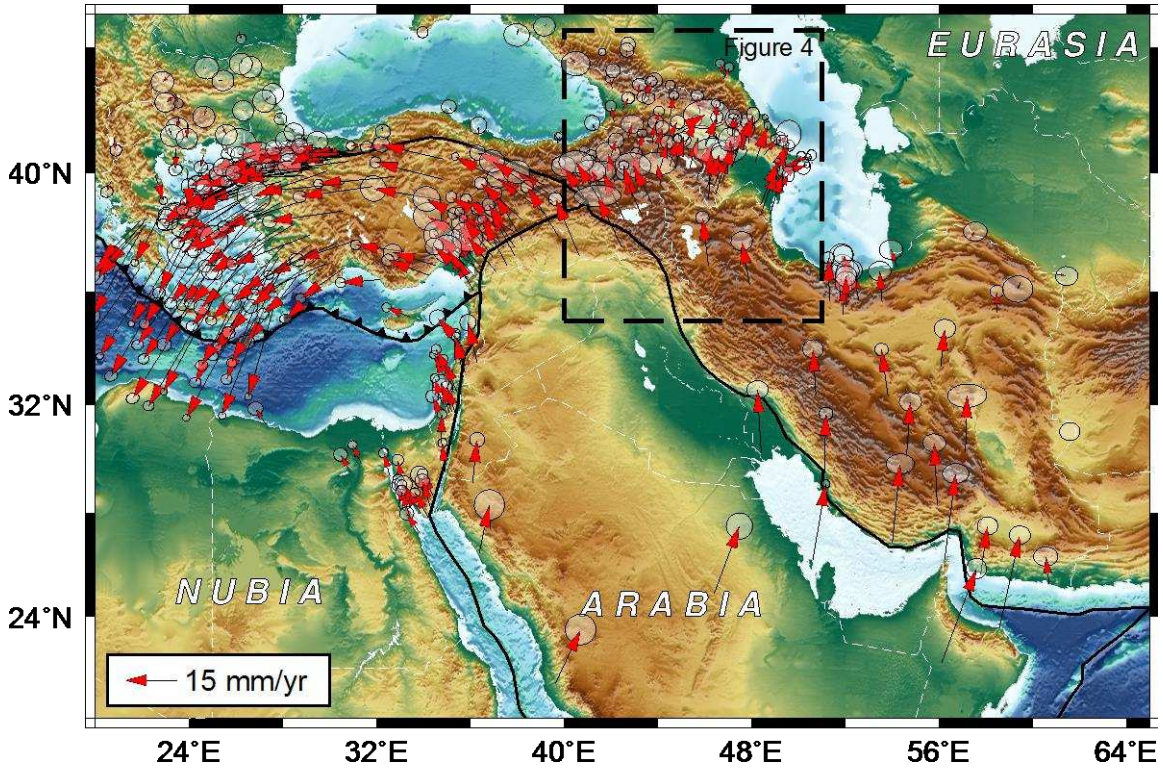


Figure 3. GPS velocities and 95% confidence ellipses with respect to Eurasia (according to Altamimi et al., 2012) within the Eastern Mediterranean from Reilinger et al. (2006), with updated velocities in Azerbaijan for the period 1994.0-2013.5. Major plate boundaries are from Bird (2003), as in Figure 1

Deformation of the Greater and Lesser Caucasus

Figure 4 shows a close-up of the GPS velocity field around the Greater and Lesser Caucasus, providing a quantitative basis to estimate the locations and slip rates and directions on the major structures that accommodate deformation. As is clear from Figure 4, the main shortening in the Arabia-Eurasia collision zone occurs along the southern boundary of the Greater Caucasus near the seismically active Greater Caucasus Fold-and-Thrust Belt (GCFTB). This is well illustrated in the series of velocity profiles in Figure 5, which show the rate of motion versus distance along profiles parallel to (5A) and traversing (5B-E) the Caucasus system (profile locations on Figure 4). Figure 5A shows the component of velocity perpendicular to the direction of the profile**;** Figures 5B-E show the component along the direction of the profile (i.e. shortening or lengthening).The plot in Figure 5A for the profile aligned along strike of the Greater Caucasus demonstrates the progressive increase in convergence rate with Eurasia from west to east, from 1-2 mm/yr near the eastern end of the Black Sea, to 13-14 mm/yr south of Baku, Azerbaijan. The absence of any consistent change in rates in the direction of the profile traversing the Lesser Caucasus (i.e., Figures 5B, 5D and 5E) constrains active shortening in the Lesser Caucasus to < 2 mm/yr. These observations, and the low level of significant seismicity in the Lesser Caucasus (Figure 1; the M6.8, 1988, Spitak, Armenia Earthquake being a notable exception), suggest that, within the resolution of our GPS observations, the Lesser Caucasus behaves like a coherent block rotating in a counter clockwise sense with respect to Eurasia, around a pole near the eastern end of the Black Sea (e.g. Lawrence, 2003; Reilinger et al., 2006; Copley, Jackson, 2006). Rotation may be related to the closure of an inter-continental back-arc basin separating the Lesser and Greater Caucasus with the Caucasian Isthmus (Kur Depression in Azerbaijan) being the last remnants currently undergoing the final stages of subduction/closure (e.g., Cowgill et al., 2012).

Geometry of the eastern GCFTB

The nature of the eastern GCFTB remains an outstanding question in Caucasus tectonics with implications for earthquake hazards in the greater Baku region (Kadirov et al., 2012). Specifically, the physical connection (i.e., faults or zones of deformation) connecting the GCFTB and the Central Caspian Seismic Zone (CCSZ) (Figure 1) remains uncertain. While both structures accommodate convergence with Eurasia, along the CCSZ it is manifest in moderately deep (~40 km) earthquakes with focal mechanisms indicative of deformation within the subducting plate rather than on the plate interface (Jackson et al., 2002), while the GCFTB has broken historically in shallow (~15-20 km) continental thrust events (e.g., Triep et al., 1995). It is possible that this differences due to differences in the nature of the crust and lithosphere (i.e., rheology) at the junction of the GCFTB and CCSZ, continental for the Kur Depression and oceanic (with very thick and consolidated sediments) in the S Caspian Basin (Knapp et al., 2004, Kadirov, Gadirov, 2014). It is also possible, perhaps likely, that the different modes of accommodating shortening at the plate interface reflect different dynamics, subduction in the CCSZ and continental collision along the GCFTB (e.g., Reilinger et al., 2006;Vernant, Chery, 2006; Copley, Jackson, 2006).

New GPS observations on the Absheron and Neftchala peninsulas, and on the southern edge of the Caspian Basin in Iran make it clear that a branch (or multiple branches) of the GCFTB follows the curved topographic break between the Kur Depression and Greater Caucasus/Absheron Peninsula, having a SSE orientation south of Baku (Figures 4 and 6b). Structures accommodating deformation may merge offshore with the thick, folded sediments south of the Absheron Peninsula. This offshore geometry is supported by GPS velocities in the SW corner of the Caspian Basin in Iran (Djamour et al., 2010) that indicate northerly motion with rates similar to those in the adjacent Lesser Caucasus to the west.

On the other hand, the set of velocity vectors from ~ 50 km SW of Baku (SHIK) to the eastern end of the Absheron Peninsula (GURK) indicate shortening at ~6 mm/yr perpendicular to the easternmost Caucasus (Figure 6a). We interpret these GPS observations to imply that crustal shortening accommodated by the GCFTB is partitioned between NE-SW shortening across the Absheron Peninsula and right-lateral, transpressive deformation S of Baku that joins the system of folded sediments in the SW Caspian Basin (Figure 4, 6a and 6b).

Implications for earthquake hazards in Azerbaijan

Earthquake hazard analysis includes estimating the most likely locations, magnitudes, and time of future earthquakes. We emphasize that it is

not possible at present to determine these parameters precisely (e.g., Jordon, 2014). However, with auxiliary information from geology (paleoseismology, geomorphology; e.g., Forte et al., 2012), and seismology (instrumental and historic; e.g., Ambraseys, Melville, 1982; Philip et al., 2001; Jackson et al., 2002), it is possible to make estimates of location and, to a lesser extent, magnitude and time of anticipated events.

Our approach involves identifying zones of rapid, spatially systematic changes in site velocities that we observe occur almost exclusively across known faults (e.g., McClusky et al., 2000; Vernant et al., 2014). To the extent that the velocity changes across the faults are due to strain accumulation, the velocity field provides direct evidence for the likely locations of future earthquakes. Some caution is needed since earthquakes are known to occur in areas of very low strain rates, including the 1988 Spitak, Armenia earthquake. While it is difficult to quantify hazards in such cases, we expect very long repeat times for similar earthquakes (e.g., Westaway, 1990), making their occurrence less likely than earthquakes on faults that are rapidly accumulating strain.

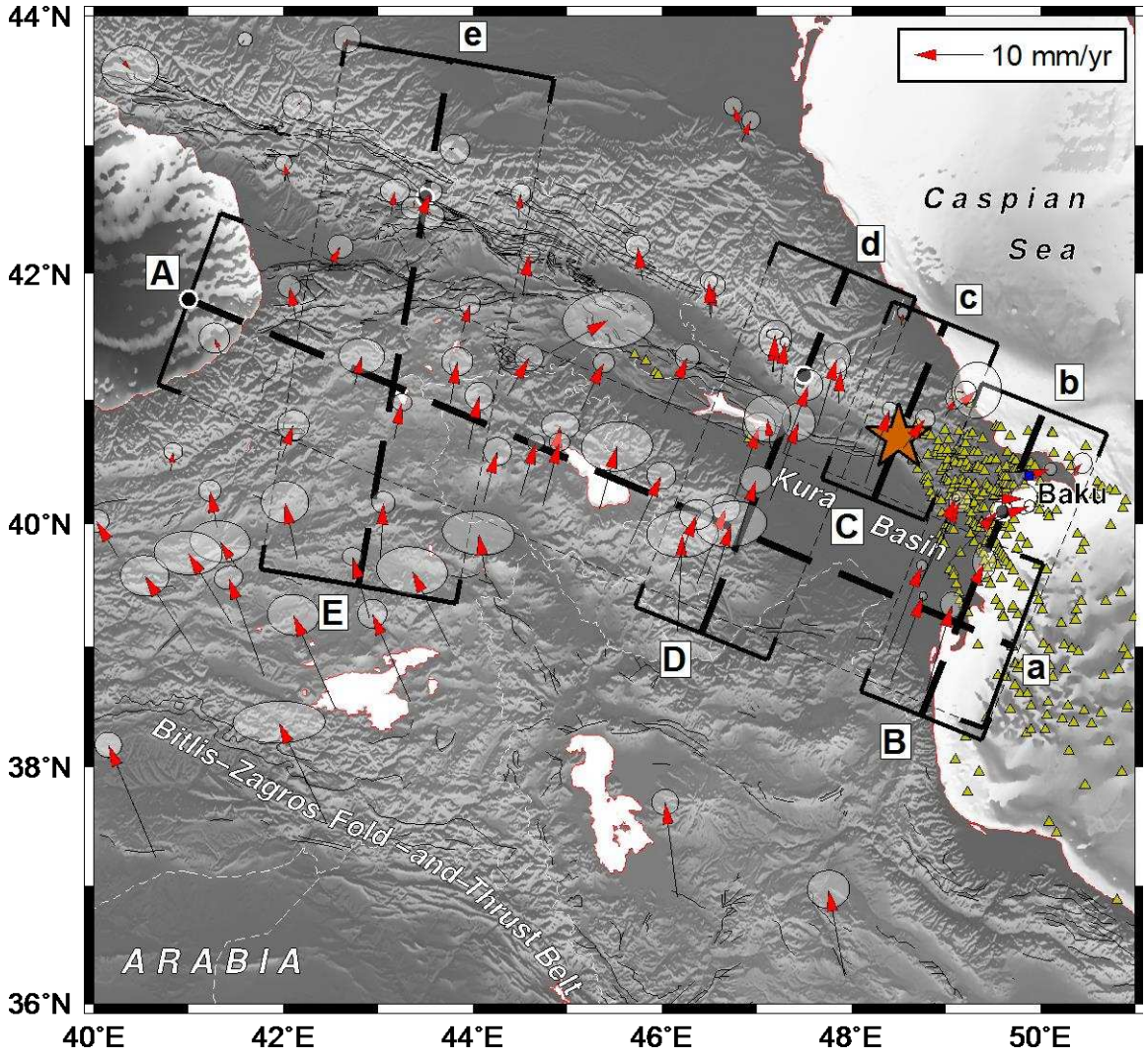
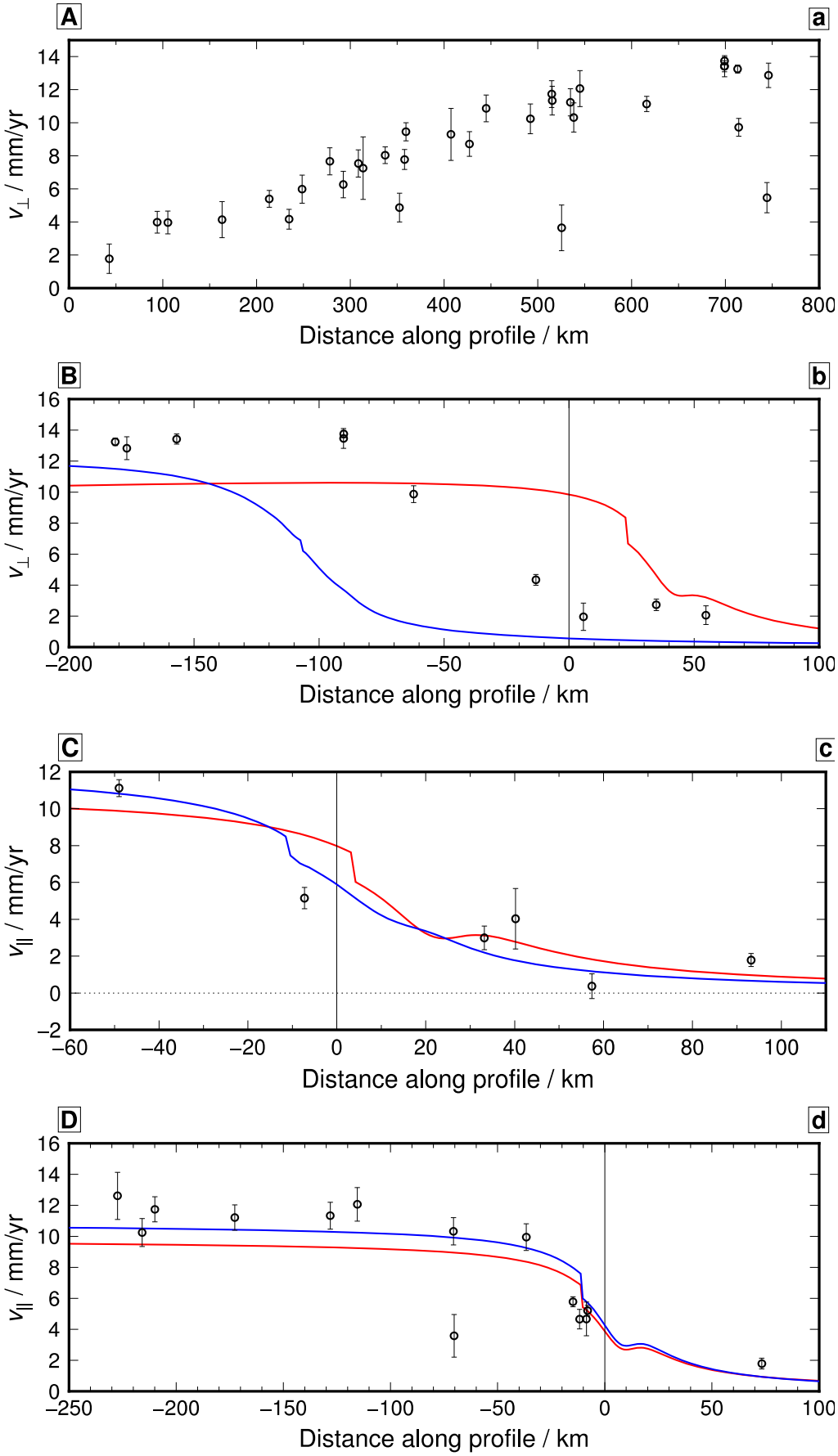


Figure 4. GPS velocities and 95% confidence ellipses w.r.t. (with respect to) Eurasia for the eastern AR-EU collision zone. Orange star shows 1902, M6.9 Shamakha earthquake epicenter. Yellow triangles represent mud volcanoes. Velocity profiles A-E are shown in Figure 5. Their origins are marked by black dots which, for profiles B-E, coincide approximately with the surface expression of the GCFTB


A
a
$v_\perp$ / mm/yr
Distance along profile / km
B
b
$v_\perp$ / mm/yr
Distance along profile / km
C
c
$v_\parallel$ / mm/yr
Distance along profile / km
D
d
$v_\parallel$ / mm/yr
Distance along profile / km

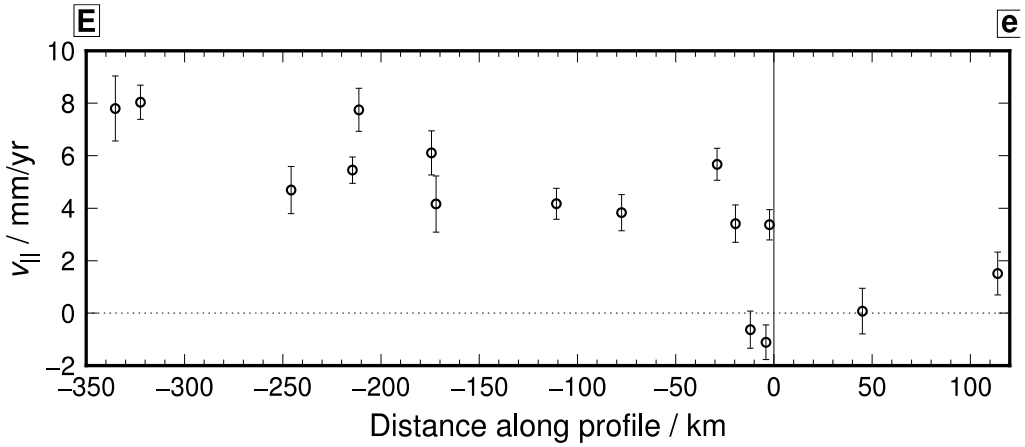


Figure 5. Plots of transverse (A) and parallel (B-E) components of velocities versus distance along the profiles shown in Figure 4. Red curves are velocity profiles from the model shown in Figure 6a, blue curves are velocity profiles from the model shown in Figure 6b (see main text for descriptions). The approximate location of the surface trace of the GCFTB is shown by the vertical line at the origin (see black dots in Figure 4). Note different scales

The magnitude of an earthquake is directly related to the total earthquake offset (co-seismic fault slip) and the surface area of the fault break (Aki, Richards, 2002; Wells, Coppersmith, 1994). Some idea of the possible size of pending earthquakes can be garnered from the historic earthquake record, and/or geological observations of surface faults (e.g., Weldon et al., 2004). With an estimate of the expected magnitude of an anticipated earthquake, we can use the time since the prior event, and the rate of offset accumulation across the fault to estimate the time until the next earthquake (i.e., when the offset accumulation equals the observed co-seismic offset in prior earthquakes).

This simple approach assumes (1) rate differences across the fault are due entirely to strain accumulation for the full time period since the prior earthquake and not permanent deformation or aseismic slip on the fault (i.e., the fault is fully coupled or locked, and the crust adjacent to the fault is not deforming an elastically); (2) the GPS-determined rate of strain accumulation is constant throughout the period since the prior earthquake; and (3) the fault will fail in an earthquake of similar magnitude to the prior event(s) (i.e., "characteristic earthquake" model; Swartz and Coppersmith, 1984).

Each of these assumptions requires consideration for each individual fault being analyzed (e.g., WGCEP, 2007). Some faults are known to fail aseismically via fault creep up to the surface, either in steady-state or by episodic creep events. Sections of the San Andreas and North Anatolian strike-slip faults are well-studied examples (e.g., Lyons, Sandwell, 2003; Cetin et al., 2014). In fact, below depths of a few 10s of km (i.e., fault locking depths), faults of all types accommodate relative motion aseismically (we exclude discussion of deep earthquakes in the subducting lithosphere). However, we are not aware of evidence for shallow, aseismic slip on continental thrust faults such as those within the GCFTB (e.g., Bird, Kagan, 2004).On the other hand, the easternmost segment of the GCFTB may curve to the south taking on a predominantly strike-slip geometry (Figure 6b). To our knowledge, this segment, located south of Baku, has not experienced strike-slip earthquakes during the instrumental period (Jackson et al., 2002). However, whether this segment is creeping aseismically or accumulating strain without generating seismicity (the case for the southern San Andreas Fault; Bennett et al., 1996; Fialko, 2006) remains conjectural.

GPS observations can help address the nature of fault coupling since the spatial pattern of deformation adjacent to a fault has a characteristic strain pattern for a locked fault (e.g., Okada, 1985), and a step-function offset for a freely slipping fault; directly identifiable "end member" cases. Furthermore, the gradient of the velocity near the fault is directly related to the fault locking depth (i.e., below this depth the fault creeps aseismically). Besides directly identifying locked fault segments (i.e., those capable of generating earthquakes), constraining the locking depth is important for estimating fault area, and thus anticipated earthquake magnitude (e.g., Aki, Richards, 2002).

Because the time between moderate to large earthquakes is long compared to the length of time precise fault monitoring observations have been

made (beginning in the 1970s with ground-based observations; e.g. Prescott, Savage, 1976), it isn't possible to directly determine the extent to which the rate and spatial geometry of strain accumulation remains constant through the period between earthquakes. While long-term slip rates estimated from offset features and topography agree well (±10%) with present-day GPS slip rates (e.g. Reilinger et al., 2006), rates of strain accumulation on faults are known to vary between earthquakes. An important, well observed case is the period of rapid surface deformation that occurs following earthquakes (postseismic period) (e.g. Nur, Mavko, 1974). Postseismic deformation is thought to be due in part to slip on the fault below the seismogenic depth (at temperatures and pressures where the crust no longer behaves elastically) as it responds to the instantaneous stress transferred by the earthquake (e.g., Pollitz, 1992). As the lower aseismic part of the fault relaxes the coseismic induced stress, it reloads the shallow, seismic segments. This mechanism can either drive after slip on the fault (in essence adding to the total coseismic slip, i.e. total earthquake slip prior to re-locking) or reload the fault, thereby advancing the fault in time towards the next earthquake. Available evidence indicates that all fault types experience postseismic deformation of some kind that impacts the nature of strain accumulation on the earthquake fault.

For the few earthquakes studied in some detail, the postseismic period of rapid strain accumulation or release is short relative to the time between earthquakes (< 5%) (e.g., Lyzenga et al., 2000; Podgorski et al., 2007; Ergintav et al., 2009) and any increase in strain accumulation is to some extent offset by after slip (i.e. after slip releases strain and stress). Although insufficient case studies are available to determine the degree to which postseismic effects bias estimates of earthquake repeat times quantitatively, for the most part we assume this uncertainty is small compared to uncertainties due to deviations from the characteristic earthquake model.

The assumption that faults fail in "characteristic earthquakes" is the most critical and the most uncertain assumption necessary for any earthquake forecast (WGCEP, 2007). Again we are hampered by the long time between earthquakes compared to the instrumental and historic records. Paleoseismic observations help fill this deficit, but the information on prior earthquakes becomes less precise with age. From the scant constraints we have, it is clear that even for faults that adhere to the characteristic earthquake model in a general way, appearing to behave quasi-periodically as evidenced by long historic records, variations in repeat times are high, introducing large uncertainties in timing and magnitude estimates (e.g., Weldon et al., 2004). In spite of this variability, repeating patterns have been reported when sufficiently long histories are available (e.g., Ambraseys, 2002; Zoller et al., 2007; Meghraoui et al., 2012), and the notion that quasi-steady strain build up (as evidenced by geodetic observations) will "periodically" overcome fault friction and lead to an earthquake is physically appealing.

Because of these outstanding uncertainties, rather than making estimates of future earthquake occurrences, we present general hypotheses that we hope will help focus ongoing studies to constrain better active geodynamic processes, present-day fault behavior (locked vs. creeping), and paleoseismic and historic earthquake studies, all of which are needed to reduce forecast uncertainties. Furthermore, our identification of faults that are potentially accumulating strain in Azerbaijan contributes to the development of earthquake scenarios for estimating seismic ground motion, and focusing earthquake preparations and responses (e.g., Jones et al., 2008).

Deformation and possible strain accumulation along the Main Caucasus thrust fault

In Figures 5B, 5C and5D we compare the results of simple, elastic models of strain accumulation for the wide profiles crossing eastern and west-central Azerbaijan (Figure 4). We consider two models; the surface outcrop of both are shown in Figures 6a and 6b, and model parameters (fault locking depth and dip) are given in the caption for Figure 6. Both models include thrusting along the segment of the GCFTB west of the Absheron Peninsula, where the fault dips northward at 30°. Model A has this same fault geometry extending to the east, south of Baku and connecting with the Central Caspian Seismic Zone. Model B has the modeled fault following the topographic break of the GCFTB west of Baku, turning to the south and extending through the Neftchala Peninsula. In this latter model, the fault dip gradually increases with the change in strike to become vertical along the Neftchala Peninsula. The models show the deformation predicted by a fault that is locked to a certain depth and freely slipping below that depth following the formulation of Okada (1985). Figure 6 shows the residual (observed minus estimated) GPS velocities for each model.

Profile D crosses the GCFTB approximately 70 km WNW of the 1902, M6.9, Shamakha Earth-

quake epicenter. For perspective, a M6.9 thrust earthquake is expected to have a surface rupture length of ~40-70km (Wells and Coppersmith, 1994). The model results for the profile shown in Figure 5D are almost identical for the 2 models considered; both models involve thrust faulting on a 30°dipping fault that is roughly coincident with the GCFTB in west-central Azerbaijan (Figure 6). The width of the zone of shortening is consistent with a fault locked to a depth of at least12 km (measured vertically from the surface) accumulating offset deficit at a rate of 10-12 mm/yr (i.e., offset deficit is the missing slip on the fault that is expected to be released in an earthquake).

Figure 5C shows the shorter and sparser profile crossing the GCFTB at the location of the 1902 Shamakha Earthquake (Figure 4). The Shamakha region experienced earlier, devastating earthquakes in 1191, and 1859. As mentioned earlier, these events were so severe that they instigated the population to move the Azerbaijan capital from Shirvan to the present location of Baku. The total amplitude (~ 11 mm/yr) and distribution of shortening (~ 70-100 km) along this short profile that crosses a segment of the fault system known to generate M~7 earthquakes, is very similar to that for Profile D. In addition, the overall kinematics and morphology of the GCFTB is generally similar along this segment of the range. However, this is approximately the location at which the major GCFTB begins to bifurcate into several potentially active structures. The relatively sparse GPS data along Profile C makes these end-member structures, as previously described and shown by the red and blue curves, indistinguishable. Nevertheless, these observations suggest that the entire GCFTB in Azerbaijan west of the Shamakha earthquake region is likely to experience earthquakes in the future, possibly similar to the historic events near Shamakha.

Profile B (Figure 5b) crosses the Kur Depression, eastern Greater Caucasus, and Absheron Peninsula near Baku (Figure 4). As described earlier, the new GPS observations presented here reveal that the trend and complexity of the eastern most GCFTB near Baku aid us in placing physical constraints on potentially active structures in an area that remains poorly understood. However, large misfits to both models confirm that there is likely to be deformation accommodated both on structures that continue east into the Central Caspian Sea and others that strike southward towards the Neftchala Peninsula. Figures 5B and 6 show that neither end-member model alone satisfactorily explain the observations. Neither model is significantly better than the other: the weighted root-mean-square (WRMS) residual to the model shown in Figure 6a is 2.04 mm/yr and the WRMS for the model shown in Figure 6b is 1.96 mm/yr, which

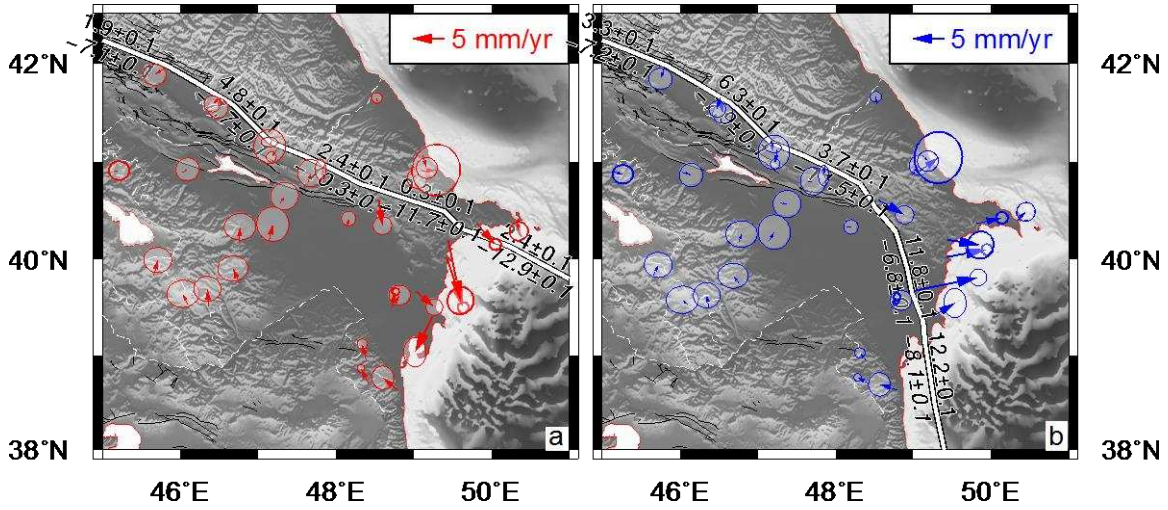


Figure 6. Map showing GPS residual velocities for the two fault models: (a) with continuation of the GCFTB eastwards towards the CCSZ, and (b) with change in strike of the GCFTB southwards along the west coast of the Caspian Sea. The common fault (west of 49.5°E) is a thrust fault dipping north at 30°. In (a), the continuation of the GCTFB is also modeled as a thrust fault dipping north at 30°; in (b) the southward change in strike of the fault is accompanied by a gradual change in dip such that the fault is vertical along the Neftchala Peninsula. All segments of the faults are locked to 12 km depth. Model fault slip rates shown along the fault traces, where the upper number is the strike-slip rate (positive is right-lateral) and the lower number in italics is the dip-slip rate (positive is extension) in mm/yr

is not a statistically significant difference. We do not consider complex models that include multiple branches of the GCFTB here since we have insufficient density of data and lack constraints on motion of the S Caspian Basin southeast of the Absheron Peninsula. We emphasize that these are highly idealized models that do not include variations in elastic properties of the crust, or complexities in the geometry of the eastern GCFTB. More realistic models will require better geodetic constraints on the spatial distribution of motions around the eastern segment.

As indicated in Figures 5 and 6, both these models do provide a good fit to the observed velocities in western Azerbaijan, the Kur Depression, and near Baku and the Absheron region. This gives us confidence about the magnitude of convergent strain rate that must be accommodated by some active structure or structures as we move from western Azerbaijan (convergence at ~ 8 mm/yr) to east (convergence at ~ 12–13 mm/yr). However, significant residual velocities in either one direction or the other exist in the area immediately south-west of the Absheron Peninsula along the coast of the Caspian Sea (Figure 6a compared to Figure 6b) indicating that the exact location and nature of these structures require further investigation. It is likely that a combination of the two modeled faults, possibly along with some other hybrid of intervening structures, is responsible for the observed deformation in this area.

In addition to its arcuate shape and the transition from a shallow dipping thrust fault in the west to a steeply dipping strike-slip fault south of Baku, the easternmost segment of the GCFTB is different in a number of ways from the central thrust segment. For example, the sedimentary section in the southern Caspian Sea south of the Absheron Peninsula reaches thicknesses of > 15 km, roughly twice the thickness of that in the eastern Kur Basin. The Caspian Basin is underlain by ocean crust as opposed to the continental crust below the Lesser Caucasus and Kur depression (e.g., Neprochnov, 1968; Kadinsky-Cade et al., 1981; Jackson et al., 2002). Furthermore, the ubiquitous nature of mud volcanoes in the E Kur Depression (Aliyev et al., 2009) attests to the importance of hydrothermal processes in the crust not present along the GCFTB to the west. How these differences may affect seismogenic structures and earthquake activity is presently unknown.

In spite of these uncertainties, the pattern of deformation across the E branch of the GCFTB (Figure 5B) is very similar to that across the central fault segment (Figures 5C and 5D) that is known to generate significant earthquakes. In addition, the discrepancies between the model fits for our two end-member models (Figures 5B and 6) appear to "bracket" the observations SW of Baku, suggesting that a hybrid-model for strain accumulation is more representative of the actual fault configuration; in this sense, the GPS observations are at least consistent with active strain accumulation. On the other hand, the broad distribution of shortening (Figure 5B) may be due to distributed, aseismic deformation associated with multiple, creeping fault branches, rather than strain accumulation on specific, major faults. Aseismic deformation within the thick, water-saturated sediments of the E Kur Depression seems plausible. We caution however, that the 2011, M9, Fukushima, Japan Earthquake unexpectedly ruptured through the thick, partially consolidated sediments offshore of Japan, producing a substantially larger earthquake than was estimated for the fault, and the accompanying destructive tsunami (e.g., Lay et al., 2011).

Conclusions

Azerbaijan has experienced large (M~7) and highly destructive earthquakes in the past and almost certainly will suffer earthquakes in the future. The geodetic observations presented in this chapter demonstrate that strain is accumulating on the 200 km long segment of the Greater Caucasus Fold-and-Thrust Belt from the Shamakha region (~70 km west of Baku) to the Azerbaijan-Georgian border. Based on the historic earthquake record (destructive earthquakes in 1191, 1859, and 1902) and the geodetic evidence we present for active strain accumulation, M7 thrust earthquakes are likely along this entire segment.

Geodetic observations across the Kur Depression and Absheron Peninsula in the densely populated and highly developed easternmost part of Azerbaijan show a similar deformation pattern across the GCFTB as the observations crossing the central and eastern segments of the fault. While this may indicate active strain accumulation that could generate earthquakes, the absence of large historic earthquakes, the change in strike of the fault west of Baku, and the thick highly saturated sediments in the eastern Kur Depression and south Caspian Basin may preclude large events like those known to occur on the fault further east. However, given the rapid increase in the population and the extensive infrastructural development in this part of Azerbaijan, and the likelihood of gaining new insights from additional geodetic observations and complex fault

models, it is essential that further studies be focused on the possibility and effects of damaging earthquakes along the eastern segment of the GCFTB. In particular, densifying GPS coverage along and across the eastern Caucasus, Kur Basin, and Greater Caucasus, constraining the subsurface geometry of the GCFTB and it's extension into the Caspian Sea with seismic studies, and investigating the historic earthquake record and paleoseismic observations to extend the earthquake record will provide the constraints needed to clarify better earthquake hazards in Azerbaijan.

Acknowledgments

We thank UNAVCO for technical support for the GPS network and survey observations. This research was supported by the Azerbaijan National Academy of Sciences, and the US National Science Foundation (NSF grant EAR-1321796).

The research was performed in international laboratory "Modern movements of Earth's crust and geodynamic hazards" at Geology and Geophysics Institute of Azerbaijan National Academy of Sciences within the framework of collaborative research from Massachusetts Institute of Technology (MIT).

REFERENCES

AKI, K., RICHARDS, P.G. 2002. Quantitative seismology. University Science Books. Sausalito, CA. 700 p.

ALLEN, M., JACKSON, J., WALKER, R. 2004. Late Cenozoic reorganization of the Arabia-Eurasia collision and the comparison of short-term and long-term deformation rates. *Tectonics, 23*, TC2008, doi:10.1029/2003TC001530.

ALIYEV, A.A., GULIYEV, I.S., RAHMANOV, R.R. 2009. Catalogue of mud volcanoes eruptions of Azerbaijan (1810-2007). Natfa-Press. Baku.

ALTAMIMI, Z., COLLILIEUX, X., LEGRAND, J., GARAYT, B., BOUCHER, C. 2007. A new release of the international terrestrial reference frame based on time series of station positions and earth orientation parameters. ITRF2005. *J. Geophys. Res*., doi:10.1029/2007JB004949.

AMBRASEYS, N.N. 2002. The Seismic activity of the Marmara Sea region over the last 2000 years. *Seismo. Soc. Am. Bull., 92*, 1-18.

AMBRASEYS, N.N., MELVILLE, C.P. 1982. A history of Persian earthquakes. Cambridge University Press. Cambridge. London, New York, New Rochelle, Melbourne, Sydney. ISBN 0 521 24112 X.

ArRAJEHI, A., McCLUSKY, S., REILINGER, R.E., DAOUD, M., ALCHALBI, A., ERGINTAV, S., GOMEZ, F., SHOLAN, J., BOU−RABEE, F., OGUBAZGHI, G, HAILEAB, B, FISSEHA, S., ASFAW, L., MAHMOUD, S., RAYAN, A., BENDIK, R., KOGAN, L. 2010. Geodetic constraints on present-day motion of the Arabian Plate: Implications for Red Sea and Gulf of Aden rifting. *Tectonics, 29*, TC3011, doi:10.1029/2009TC002482.

AVDEEV, B., NIEMI, N.A. 2008. Constraints on the rates and timing of exhumation of the Greater Caucasus from low-temperature thermochronology. *Eos, Trans. Am. Geophys. Union, 89*, 53.

BARAZANGI, M., SANDVOL, E., SEBER, D. 2006. Structure and tectonic evolution of the Anatolian plateau in eastern Turkey, *Geol. Soc. Am. Special Paper, 409*.

BENNETT, R.A., RODI, W., REILINGER, R. 1996. Global Positioning System constraints on fault slip rates in southern California and northern Baja, Mexico. *J. Geophys. Res., 101*, 21,943-21,960.

BIRD, P. 2003. An updated digital model of plate boundaries. *Geochemistry, Geophysics, Geosystems*, 4(3), 1027, doi: 10.29/2001GC000252.

BIRD, P., KAGAN, Y.Y. 2004. Plate-tectonic analysis of shallow seismicity: Apparent boundary width, beta, corner magnitude, coupled lithosphere thickness, and coupling in seven tectonic settings. *Seismo. Soc. Am. Bull., 94*, 2380-2399.

BLEWITT, G., LAVALLEE, D. 2002. Bias in geodetic site velocity due to annual signals. In: *Vistas for Geodesy in the New Millenium*, Int. Assoc. Geod.Symposia, 125, 499-500.

CETIN, E., CAKIR, Z., MEGHRAOUI, M., ERGINTAV, S., AKOGLU, A.M. 2014. Extent and distribution of aseismic slip on the Ismetpasa segment of the North Anatolian Fault (Turkey) from Persistent Scatterer InSAR. *Geochem. Geophys.Geosyst*., 15, doi:10.1002/ 2014GC005307.

COPLEY, A., JACKSON, J. 2006. Active tectonics of the Turkish-Iranian Plateau. *Tectonics, 25*, TC6006, doi: 10.1029/2005TC001906.

COWGILL, E., NIEMI, N.A., FORTE, A.M., ELASHVILI, M., JAVAKISHVILI, Z., MUMLADZE, T. 2012. Orogen-scale structural architecture and potential seismic sources resulting from Cenozoic closure of a relict Mesozoic ocean basin in the Greater Caucasus. S43J-07, 2012 Spring AGU Meeting.

DIXON, T. 1991. An introduction to the Global Positioning System and some geological applications. *Reviews of Geophys., 29*, 249-276.

DJAMOUR, Y., VERNANT, P., BAYER, R., NANKALI, H.R., RITZ, J.F., HINDERER, J., HATAM, Y., LUCK, B., LEMOIGNE, N., SEDIGHI, M., KHORRAMI, F. 2010. GPS and gravity constraints on continental deformation in the Alborz mountain range, Iran. *Geophys. J. Int., 183*, 1287-1301.

ENGDAHL, E.R., VAN DER HILST. R., BULAND, R. 1998. Global teleseismic earthquake relocation with improved travel times and procedures for depth determination. *Bull. Seismol. Soc. Am., 88,* 722-743,

ERGINTAV, S. et al. 2009. Seven years of postseismic deformation following the 1999, M=7.4, and M=7.2 Izmit-Duzce, Turkey earthquake sequence. *J. Geophys. Res.,* doi: 10.1029/2008JB006021.

FIALKO, Y. 2006. Interseismic strain accumulation and the earthquake potential on the southern San Andreas fault system. *Nature, 441*, 968-971,

FORTE, A., COWGILL, E., BERNARDIN, T., KREYLOS, O., HAMANN, B. 2012. Late Cenozoic deformation of the Kura fold-thrust belt, southern Greater Caucasus. *Geological Society of America Bulletin, 122,* 3-4, 465-486, doi: 10.1130/B26464.1.

GOK, R., SANDVOL, E., TURKELLI, N., SEBER, D., BARAZANGI, M. 2003. Snattenuation in the Anatolian and Iranian plateau and surrounding regions. *Geophys. Res. Lett., 30*, 24, doi: 10.1029/2003GL018020.

HAGER, B.H., KING, R.W., MURRAY, M.H. 1991. Measurements of crustal deformation using the Global

Positioning System. *Ann. Rev. Earth Planet Sci., 19,* 351-382.

HERRING, T.A., KING, R.W., McCLUSKY, S.M. 2010. Introduction to GAMIT/GLOBK Release 10.4. Mass. Inst. of Technology, 48p.

JACKSON, J. 1992. Partitioning of strike-slip and convergent motion between Eurasia and Arabia in eastern Turkey. *J. Geophys. Res., 97*, 12471-12479.

JACKSON, J., McKENZIE, D. 1984. Active tectonics of the Alpine-Himalayan belt between western Turkey and Pakistan. *Geophys. J. R. Astr. Soc., 77*, 185-246,

JACKSON, J., MCKENZIE, D. 1988. The relationship between plate motions and seismic tremors, and the rates of active deformation in the Mediterranean and Middle East. *Geophys. J. R. Astr. Soc., 93*, 45-73.

JACKSON, J., PRIESTLEY, K., ALLEN, M., BERBERIAN, M. 2002. Active tectonics of the south Caspian Basin. *Geophys. J. I, 148*, 214-245.

JONES, L. and 13 others. 2008. The Shake Out Scenario, U.S. Geological Survey Open File Report 2008-1150. California Geological Survey Preliminary Report 25, version 1.0.

JORDAN, T.H. 2014. The prediction problems of earthquake system science. *Seismol. Res. Lett., 85*, 767-769.

KADINSKY-CADE, K., BARAZANGI, M., OLIVER, J., ISACKS, B. 1981. Lateral variations of high-frequency seismic wave propagation at regional distances across the Turkish and Iranian Plateaus. *Journal of Geophysical Research*, 86: doi: 10.1029/JB080i010p09377. issn: 0148-0227.

KADIROV, F., MAMMADOV, S., REILINGER, R.E., McCLUSKY, S. 2008. Some new data on modern tectonic deformation and active faulting in Azerbaijan (according to Global Positioning System measurements). *Proceedings of the Azerbaijan National Academy of Sciences*, *The Sciences of the Earth, 1*, 82-88.

KADIROV, F., FLOYD, M. ALIZADEH, A., GULIEV, I., REILINGER, R.E., KULELI, S., KING, R., TOKSOZ, M.N. 2012. Kinematics of the eastern Caucasus near Baku, Azerbaijan. *Natural Hazards,* 63, 2, 997-1006; DOI 10.1007/s11069-012-0199-0.

KADIROV, F.A., GADIROV, A.H. 2014. A gravity model of the deep structure of South Caspian Basin along submeridional profile Alborz–Absheron Sill. *Global and Planetary Change, 114,* 66-74, DOI: 10.1016/j.gloplacha.

KNAPP, C.C., KNAPP, J.H., CONNOR, J.A. 2004. Crustal-scale structure of the South Caspian Basin revealed by deep seismic reflection profiling. *Marine and Petroleum Geology 2,* 1073-1081.

KONDORSKAYA, N.V., SHEBALIN, N.V. (Eds.). 1982. New catalogue of strong earthquakes in the USSR from ancient times through 1977. *World Data Centre A for Solid Earth Geophysics, Report SE-31*, English translation of Russian original, Boulder, Colorado, USA, 608 pp.

KOPP, M.L., SHCHERBA I.G. 1985. Late Alpine development of the east Caucasus. *Geotectonics*, *19*(6), 497-507.

KRÁL, J., GURBANOV, A.G. 1996.Apatite fission track data from the Greater Caucasus pre-Alpine basement. *Chemieder Erde, 56,* 177-192.

LAWRENCE, S.A. 2003. Kinematically consistent, elastic block model of the Eastern Mediterranean constrained by GPS measurements. M.S. Thesis, Massachusetts Institute of Technology, Cambridge, MA.

LAY, T., YAMAZAKI, Y., AMMON, C.J., CHEUNG, K.F., KANAMORI, H. 2011. The 2011 Mw 9.0 off the Pacific coast of Tohoku Earthquake: Comparison of deep-water tsunami signals with finite-fault rupture model predictions. *Earth Planets Space, 63*, 797-801.

LYONS, S., SANDWELL, D. 2003. Fault creep along the southern San Andreas from interferometric synthetic aperture radar, permanent scatterers, and stacking. *J. Geophys. Res., 108, B1*, 2047, doi:10.1029/2002JB001831.

LYZENGA, G.A., PANERO, W.R., DONNELLAN, A. 2000. Influence of anelastic surface layers on postseismic thrust fault deformation. *J. Geophys. Res., 105*, 3151-3157.

MEGHRAOUI, M., AKSOY, M.E., AKYÜZ, H.S., M. FERRY, DIKBAŞ, A., ALTUNEL, E. 2012. Paleoseismology of the North Anatolian Fault at Güzelkoy (Ganos segment, Turkey): Size and recurrence time of earthquake ruptures west of the Sea of Marmara. *Geochem. Geophys. Geosys., 13,* Q04005, doi:10.1029/2011GC003960.

McCLUSKY, S, .BALASSANIA, A., BARKA, A., DEMIR,C., ERGINTAV, S., GEORGIEV, I., GURKAN, O., HAMBURGER, M., HURST, K., KAHLE, H., KASTENS, K., KEKELIDZE, G. KING, R. KOTZEV, V. LENK, O., MAHMOUD, S. MISHIN, A. NADARIYA, T.M., OUZOUNIS, A., PARADISSSIS, D., PRILEPIN,P., REILINGER, R.E., SANLI, I., SEEGER, H., TEALEB, A., TOKSOZ, M.N., VEIS, G. 2000. GPS constraints on plate kinematics and dynamics in the eastern Mediterranean and Caucasus. *J. Geophys. Res*., *105,* 5695-5719.

McCLUSKY, S., REILINGER, R., MAHMOUD, S., BEN SARI, D., TEALEB, A. 2003. GPS constraints on Africa (Nubia) and Arabia plate motion. *Geophys. J. Int., 155,* 126-138.

McQUARRIE, N., STOCK, J.M., VERDEL, C., WERNICKE, B.P. 2003. Cenozoic evolution of Neotethys and implications for the causes of plate motions. *Geophys. Res. Lett*., 30, doi:10.1029/2003GL017992.

McQUARRIE, N., VAN HINSBERGEN, D.J.J. 2013. Retrodeforming the Arabia-Eurasia collision zone: Age of collision versus magnitude of continental subduction. *Geology, 41*, 315-318.

McKENZIE, D.P. 1970. Plate tectonics of the Mediterranean region. *Nature, 226*, 239-243.

McKENZIE, D.P., DAVIES, D., MOLNAR, P. 1970. Plate tectonics of the Red Sea and East Africa. *Nature, 226,* 243-248.

McKENZIE, D.P. 1972. Active tectonics of the Mediterranean region. *Geophys. J. R. Astron. Soc., 30*, 109-185.

MUELLER, I.I., BEUTLER, G. 1992. The International GPS Service for Geodynamics – Development and Current Structure. *Proceedings of the 6th Symposium on Satellite Positioning*, Ohio State University, Columbus, Ohio.

MUSHKETOV, I.V., ORLOV, A.P. 1893. Catalogue of earthquakes of the Russian Empire. *Notes of Russian Geographic Soc., St.Peterburg, 26*, 582 pp (in Russian).

NEPROCHNOV, Y.U. 1968. Structure of the earth's crust of epicontinental seas: Caspian Black and Mediterranean. *Canad. J. Earth Sci., 5*, 1037-1043.

NUR, A., MAVKO, G. 1974. Postseismic Viscoelastic Rebound. *Science,*183, 204-206.

OKADA, Y. 1985. Surface deformation due to shear and tensile faults in a half-space. *Bull. Seismol. Soc. Am., 75*, 1135-1154.

PHILIP, H., CISTERNAS, A., GVISHIANI, A., GORSHKOV, A. 1989. The Caucasus: An actual example of the initial stages of continental collision. *Tectonophysics, 161*, 1-21, doi: 10.1016/0040-1951(89)90297-7,

PHILIP, H., AVAGYAN, A., KARAKHANIAN, A., RITZ, J.-F., REBAI, S. 2001. Estimating slip rates and recurrence in-

tervals for strong earthquakes along an intracontinental fault: Example of the Pambak-Sevan-Sunik fault (Armenia). *Tectonophysics, 343*, 205-232, doi:10.1016/S0040-1951(01)00258-X.

PODGORSKI, J., HEARN, E., MCCLUSKY, S., REILINGER, R.E., TAYMAZ, T., TAN, O. 2007. Postseismic deformation following the 1991 Racha, Georgia, earthquake. *Geophys. Res. Lett., 34*, L04310, doi:10.1029/2006GL028477.

POLLITZ, F.F. 1992. Postseismic relaxation theory on the spherical earth. *Bull. Seismo.Soc. Am., 82, 1*, 422-453.

PRESCOTT, W.H., SAVAGE, J.C. 1976. Strain accumulation on the San Andreas Fault near Palmdale, California. *J. Geophys. Res., 81*, 4901-4908

REILINGER, R.E., McCLUSKY, S., VERNANT, P., LAWRENCE, S., ERGINTAV, S., CAKMAK, R., OZENER, H., KADIROV, F., GULIEV, I., STEPANYAN, R., NADARIYA, M., HAHUBIA, G., MAHMOUD, S., SAKR, K., ArRAJEHI, A., PARADISSIS, D., AL-AYDRUS, A., PRILEPIN, M., GUSEVA, T., EVREN, E., DMITROTSA, A., FILIKOV, S.V., GOMEZ, F., AL-GHAZZI, R., KARAM, G. 2006. GPS constraints on continental deformation in the Africa-Arabia-Eurasia continental collision zone and implications for the dynamics of plate interactions. *J. Geophys. Res.,* BO5411, doi:10.1029/2005JB 004051.

SENGOR, A.M.C., GORUR, N., SAROGLU, F. 1985. Strike-slip faulting and related basin formation in zones of tectonic escape: Turkey as a case study, in Strike-slip Faulting and Basin Formation. (Biddle, K.T. and N. Christie-Blick, eds.). *Society of Econ. Paleont. Min. Sec. Pub, 37,* 227-264.

SENGOR, A.M.C., TUYSUZ, O., IMREN, C., SAKINC, M., EYIDOGAN, H., GORUR, N., LePICHON, X., RANGIN, C. 2004. The North Anatolian fault: A new look. *Ann. Rev. Earth Planet. Sci., 33,* 1-75.

SWARTZ, D.P., COPPERSMITH, K.J. 1984. Fault behavior and characteristic earthquakes: Examples from the Wasatch and San Andreas Fault Zones. *J. Geophys. Res., 49*, 5681-5698.

TRIEP, E.G., ABERS, G.A., LERNER-LAM, A.L., MISHATKIN, V., ZAKHARCHENKO, N., STAROVOIT, O. 1995. Active thrust front of the Greater Caucasus: The April 29, 1991 Racha earthquake sequence and its tectonic implications. *J. Geophys. Res., 100*, 4011-4033.

VERNANT, P., CHERY, J. 2006. Low fault friction in Iran implies localized deformation for the Arabia–Eurasia collision zone. *Earth and Planetary Sci. Lett.,246*, 197-206.

VERNANT, P., REILINGER, R.E., McCLUSKY, S. 2014. Geodetic evidence for low coupling on the Hellenic subduction plate interface. *Earth, Planet.Sci.,385,* 122-129.

VINCENT, S.J., MORTON, A.C., CARTER, A., GIBBS, S., TEIMURAZ, G.B. 2007. Oligocene uplift of the Western Greater Caucasus: An effect of initial Arabia-Eurasia collision. *Terra Nova. 19*, 160-166, doi:10.1111/j.1365-3121.2007.00731.x.

WELDON II, R. J., SCHARER, K., FUMAL, T., BIASI, G. 2004. Wrightwood and the earthquake cycle: what a long recurrence record tells us about how faults work. *GSA Today, 14(9)*, 4-10.

WELLS, D.L., COPPERSMITH, K.J. 1994. New empirical relationships among magnitude, rupture length, rupture width, rupture area, and surface displacement. *Bull. Seism. Soc. Am., 84*, 974-1002.

WESTAWAY, R. 1990. Seismicity and tectonic deformation rate in Soviet Armenia: Implications for local earthquake hazard and evolution of adjacent regions. *Tectonics*, *9(3)*, 477-503, doi:10.1029/TC009i003p00477.

WORKING GROUP ON CALIFORNIA EARTHQUAKE PROBABILITIES (WGCEP). 2008. The Uniform California Earthquake Rupture Forecast, Version 2 (UCERF 2): U.S. Geological Survey Open-File Report 2007-1437 and California Geological Survey Special Report 203 [http://pubs.usgs.gov/of/2007/1091/].

ZOLLER, G., BEN-ZION, Y., HOLSCHNEIDER, M., HAINZ, S. 2007. Estimating recurrence times and seismic hazard of large earthquakes on an individual fault. *Geophys. J. Int.,* 170, 1300-1310.

ZONENSHAIN, L.P., Le PICHON, X. 1986. Deep basins of the Black Sea and Caspian Sea as remnants of Mesozoic back-arc basins. *Tectonophysics, 123*, 181-211, doi: 10.1016/0040-1951(86)90197-6.

© F.A.Kadirov, B.G.Ahadov, A.H.Gadirov, G.R.Babayev, S.G.Mammadov, R.T.Safarov, 2015

MICROTREMOR SURVEY AND SPECTRAL ANALYSES OF H/V RATIO FOR BAKU CITY (AZERBAIJAN)

F.A.Kadirov, B.G.Ahadov, A.H.Gadirov, G.R.Babayev, S.G.Mammadov, R.T.Safarov

Institute of Geology and Geophysics, Azerbaijan National Academy of Sciences, 119, H.Javid ave., Baku, AZ1143

In this study, ground response analysis on different 255 sites in Baku city of Azerbaijan was done. The damage distribution is estimated on the basis of local site effects. Aiming to estimate local site effect, analysis of the ratio of horizontal to vertical (H/V) spectra of microtremor records was performed. The records are conducted with the Guralp CMG-5TD accelerometer and, with the Nakamura's approach, dynamic characteristics of surface ground are estimated. The maps showing the distribution of the amplification and resonance frequency for the grounds of Baku city were produced, which demonstrate variability and heterogeneity of ground characteristics in the city. The results can be used for urban seismic hazard assessment researches in the future.

Introduction

Seismic noise can be analyzed in different ways depending on the objective of the study. A popular analysis method is the H/V spectral ratio method. This method was first proposed by Nogoshi and Igarashi (1971) and years later it was summarized by Nakamura (1989). During the decade of the 1990´s almost 80% of the published works about seismic noise were using the H/V spectral ratio method (Bard, 1998; Bonnefoy-Claudet et al., 2006). It is very useful tool in identifying seismic ground motion amplification for earthquake hazard assessment, because it is very simple and economical in operation.

Baku is a fast growing megacity (availability of multi-stored buildings, residential places, industrial constructions, new roads, bridges, tunnels, fashionable hotels) that influences the economic and industrial developments in the country. This region has experienced many earthquakes since ancient times and faces severe seismic threats from the Caspian and Absheron seismic events. It lies in the zone VIII of seismic zoning map of Azerbaijan (MSK 64). Within the historical time period, peninsula, as well as, Baku city have shaken as a result of occurrences of a number of seismic events, such as 1842 Mashtagi earthquake with magnitude M=5 (25 km northward from Baku), 1983 Nardaran-Bilgyah earthquake with M=5, 1986, 1989 Caspian earthquakes with M=6.0-6.5, the last strong 2000 earthquake with M=6.3, which occurred southward from Baku city. Intensive city planning, erroneous land using, construction of many industrial and residential buildings, roads, tunnels, bridges, change of soil conditions due to the various geodynamic and seismic processes, lack of knowledge about modern ground characteristics of Baku city accentuate the necessity to apply microtremor measurements technique which is one of the useful method in investigating ground characteristics and estimating local sites effects, especially in the urbanized areas.

Geology of the area

The study area is located in the southeast side of the Greater Caucasus mega-anticlinorium. The region has specific geologic structures and tectonics.

Fig. 1 gives the tectonic and geological scheme of the area (Kadirov, 2000). In the region, mud-volcanic and diapir folds are widespread. The Tengi-Beshbarmag anticlinorium, Shahdag-Khizi, Zagatala-Govdag, Shamakha-Gobustan synclinorium, Absheron and the Lower Kur basins are the main tectonic structural elements (Shikhalibeyli, 1972). The area embraces the whole of the Absheron oil and gas-bearing region, a large part of the Shamakha-Gobustan region, some parts of the Baku Archipelago, the Lower Kur and near-Caspian oil and gas-bearing regions. Intensive subsidence in the Shamakha-Gobustan synclinorium began in the Cretaceous and Paleogene periods. The great thicknesses of the Paleogene-Neogene deposits and the clearly expressed boundaries of their occurrence, represented in the west by Zangi and in the east by Goradil thrusts, lend support to this subsidence. A comparison of geological and geophysical data from the Shamakha-Gobustan synclinorium indicates that the structural features of the Mesozoic and Cenozoic strata are discordant. The synclinorium is considered as a superimposed trough of complicated struc-

ture. Its south-west boundary is made up of the Lengebiz-Alyat anticline zone. The present structure of the Lengebiz-Alyat zone was formed in the late Pliocene-Quaternary period. The Absheron periclinal trough is superimposed in character and represents an extreme eastern structural element of the Greater Caucasus mega-anticlinorium. In the west, the trough is limited by the Yashma flexure, the origin of which is related to the Cenozoic subsidence of the Caspian basin. As a consequence, substantial sinking of the Absheron peninsula and of the North Absheron aquatorium, along with the islands and banks, occurred. Simultaneously, the eastern part of the Shamakha-Gobustan synclinorium the Jeyrankechmez depression, composed of Paleogene and Miocene sediments, was involved in this process.

According to the borehole and geophysical data, the depth of the Mesozoic top within the study area varies in the range of 1–10 km. In the central part of the Jeyrankechmez depression, the top of the Paleogene-Miocene complex lies below 3-4 km and that of the Mesozoic is within 8-10 km. The Lower Kur basin is the deepest among the basins of the Kur basin system. The major part of the Lower Kur basin is covered with Quaternary strata. The boundaries of the Lower Kur basin are the West Caspian fault and the Lengebiz-Alyat rise in the southwest and northeast, respectively. In the Lower Kur basin,

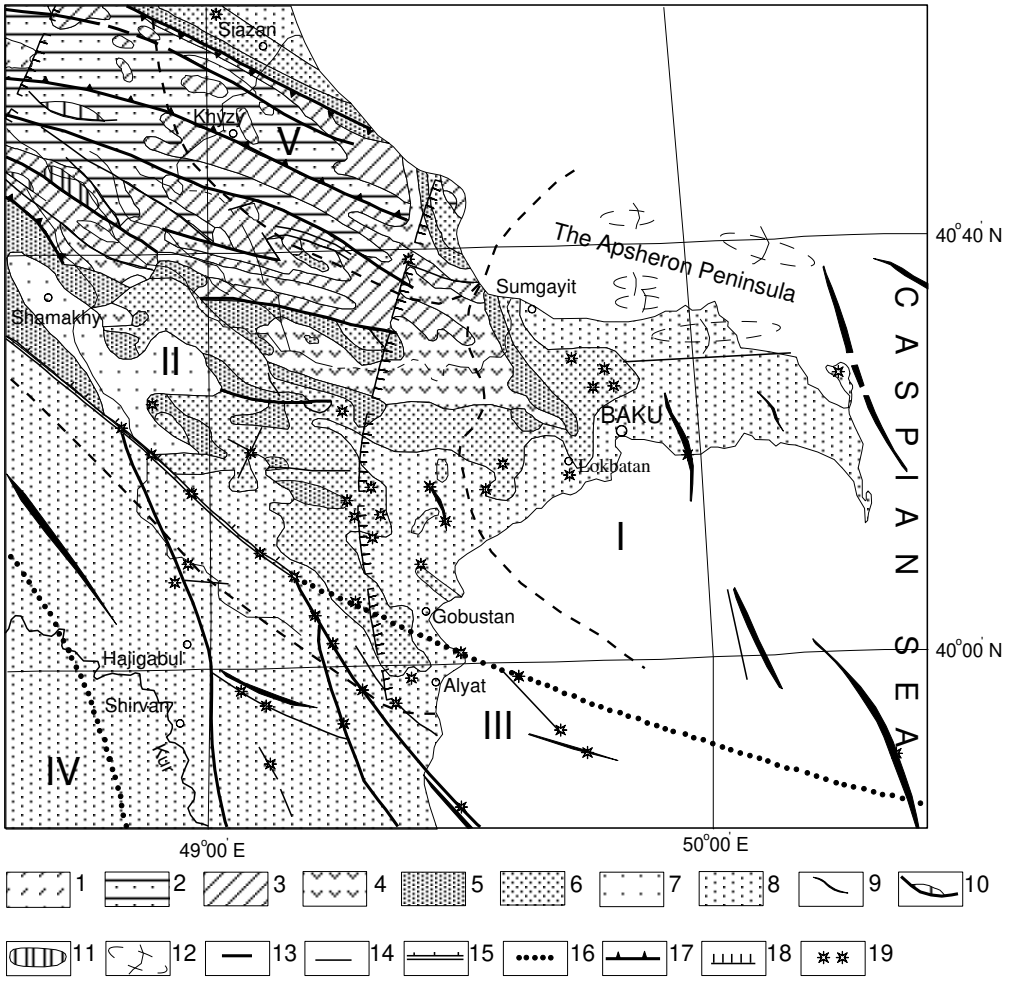


Figure 1. Tectonic and geological scheme of the study area. Alpine geosynclinals sub-complexes: 1 – early geosynclinals epoch, late geosynclinals epoch: 2 – lower epoch, 3 – middle epoch, 4 – upper epoch. Alpine orogenesis sub-complexes: 5 – early orogenesis sub-epoch, 6 – early orogenesis upper epoch o12., 7 – late orogenic epoch up to 800 m., 8 – late orogenic epoch 800 m and greater (O_2). Structural elements, fold types and dislocations with a break in continuity: 9 – axes of large anticlinal folds, 10 – scale-shaped folds, 11 – tectonic nappe, 12 – buried folds, 13 – normal faults with thousands of meters of amplitude, 14 – normal faults with hundreds of meters of amplitude, 15 – crustal faults manifested at the surface by thrusts and over faults, 16 – buried faults, 17 – thrusts and over faults with thousands of meters of amplitude, 18 – buried flexure, 19 – mud volcano. Oil- and gas-bearing regions: I – Absheron region, II – Shamakha-Gobustan region, III – Baku Archipelago, IV – Lower Kur region, V – near-Caspian region (Kadirov, 2000)

the thickness of the sedimentary pile is around 15 km, of which over 8 km is made up of the Pliocene-Quaternary sediments. The study area is an element of the Alpine folded belt of Eurasia. The Greater Caucasus and the Kur basin experienced tectonic evolution spanning the Late Proterozoic to the Anthropogenic period. In general, three periods are differentiated in the geological evolution of Azerbaijan: Baikalian, Hercynian and Alpine. The area along the Greater Caucasus axis and its south slope is supposed to belong to the Paleozoic geosyncline (Azizbekov et al., 1972).

Methodology

There are different methods to perform and interpret microtremor measurements, which require several instrumentation set-ups and assumptions. This study focuses on applications and interpretation of microtremors, with the emphasis on the method proposed by Nakamura (1989). Damages caused by the recent earthquakes are concluded as a direct result of local geological condition affecting the ground motion. Best approach for understanding ground conditions is through direct observation of seismic ground motion, but such studies are restricted to areas with relatively high rates of seismicity. Because of these restrictions in other methods, such as high rates of seismicity and the availability of an adequate reference site, non-reference site methods have been applied to site response studies. Microtremor is a very convenient tool to estimate the effect of surface geology on seismic motion without needing other geological information (Kanai et. al., 1954). Many observations and experiences on microtremor records show that microtremor consists of both body and surface waves, but there is no established theory concerning what kinds of wave motions the microtremor is made up from. In Nakamura (1989), the purpose of the author was the estimation of the amplification factor caused by multiply-refracted vertical incident SH waves. For this purpose, Rayleigh wave contained by microtremor was considered as noise and eliminated inside the H/V process. Nakamura (1989) gives theoretical definition of the H/V technique with multiple refraction of SH waves. On the other hand, there is a group of researchers who try to explain the peak of H/V ratio with the evidence of Rayleigh waves. As it is mentioned before, microtremor consists of many kinds of waves. Linking to the surface waves is based on the assumption that noise predominantly consists of surface waves. Figure 2 shows two of these examples for the microtremor records in Hakodate, Japan. It can be clearly seen from this figure that, energy of Rayleigh wave does not appear on the peak of H/V of Rayleigh wave. Rayleigh wave energy gets its maximum on later frequencies at minimum group velocity of Rayleigh wave and this is nearly equal to trough frequency which is almost two times of the H/V peak frequency (Nakamura, 2000).

From this view point, the Rayleigh wave plays as a noise and it is necessary to reject the effect of the Rayleigh wave. It is possible to understand that the surface layer behaves as a high-pass filter for the Rayleigh wave propagating in the surface layer. Rayleigh wave can not propagate in the frequency range under the predominant frequency of surface ground and can transmit the energy peak around the frequency of minimum group velocity.

Here microtremor is divided into two parts considering that it contains Rayleigh wave and other waves. Then, horizontal and vertical spectra on the surface ground of the sedimentary basin (H_f, V_f) can be written as follows (Nakamura, 2000):

$$H_f = A_h * H_b + H_s, \; V_f = A_v * V_b + V_s,$$

where A_h and A_v are amplification factor of horizontal and vertical motions of vertically incident body wave. H_b and V_b are spectra of horizontal and vertical motion in the basement under the basin (outcropped basin). H_s sand V_s are spectra of horizontal and vertical directions of Rayleigh waves.

Main waves consisting of microtremors are either body waves or Rayleigh waves, or depending on the location and other conditions they can be mixture of both waves. More explanation regarding Rayleigh waves can be found in Nakamura (1996).

Microtremor survey and spectral analyses

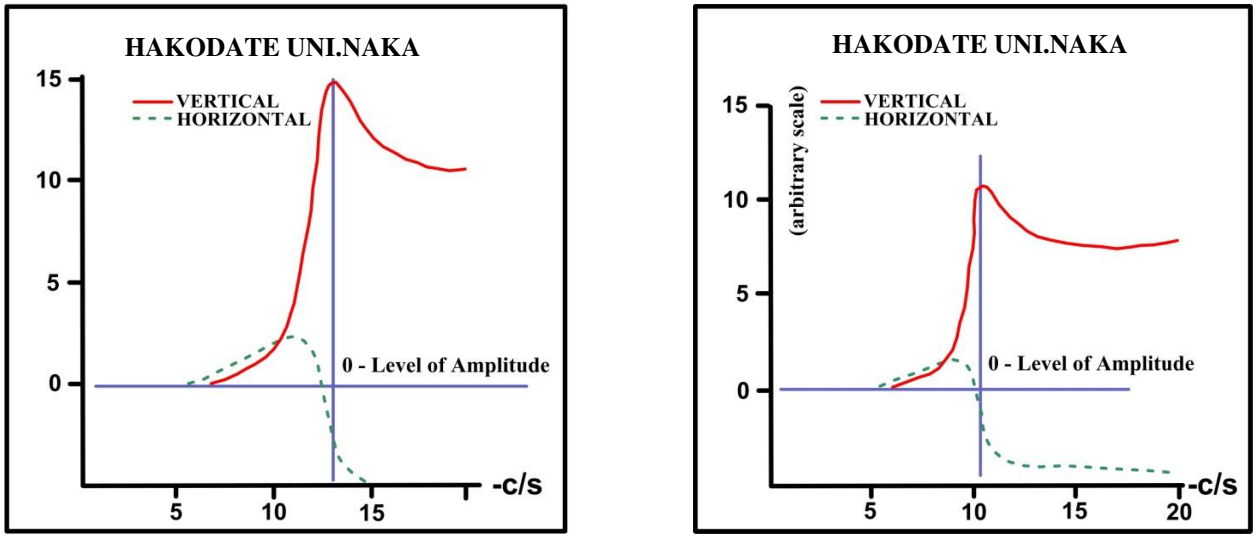
The objective of the present study is to analyze microtremors for investigation of ground characteristics in Baku city by estimating local site effects through the H/V ratio technique. The parameters that were analyzed are amplitude spectra, soil classification, H/V spectral ratio, resonance frequency and amplification ratio in site location. In this study, microtremor measurements were done in 255 points in Baku city. The measurement points have been selected in such a way so that they could give a good coverage of the study area, a large selection of different quaternary sediments and sedi-

ment thicknesses (Kadirov et al., 2012). Recording duration is 30 minutes. Measurements have been conducted at the distance of every 500 m taking into account environmental impact after getting results of primary analyses observations have been repeated every 250 m.

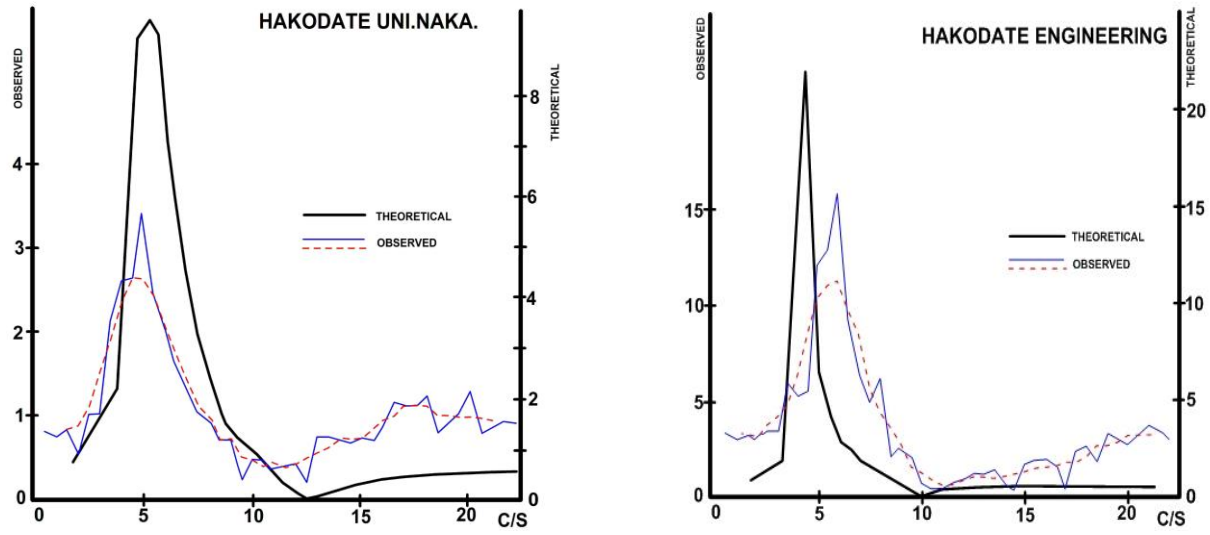
Figure 3 shows microtremor measurements points in throughout Baku city.

The resulting 255 H/V spectral ratios were systematically analyzed considering the recommendations proposed by the SESAME consortium (SESAME WP12 team 2005). Here we used the program "Matlab programming language" for H/V spectral analysis. (Figure 4 shows calculated of spectral analyzes for point 14, as an example).

The data processing for both data sets was as follows: each noise recording was divided into 30s window length. Each window was tapered at both ends with a 5% cosine taper and its Fast Fourier Transform (FFT) calculated. The FFT have been smoothed using a Konno-Ohmachi window (Konno and Ohmachi, 1998) fixing the parameter b to 20.



a)



b)

Figure 2. Example of horizontal and vertical components of rayleigh wave in Hakodate area, Japan (in (a) x axis represents velocity of S-waves; in (b) x axis represents frequency in unit, while y axis indicates H/V of Rayleigh wave)

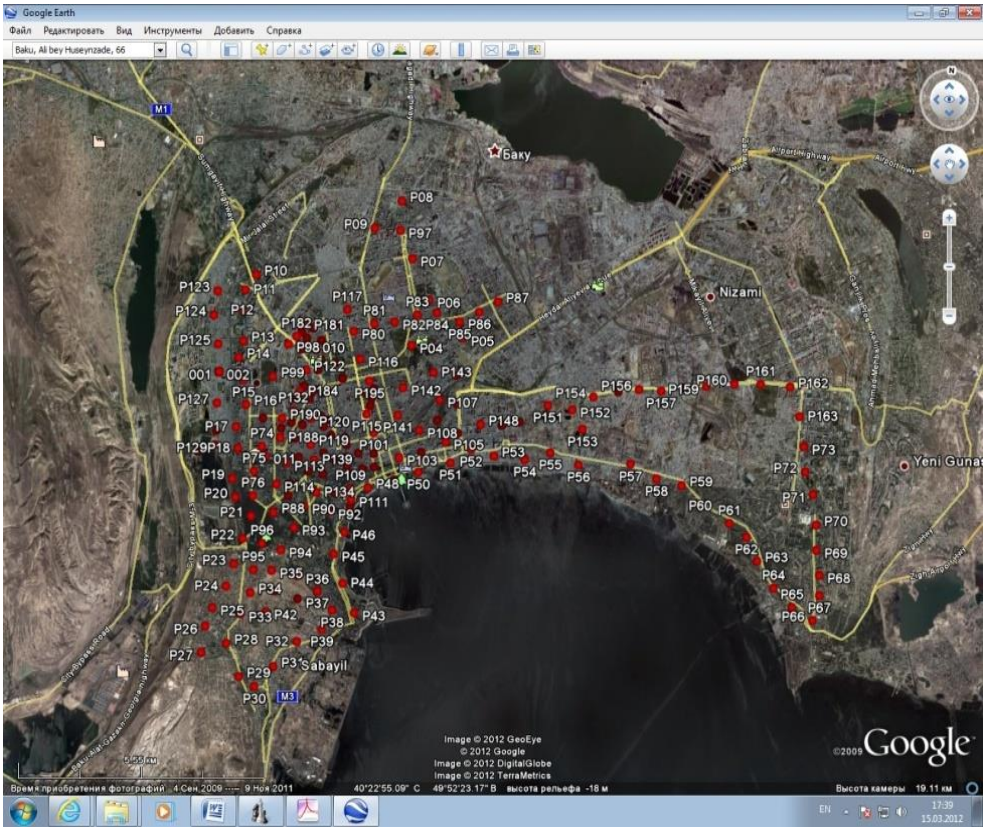


Figure 3. Measurements points

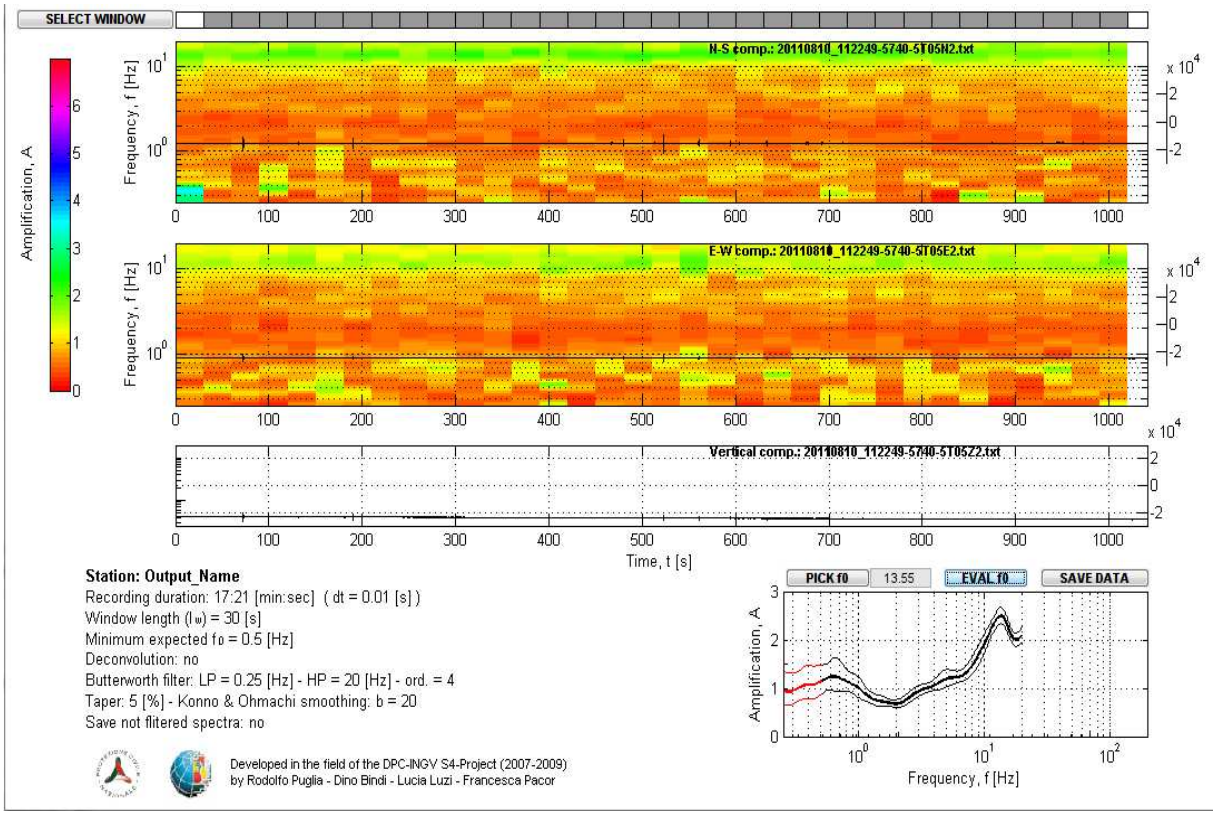


Figure 4. Spectral analyzes for point 14 (parametric entry was done by Ahadov B.)

Results

In the present study we have investigated the use of HVNSR analysis using microtremors in the Baku city to map the fundamental frequency and amplification factor of soils. Figure 5 and 6 demonstrate the map of the amplification factor and fundamental frequency of grounds in the Baku city, respectively. The results indicate that the ambient noise analysis can be an efficient tool for exploring soil conditions in urban areas. As a result of thorough investigation and observation of two above-mentioned maps, it was found out three zones with various ground conditions appeared over the area of study: hard soil, soft soil and intermediate type of soil. Preliminary analysis of amplitude-resonance properties of soil demonstrates that the larger part of the study area is covered by hard soil types. Intermediate type of soil can be observed in the north-western and north-eastern parts of the city. The soft soil types are mainly spread in the shoreline area and across the central part of the city. It is worth mentioning that with this approach, it is possible to reveal the influence of uncertainties on the resonance properties of the ground. Amplification factor ranges 0.6-4. Maximum amplification factor is observed in the western part. Fundamental frequency ranges 0.5Hz-9Hz. Also, maximum frequency is observed in the north – western part.

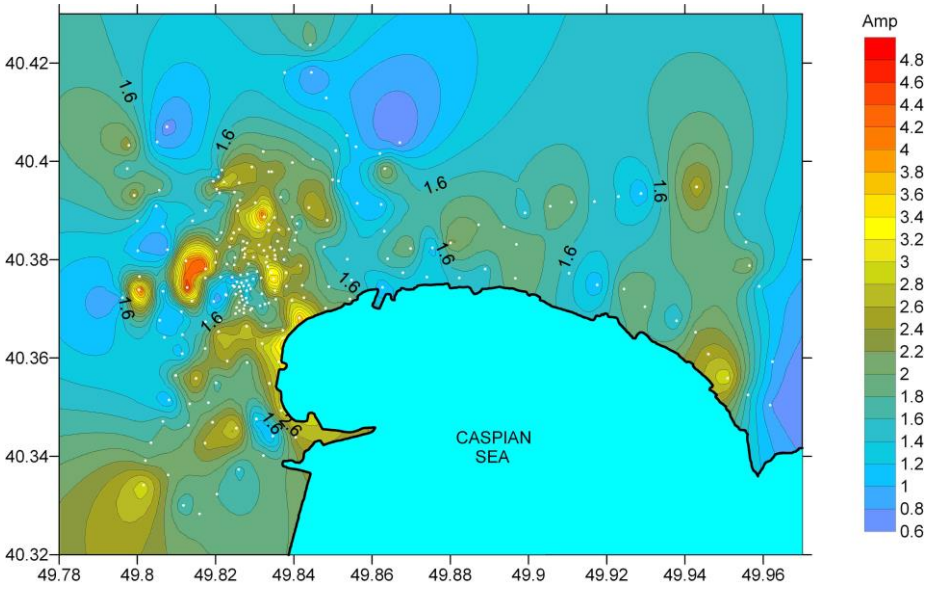


Figure 5. Map of the ground amplification distribution for Baku city

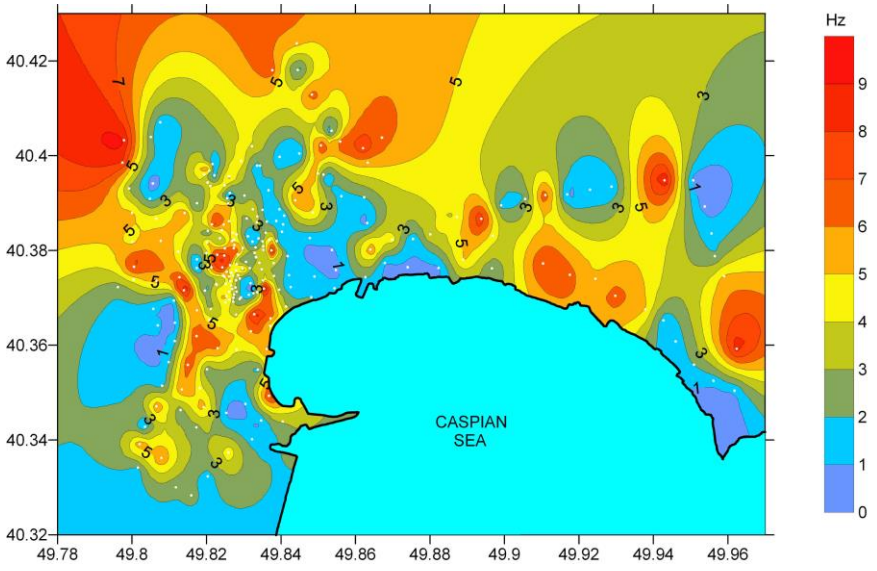


Figure 6. Map of fundamental frequency of resonance distribution for Baku city

In general, the site effects are usually associated with local subsurface conditions. From those two models, one can resume that where high frequency is observed at 5-8Hz, amplification normally dampens towards 0.6. This is most probably due to the heterogeneous content of the soils, such as within the hard rocks there might be existence of water-saturated soils, loose sediments (such as sands, sandy clays and clayey sands). Additionally, in those specific areas, more extensive measurements are necessary to perform in order to more clearly trace the obtained results of predominant frequency behavior and amplification factor correlated with the geological conditions of the study area.

Future plans

The resultant information obtained for the first time, will be used for preparation of the exact seismic hazard and risk maps and implementation of the effective plan to reduce the scale of destruction for Baku city.

Models of seismic hazard plotted up to the present time for Baku city have been prepared without information of real seismic motion, compiled theoretically, however for practical investigation it is necessary to use factual data. Besides, the establishment of 3D seismic models is very important for the city.

Acknowledgments

This work was supported by the Science Development Foundation under the President of the Republic of Azerbaijan (grant no. EIFF201001(1) 40/188MM21). The research was performed in international laboratory "Modern movements of Earth's crust and geodynamic hazards" at Geology and Geophysics Institute of Azerbaijan National Academy of Sciences.

We are very thankful to Prof. Hakan Karsli from Department of Geophysical Engineering, Karadeniz Technical University for his incredible comments and suggestions while reviewing the paper.

REFERENCES

AZIZBEKOV, SH.A., AGABEKOV, M.G., GRIGORYANTS, B.V., SHIKALIBEYLI, E.SH., MAMEDOV, A.V. 1972. The history of the geological evolution. In: Azizbekov, Sh.A. Ed.: *Geology of the USSR, Azerbaijan vol. XLVII.* Nedra, Moscow, 441-503 (in Russian).

BARD, P.Y., JONATHAN, F. 1998. Springer Science & Business Media. 473 p.

BONNEFOY-CLAUDET, S., KÖHLER, A., CORNOU, C., WATHELET, M., BARD, P.Y. 2008. Effects of love waves on microtremor H/V Ratio. *Bull. seism. Soc. Am.,* 98(1), 288-300.

KADIROV, F.A. 2000. Application of the Hartley transform for interpretation of gravity anomalies in the Shamakhy-Gobustan and Absheron oil- and gas-bearing regions, Azerbaijan. *Journal of applied geophysics,* 45 (1), 49-61.

KADIROV, F., BABAYEV, G., GADIROV, A. 2012. Analysis of horizontal to vertical spectra of microseisms for Baku City. *Problems of Cybernetics and Informatics (PCI),* 2012 IV International Conference.

KADIROV, F.A., BABAYEV, G.R., GADIROV, A.G., SAFAROV, R.T., MUKHTAROV, A.S. 2012. Microzonation of the Baku city using mikrotremor measurements. In the book: *Problems of reduction of natural hazards and risks*. International scientific and practical conference "GEORISK 2012". In 2 Vols. Volume 1. Moscow. Peoples' Friendship University of Russia (PFUR). 348, 94-98.

KANAI, K., TANAKA, T. 1954. Measurement of the microtremor. Bull. *Earthq. Res. Inst. Tokyo Univ*., 32, 199-209.

KONNO, K., OHMACHI, T. 1998. Ground motion characteristics estimated from spectral ratio between horizontal and vertical components of microtremors. *Bull. Seism. Soc. Am.,* 88-1, 228-241.

NAKAMURA, Y. 1989. A method for dynamic characteristics estimation of subsurface using ambient noise on the ground surface. *QR Railway Tech. Res. Inst*., 30, 25-33.

NAKAMURA, Y. 1996. Real time information systems for seismic hazards mitigation UrEDAS, HERAS and PIC. *Quarterly Report of RTRI*, 37, 3, 112-127.

NAKAMURA, Y. 2000. Clear identification of fundamental idea of Nakamura's technique and its applications. 12WCSEE: 12th World conference on earthquake engineering, Auckland, New Zealand.

NOGOSHI, M., IGARASHI, T. 1971. On the amplitude characteristics of microtremor (Part 2). *Jour. Seism. Soc.* Japan, 24, 26-40 (in Japanese with English abstract).

SESAME EUROPEAN RESEARCH PROJECT WP12 – Deliverable D23.12 2004.

SHIKHALIBEYLI, E. 1996. Some problematic aspects of geological structures and tectonics of Azerbaijan. Elm. Baku.

© L.Eppelbaum, 2015

COMPARISON OF 3D INTEGRATED GEOPHYSICAL MODELING IN THE SOUTH CAUCASIAN AND EASTERN MEDITERRANEAN SEGMENTS OF THE ALPINE-HIMALAYAN TECTONIC BELT

L.Eppelbaum

Tel Aviv University,
Ramat Aviv 69978, Tel Aviv, Israel

South Caucasus (including Azerbaijan) and Easternmost Mediterranean (including Israel) are located within the Alpine-Himalayan tectonic belt and are characterized by complex and variable tectono-geological pattern. To study deep structure of these regions several regional interpreting profiles indicating results of 3D combined gravity-magnetic modeling were selected. Development of the initial physical-geological models (***PGM***s) is realized by utilization of the known surface geology, drilling data examination, previous seismic, magnetotelluric and thermal data analysis, careful investigation of the petrophysical (including paleomagnetic) data, as well as qualitative and quantitative analysis of gravity-magnetic materials. After that an iterative 3D modeling accompanied by changing geometrical boundaries of geological bodies (and assuming new targets) and varying physical properties (density, magnetization and magnetic vector inclination) is started. This process has been completed by development of final ***PGM***s. Creating the final ***PGM***s means not only determination of minimal difference between the observed and computed gravity and magnetic fields, but also compliance of the models with the known geological principles (complex geological ***PGMs*** of the regions under study often compose intricate structural-tectonic puzzles). The final ***PGM***s reflect the key structural-tectonic specifics of the regional geological structure, beginning from the subsurface (hundreds of meters) up to the Moho discontinuity (tens of kilometers). The ***PGM***s revealed primarily the boundaries of tectonic blocks, masked faults, buried uplifts of basement, occurrence and form of various magmatic bodies, some common factors controlling ore- and hydrocarbon bearing formations, and some other features. This investigation briefly summarizes the principles and possibilities of advanced 3D combined modeling of gravity and magnetic fields and presents several essential ***PGM***s for the regions under study.

Introduction

The Alpine-Himalayan tectonic belt (AHTB) includes an array of mountain ranges which extends along the southern margin of Eurasia, stretching from islands of Java and Sumatra through the Himalayan Mts., Mediterranean Sea, and out into the Atlantic Ocean, on the total distance of about 16,000 km (Khain, 2000). The AHTB is a typical collision-type orogenic belt formed during tens of million years after the closure of the Mesozoic – Early Cenozoic Tethys Ocean. It is characterized by an intensive mountain building and rifting which were accompanied by extensive plateau basaltic and andesite-latite magmatism (Sharkov et al., 2015).

The South Caucasus and Easternmost Mediterranean are the central segments of this tectonic belt, but their geological structure is strongly differing (see corresponding sections below). Seismic analysis is accepted now as a leading (and expensive) geophysical method for deep structure investigation. However, not in all situations (especially for the areas with the predominant distribution of subvertical targets) seismic analysis may provide effective and reliable results. At the same time comprehensive analysis of comparatively inexpensive gravity-magnetic data can not only to significantly extend the seismic data interpretation, but also to obtain data which are not unattainable by the seismic data examination. A 3D combined gravity-magnetic modeling is the most powerful and simultaneously is the most complex interpretation tool of potential geophysical field analysis. Its effective application suggests besides the obvious physical-mathematical basis the good knowledge of geological methods of analysis on the whole and familiarity with a concrete geology of the region under study.

Preferences of integrated interpretation

Gravity-magnetic data processing is generally intended to reduce and eliminate noise factors of different origins and intensities. The main problem faced by qualitative interpretation is to single out a desired target, whereas quantitative interpretation needs to determine and refine the target parameters. Thus, geological problems need to be resolved in terms of: (1) the capabilities of the geophysical method selected for measurements of the field containing the information required, (2) the physical

properties of the medium under study and their capability to generate detectable signals (anomalies), (3) the methods for data processing and interpretation; namely, their ability to extract information from geophysical fields and reveal the effects from the geological targets. Figure 1 presents a general flow-chart for analysis and synthesis of geophysical data for complex regions. Each step in this flow-chart is divided into sub-steps with more concrete formulation (Khesin et al., 1996).

Estimation of efficiency of geophysical integration from the probabilistic and information points of view is considered in detail in Eppelbaum (2014b). Interestingly that from analysis of a classical "Four Color Problem" follows that two geophysical method applications theoretically is sufficient for successive mapping of the area of any geological complexity (Eppelbaum, 2014a). Undoubtedly this fact supports the theoretical basement of 3D combined gravity-magnetic field modeling.

Short description of the employed algorithm

The *GSFC* (Geological Space Field Calculation) program was developed for solving a direct 3-D gravity and magnetic prospecting problem under complex geological conditions (Khesin et al., 1996; Eppelbaum and Khesin, 2004). This program has been designed for computing the field of Δg (Bouguer, free-air or observed value anomalies), components of magnetic field ΔZ, ΔX, ΔY, total magnetic field ΔT, as well as second derivatives of the gravitational potential under conditions of rugged relief and inclined magnetization. The geological space can be approximated by (1) three-dimensional, (2) semi-infinite bodies, and (3) those infinite along the strike closed, left hand (LH) non-closed, right hand (RH) non-closed, and open bodies (Figure 2). Geological bodies are approximated by horizontal polygonal prisms with arbitrary number of characteristic points (a simplified example is given in Figure 3).

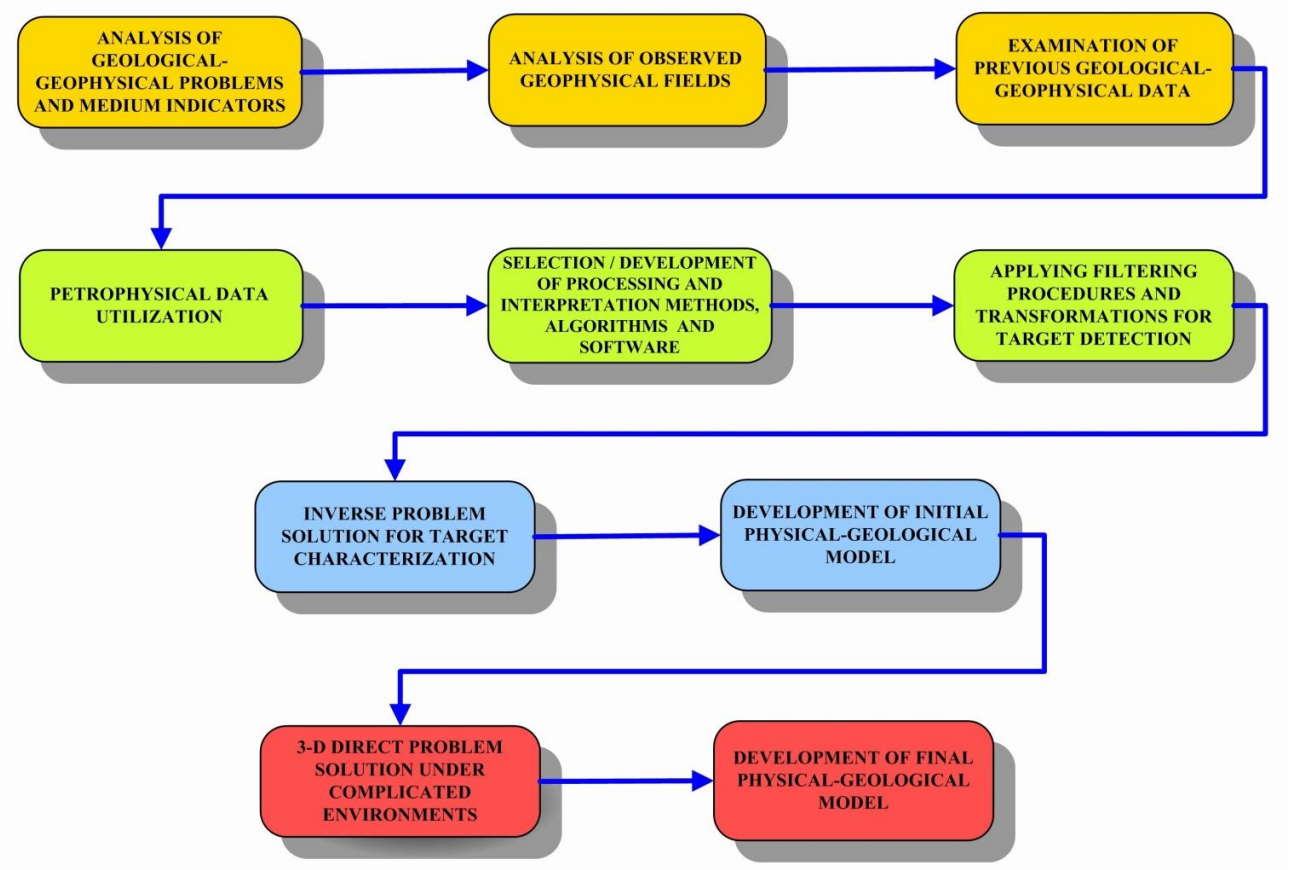


Figure 1. Interpretation of geophysical fields under complex environments: A general scheme

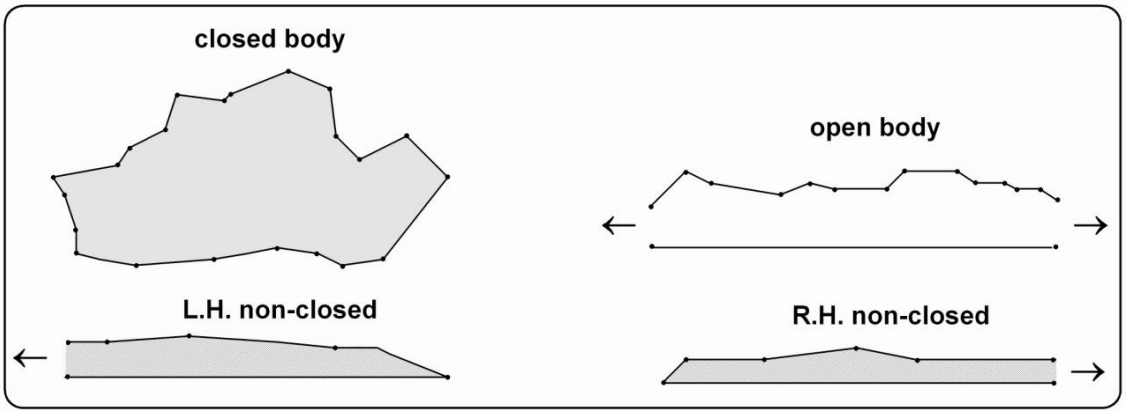


Figure 2. Types of geological bodies used in modeling

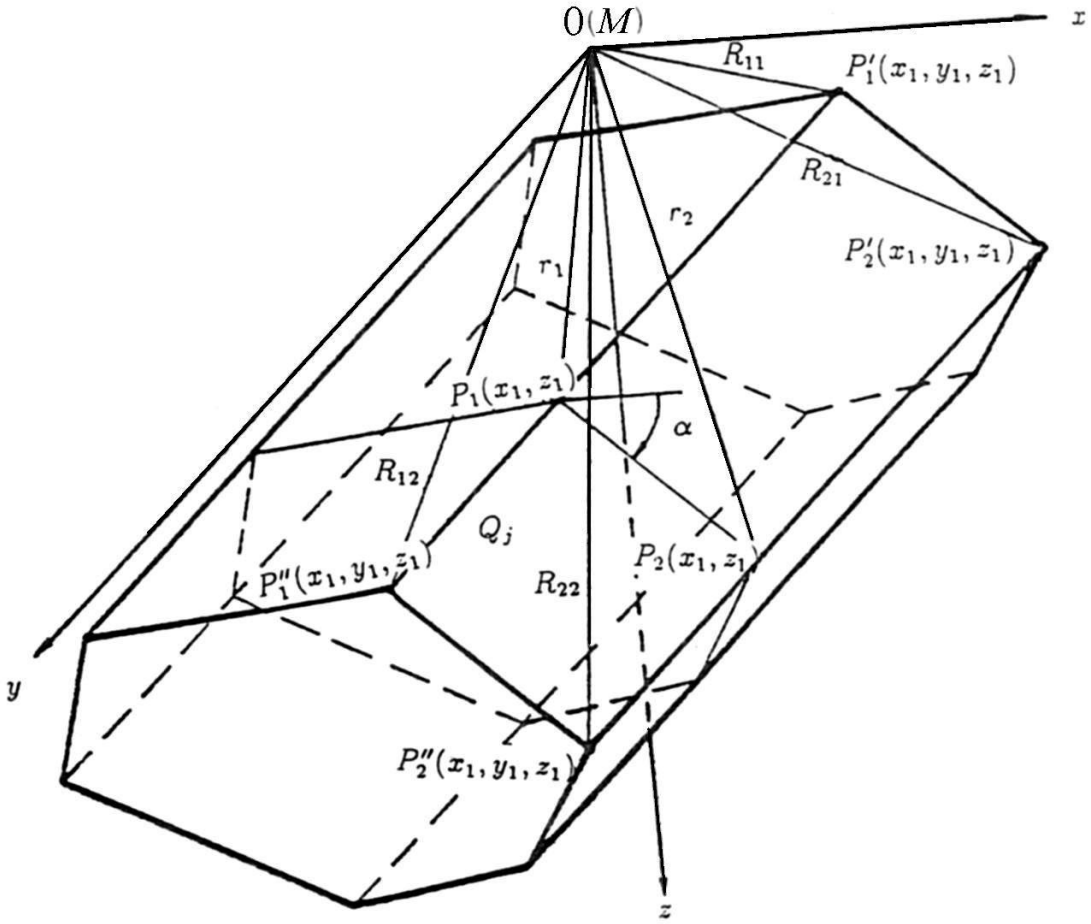


Figure 3. Computing derivatives of gravity potential for a horizontal polygonal prism

The program has the following main advantages (besides above-mentioned ones): (1) Simultaneous computing of gravity and magnetic fields; (2) Description of the terrain relief by irregularly placed characteristic points; (3) Computation of the effect of the earth-air boundary directly in the process of interpretation; (4) Modeling of the interpreting profiles draping over rugged relief or at various arbitrary levels (using characteristic point description); (5) Simultaneous modeling of several profiles; (6) Description of a large number of geological bodies and fragments (up to 1,000). The basic

algorithm realized in the GSFC program is the solution of the direct 3-D problem of gravity and magnetic prospecting for the horizontal limited in the strike polygonal prism (Figure 3). In the developed algorithm integration over a volume is realized on the surface limiting the anomalous body.

Analytical expression for the first vertical derivative of gravity potential of (*m*-1) angle horizontal prism (Figure 3) has been obtained by integrating a common analytical expression:

$$W_{z'} = -\int_s \frac{z}{(R+y)R} dxdz \Big|_{y_1}^{y_2}, \qquad (1)$$

where $R = \sqrt{x^2 + y^2 + z^2}$, *S* is the area of normal section of the prism by the plane of *xOz*.

$$W_{z\tau} = \left\{ \begin{array}{l} -f\sigma \sum_{j=1}^{m-1} \left[V_j \sin\alpha_j \left(\ln \frac{R_{12j} + y_2}{R_{22j} + y_2} - \ln \frac{R_{11j} + y_1}{R_{21j} + y_1} \right) \right. \\ + V_j \cos\alpha_j \left(\mathrm{sgn}(y_2 V_j) \arccos \frac{V_j^2 R_{12j} R_{22j} + U_{1j} U_{2j} y_2^2}{r_{1j} r_{2j} (y_2^2 + V_j^2)} \right) \\ - \left(\mathrm{sgn}(y_1 V_j) \arccos \frac{V_j^2 R_{11j} R_{21j} + U_{1j} U_{2j} y_1^2}{r_{1j} r_{2j} (y_2^2 + V_j^2)} \right) \\ \left. + \cos\alpha_j \left(y_2 \ln \frac{R_{12j} + U_{1j}}{R_{22j} + U_{2j}} - y_1 \ln \frac{R_{11j} + U_{1j}}{R_{21j} + U_{2j}} \right) \right] \end{array} \right\}, \qquad (2)$$

here *f* is the gravitational constant, σ is the density of the body and α_j is the angle of the prism's side inclination.

$$\left. \begin{array}{l} \cos\alpha_j = \frac{x_{2j} - x_{1j}}{r_{12j}} \\ \sin\alpha_j = \frac{z_{2j} - z_{1j}}{r_{12j}} \end{array} \right\}, \qquad (3)$$

x_{1j}, z_{1j} and x_{2j}, z_{2j} are coordinates of points P_{1j} and P_{2j} (angle points of *j*-side of (*m*-1) polyhedron); r_{12j} is the length of *j*-side of this polyhedron:

$$r_{12j} = \sqrt{(x_{2j} - x_{1j})^2 + (z_{2j} - z_{1j})^2}, \qquad (4)$$

r_{1j} and r_{2j} are distances from the selected point *M* to the points P_{1j} and P_{2j}, respectively:

$$\left. \begin{array}{l} r_{1j} = \sqrt{x_{1j}^2 + z_{1j}^2} \\ r_{2j} = \sqrt{x_{2j}^2 + z_{2j}^2} \end{array} \right\}, \qquad (5)$$

R_{11j}, R_{21j}, R_{12j}, R_{22j} are distances from the selected point *M* to angle points $R_{1j'}$, $R_{2j'}$, $R_{1j''}$ and $R_{2j''}$, respectively, for *j*-side of the prism:

$$\left. \begin{array}{l} R_{11j} = \sqrt{r_{1j}^2 + y_1^2} \\ R_{21j} = \sqrt{r_{2j}^2 + y_1^2} \\ R_{12j} = \sqrt{r_{1j}^2 + y_2^2} \\ R_{22j} = \sqrt{r_{2j}^2 + y_2^2} \end{array} \right\}. \qquad (6)$$

U_{1j}, U_{2j} and V_j are the visible solid angles of corresponding parts of the prism's *j*-th side (see Figure 3).

The values of the gravitational and magnetic fields at the selected point *M* are determined using the following formulas:

$$\Delta g = CMf\sigma U_{z'}, \qquad (7)$$

$$\Delta Z = I_z U_{z'z'} + I_x U_{x'z'} + I_y U_{y'z'}, \qquad (8)$$

$$\Delta X = I_x U_{x'z'} - I_x \left(U_{z'z'} + U_{y'y'} \right) + I_y U_{x'y'}, \qquad (9)$$

$$\Delta Y = I_z U_{y'z'} + I_{x'y'} + I_y U_{y'y'}, \qquad (10)$$

$$\Delta T = W_{zz} U_{z'z'} + W_{zx} U_{z'x'} + W_{yy} U_{y'y'} + W_{yz} U_{y'z'} + W_{xy} U_{x'y'}, \qquad (11)$$

where *CM* is the scale of the chart; *f* = 0.00667 (gravitational constant is given in 10^{-8} SI unit, i.e. measured in 10^{-8} m^3 $kg^{-1}s^{-2}$); σ is the body's excess density determined using the formula:

$$\sigma = \sigma_d - \sigma_s. \qquad (12)$$

Here σ_d and σ_s are the densities of the anomalous body and the surrounding medium, respectively. Density is given in 10^3 SI unit (10^3 kg/m^3), i.e. in g/cm^3. At such dimensions of the density and gravitational constant, the computed gravity field will be obtained in 10^{-5} SI unit (10^{-5}m/s^2 = milliGal (mGal)). I_z, I_x and I_y are the components of the excess magnetization vector determined using the following formulas (revised after Khesin et al., 1996):

$$I_z = 0.1\left[I_d \sin J_d - I_s \sin J_s \right], \qquad (13)$$

$$I_x = 0.1\left[I_d \cos J_d \cos(A_d - A_x) - I_s \cos J_s \cos(A_s - A_x) \right], \qquad (14)$$

$$I_y = 0.1\left[I_d \cos J_d \sin(A_d - A_x) - I_s \cos J_s \sin(A_s - A_x) \right], \qquad (15)$$

where I_d and I_s are magnetization values for the anomalous body and the surrounding medium, respectively; the coefficient 0.1 is introduced to obtain the magnetic field plots in nanoTesla (nT); J_d and J_s are the inclinations of the magnetization vector of the body and the medium to the horizon, respectively; A_d and A_s are azimuths of the magnetization vector horizontal projections for the anomalous body and the medium, respectively; A_x is the azimuth of the interpreting profile. Detailed description of analytical expressions for the first and second derivatives of gravity potential of the approximation model of the horizontal polygonal prism and their connection with magnetic field is presented in Khesin et al. (1996) and Eppelbaum et al. (2000).

Let us discuss shortly the constantly arisen problem of development of an automatic system of 3D combined gravity-magnetic field modeling. Suppose we conduct 3-D integrated gravity and magnetic modeling over a geological section consisting of ten geological bodies. Each geological body has three petrophysical variables (density, value and inclination of the magnetization vector), and geometric variables: geometric parameters in the plane of geological section (x_i, z_i), left-hand (y_{i1}) and right-hand (y_{i2}) end faces of each body. Number of points (variables) necessary for describing bodies in the plane of section *a priori* is unknown. For simplicity and taking into account that many of these points are calculated two times by contouring objects, we can assume that the number of these points is ten. To calculate the possible number of combinations of all variables by the integrated 3-D modeling, we should carry out approximated ranging of variables (Table 1). Undoubtedly, this ranging is relative and is executed only for an estimation of necessary order number of combinations.

Applying known combinatorial analysis (e.g., Riordan, 2014), for one body we have the number of combinations $C_{30}^1 \cdot C_{60}^1 \cdot C_{24}^1 \cdot C_{30}^1 \cdot C_{30}^1 \cdot C_{100}^1 \approx 4 \cdot 10^9$. Correspondingly, for ten bodies we have $\approx 4 \cdot 10^{90}$ combinations. Obviously, such a number of combinations considerably complicates an automatic 3-D integrated gravity-magnetic modeling even using supercomputers.

Description of interpretation methodology

The most complete description of the interpretative process structure was given by Strakhov (1976). An interpretation process may be roughly subdivided into the following stages: (1) summarizing prior information; (2) sequential analysis, and (3) geological synthesis.

The development of 3-D ***PGM*** is usually performed using these three stages.

The first stage (summarizing prior information) is as follows:

(A) First of all the main geological-geophysical conception of tectonic development of the region under study must be analyzed and adopted (without it the process of *PGM* construction will be not successive and logical). Construction of geological section includes compilation of all intrusive, effusive and other associations, as well as faults and the surface of folded foundation on the basis of geological data within a strip of 15-20 km (in some cases – 20-40 km) wide. The interpreting section is located in the middle of this strip. Undoubtedly, geophysicist-interpreter must have a good knowledge of the region under study.

Such a section characterizes the upper portion of the Earth's crust with a thickness from 2-3 to 5-8 km from the Earth's surface to the Baikalian (this complex is termed as Cadomian in western publications (Khain, 2007)) basement. Deeper parts of the intrusive bodies and certain faults are formed by extrapolation of the available constructions, general geological considerations and the results of previous geophysical analyses.

Table 1

Calculation of the number of possible combinations of variables

Variable	Interval of changing	Ranging	Number of combinations
Density, g/cm^3	2.30-2.60	0.01	30
Magnetization, mA/m	0-3000	50	60
Inclination of magnetization, degree	0-360	15	24
Left-hand end face, y_1/x_m*	0-20	non-linear	30
Right-hand end face, y_2/x_m	0-20	non-linear	30
Geometrical coordinates of geological body in the plane of geological section	min 10 points	–	min 10·10

*x_m is the maximum length of interpreting profile.

(**B**) A preliminary petrophysical model of the section is developed. Here all the geological bodies acquire density and magnetization values according to the preceding petrophysical data analysis and results of geophysical field interpretation. When no data are available on the magnetization direction, it is assumed to be parallel to the normal geomagnetic field in the region under study. Further, the magnetization direction is refined in the process of physical-geological modeling. Density properties are received from the borehole sample examination and converted from the seismic data by the known method (e.g., Barton, 1986). The petrophysical model includes deep-seated layers (slabs) of the Earth's crust: (1) the "basaltic", (2) the intermediate between the crust and the upper mantle, and (3) the upper mantle. Their surfaces are constructed and physical properties are associated with them according to the data from previous seismic, magnetotelluric, thermal and other geophysical studies. Paleomagnetic data examination may be of a high significance (it is shown below on example of the Easternmost Mediterranean).

(**C**) The initial (preliminary) petrophysical model includes hidden bodies as well. Their location, thickness, depth, density and magnetization are obtained from the quantitative analysis of magnetic and gravity fields as well as from seismic data examination.

The second stage (sequential analysis) includes application of combined gravity and magnetic field modeling along the interpreting profiles using 3D *GSFC* program (sometimes other software – EMIGMA – was applied). Each time the gravity-magnetic effects from different bodies, groups of bodies and the total computed model are displayed and compared to the observed gravity and magnetic fields. Using the results of this comparison, the changes that match the gravity and magnetic effects into the model of the medium are introduced. The computations and comparisons of fields and model modifications are repeated until the desired fit between the computed and observed fields is obtained.

Then, a regional gravity (and sometimes magnetic) field is roughly selected. As a rule, the densities of deep-seated complexes are not changed; the modifications only affect the shape of their roof. Next, geophysical fields of local bodies are selected. If necessary, this is followed by a verification of the regional fields and the fields of the local bodies.

At each computational step, a separate analysis of gravity and magnetic fields is carried out. Geometrical coordinates of geological bodies are verified in the subsequent steps, and then introduced into the model. This procedure leads to an integrated qualitative and quantitative interpretation for anomalous gravity and magnetic fields. The modeling completes when the computed gravity and magnetic fields coincide accurately with the observed fields. All this modeling process must be carried out in a full compliance with the known geological principles.

The third stage (geological synthesis) involves a detailed geological interpretation of these models. A 3-D ***PGM*** of the area under investigation is developed based on the geological data obtained at the previous stages and qualitative and quantitative geophysical data examination. This yields the final physical-geological sections, and the models are characterized by a more complete rendering of the geological targets, including crustal blocks, intrusions, faults, and economic deposits.

The geological interpretation of the geological associations, complexes and local bodies of the constructed (final) petrophysical model does usually not consist of a hard problem since in the implementation of the interactive selection system almost all the bodies in the ***PGM*** acquire some specific geological content. The geological nature of new sources introduced into the model during the iterative modeling and reflected either in the initial geological section, or in the initial ***PGM***, is determined according to the similarity of their physical properties, dimensions, and depth of occurrence with respect to the known targets. The age of the bodies is determined according to their interrelations with the surrounding (host) rocks.

Application of 3D combined modeling of gravity-magnetic fields in the South Caucasus and Eastern Mediterranean

South Caucasian segment of the Alpine-Himalayan tectonic belt

Brief geological-geophysical background

The complexity of Azerbaijan's territory geological structure stems from its location in the AHTB (e.g., Khain and Alizadeh, 2005; Leonov, 2008). The NE part of Azerbaijan is a fragment of the Pre-Caucasian foreland filled by Cenozoic terrigenous sediments. A heterogenic Nakhichevan folding system is located in the SW part, where carbonate Paleozoic strata and Cenozoic magmatic formations are mixed (Figure 4). At the mega-anticlinorium of the Greater Caucasus, stratified Ceno-

zoic and Mesozoic thick (predominantly, sedimentary) strata are presented. The prevalence of Mesozoic magmatic formations is typical of the mega-anticlinorium of the Lesser Caucasus. The Kura mega-synclinorium, dividing the Greater and Lesser Caucasus, is characterized by an accumulation of thick (up to several kilometers) Cenozoic terrigenous sediments. The Talysh anticlinorium is located on the SE flank of the Kura depression, where Paleogene magmatic associations are widely distributed (Khain and Alizadeh, 2005).

According to Khain (2000), the most ancient Pre-Baikalian structural complex is characterized by a sub-meridional strike. A less metamorphosed Baikalian complex is rumpled to latitudinal folds in separate areas. The Caledonian complex is practically unknown. The Hercynian complex is characterized by a Caucasian strike identical to the overlying Mesozoic rocks.

The Alpine tectono-magmatic cycle is characterized by more complete geological data. As a whole, for Azerbaijan territory is typical the frequently changing geological associations on the vertical and lateral axes, the presence of multifarious fold and fault structures of different orders, and regional and local metamorphism (Alizadeh, 2012). All these factors make the development of reliable models of these media sufficiently complex.

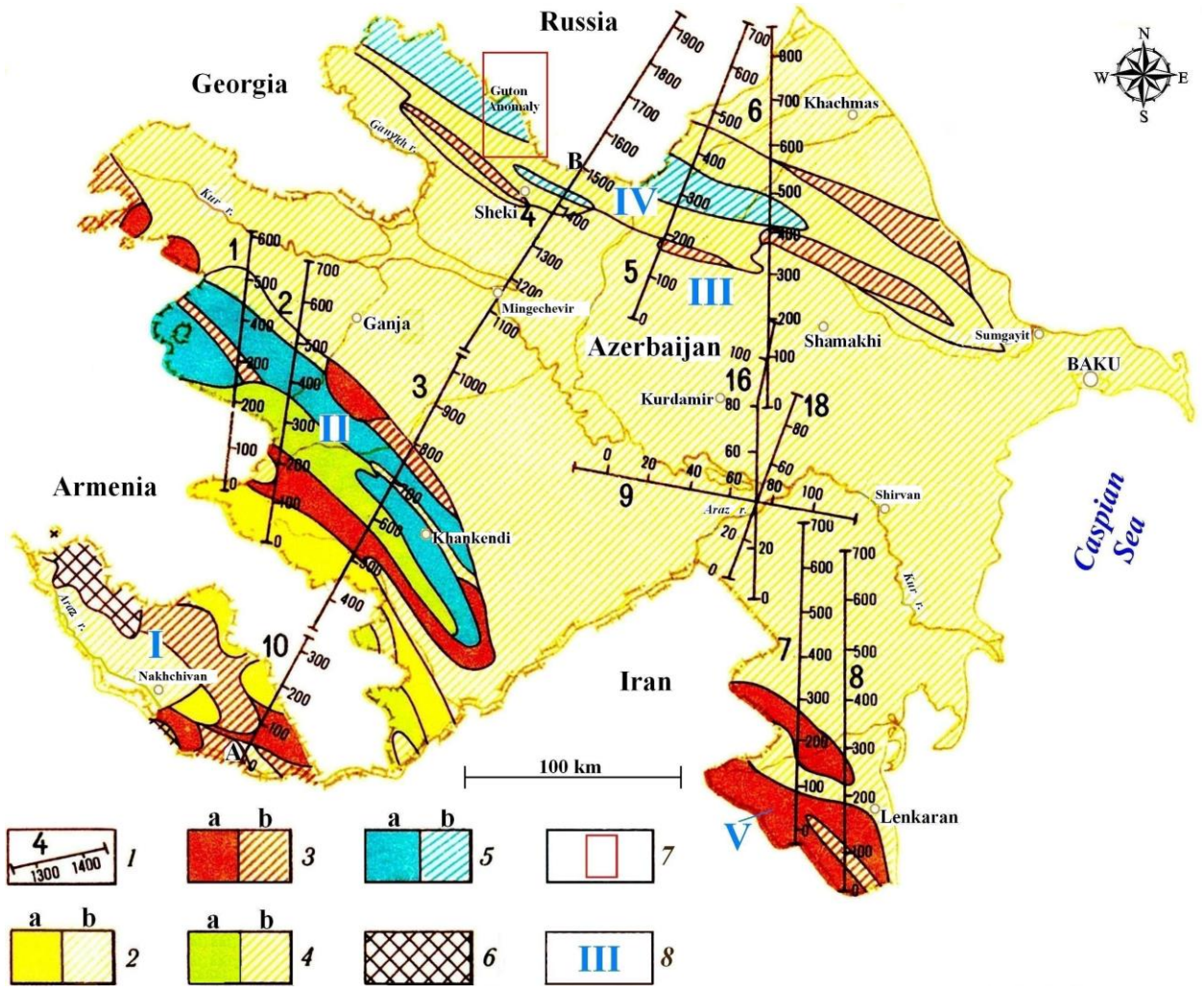


Figure 4. Areal map of some profiles used for physical-geological modeling in Azerbaijan and adjacent regions
(1) profiles and pickets, (2) Pg_3-Q: (a) orogenic magmatic associations, (b) background sedimentary deposits, (3) K_2-Pg_2: (a) pre-orogenic magmatic associations, (b) background sedimentary deposits, (4) J_3-K_1: (a) magmatic associations of the Late Alpine sub-stage, (b) background sedimentary deposits, (5) J_1-J_2: (a) magmatic associations of the Early Alpine sub-stage, (b) background sedimentary deposits; (6) Pz deposits, (7) contour of the Guton magnetic anomaly, (8) tectonic regions: I – Nakhchivan folding region, II – SE part of the Lesser Caucasus mega-anticlinorium, III – central and SE parts of the Kura mega-synclinorium, IV – SE part of the Greater Caucasus mega-anticlinorium, V – Talysh anticlinorium

The first models of the Earth's crust of Azerbaijan were put forward in the mid-1960s (Gadjiev, 1965; Tzimelzon, 1965; Shekinsky et al., 1967). These models were subsequently evaluated in the works of Tzimelzon (1970), Azizbekov et al. (1972), Shikhalibeyli (1972), Alexeyev et al. (1988), and later by Khesin et al. (1993, 1996). Rappel and McNutt (1990) studied the regional compensation of the Greater Caucasus using the Bouguer gravity. Sarker and Abers (1998) attempted to apply *P* and *S* wave tomography for examination of the Greater Caucasus deep structure. After that new models developed on the basis of gravity field analysis were presented in Kadirov (2000).

Some significant regional peculiarities of the deep structure of the South Caucasus were reflected in: Alexidze et al. (1993), Pilchin and Eppelbaum (1997), Artyushkov et al. (2000), Gasanov (2001), Kaban (2002), Brunet et al. (2003), Guliyev and Panachi (2004), Alizadeh (2005), Khain and Alizadeh (2005), Allen et al. (2006), Kadirov (2006), Khalafly (2006), Reilinger et al. (2006), Saintot et al. (2006), Spichak (2006), Gamkrelidze and Shengelia (2007), Khain (2007), Leonov (2008), Ricketts et al. (2008), Mamedov (2009), Mosar et al. (2010), Eppelbaum and Khesin (2012), Koulakov et al. (2012), Etirmishli and Kazimova (2013), Forte et al. (2013), Mederer et al. (2013), Ruban (2013), Mumladze et al. (2015). and others. In their recent publication Kadirov and Gadirov (2014) demonstrated an effective gravity field modeling along profiles crossing the South Caspian Basin.

Thus, it was recognized that 3D gravity-magnetic modeling is a powerful tool for studying the variable deep structure of the South Caucasus. This study must be preceded by a combined qualitative and advanced quantitative gravity/magnetic data analysis supported by integrated examination of available geological, seismic, magnetotelluric and thermal data, and utilization of numerous magnetic, paleomagnetic and density properties of geological samples from the region under study. Final product of such an investigation is development of series of 2.5 and 3D ***PGM***s. These ***PGM***s can be used not only for substantiation of various types of prospective economic deposits, but also to delineation of the tectonic-structural factors affecting the long-term seismological prognosis (Eppelbaum and Khesin, 2012).

Results of 3D combined gravity-magnetic modeling

Advanced interpretation methods (improved modifications of tangents, characteristic point methods and areal method) were applied to study gravity and magnetic anomalies along all profiles surrounding SuperDeep borehole SD-1 in Saatly area of Azerbaijan. A fragment of this interpretation along Profile 18 is shown in Figure 5. First of all, note that the behavior of the magnetic ΔZ curve and graph $\partial \Delta g_B / \partial x$ are very simular, which testifies to the fact that these anomalies are due to the same geological objects. A quantitative analysis of the magnetic curve allowed to delineate two magnetic targets. The main target apparently is a source of the Talysh-Vandam gravity anomaly (its upper edge coincides with the data obtained by SD-1 drilling) (Khain and Alizadeh, 2005). The obtained data were utilized by construction of a ***PGM*** of first approximation for 3D combined physical-geological modeling (Eppelbaum and Khesin, 2012).

A visual example of 3D combined modeling of gravity and magnetic fields along Profile 1 (see scheme of profiles presented in Figure 4) is shown in Figure 6. Profile 1 crossing the Lesser Caucasus illustrates the very complex geological structure of this region. The Late-Alpine effusives in the ***PGM***s compose an ophiolite zone (relic of the ocean crust). It is thought that the same rocks occur in the NE immersion of the Lesser Caucasus. Pre-orogenic and orogenic intrusive and effusive rocks are fixed in the southern parts of the ***PGM***. Thick sedimentary deposits are developed in northern part of this profile. A smooth high of the Moho discontinuity is observed from south to north from a depth of 52 km up to 42 km (Eppelbaum and Khesin, 2012). Such a Moho boundary behavior on the whole agrees with the latest data of deep seismic profile re-interpretation (Pavlenkova, 2012). Depths of the magnetized bodies lower edges were estimated on the basis of various geophysical field analyses (Pilchin and Eppelbaum, 1997). Here were revealed such classes of disturbing objects as acid intrusions of lower density and magnetization, basic magmatic rocks of increased density and magnetization, and fault zones. It was determined that the clearest density boundaries were associated with the base of the Cenozoic sedimentary strata and, to a lesser degree, with the base of the Alpine complexes. According to the performed modeling geomagnetic boundaries are associated mainly with the roof and bottom of the Mesozoic floor of heightened magnetization.

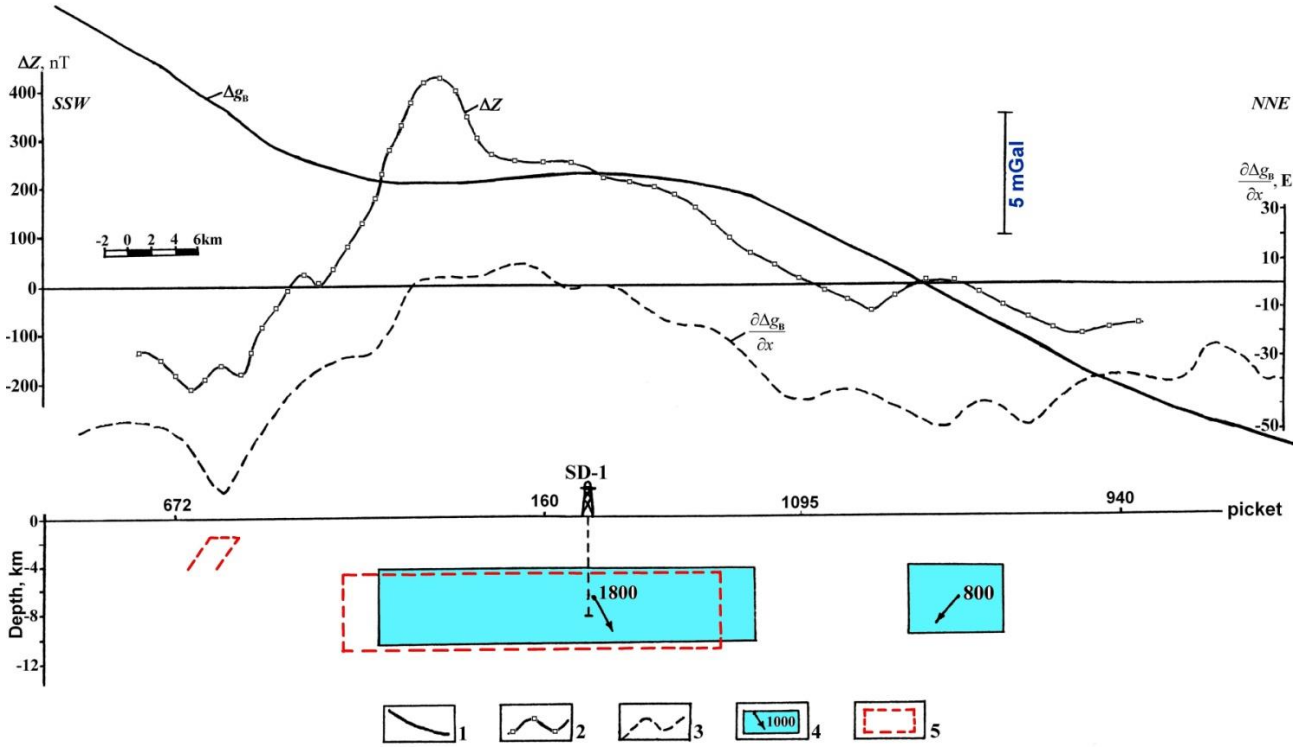


Figure 5. Fragment of gravity and magnetic field analysis along profile 18 (location of this profile is shown in Figure 4) (1) Bouguer gravity field Δg_B, (2) magnetic field ΔZ, (3) first horizontal derivative of gravity field $\partial \Delta g_B / \partial x$, (4) contour of magnetized body and position of magnetization vector, (5) contour of body determined by analysis of $\partial \Delta g_B / \partial x$

Eastern Mediterranean segment of the Alpine-Himalayan tectonic belt

The Easternmost Mediterranean (EMM) is a tectonically complex region evolving in the long term and located in the midst of the progressive Afro-Eurasian collision within the AHTB (Khain, 1984; Ben-Avraham et al., 2002) (Figure 7). Both rift-oceanic systems and terrane belts are known to have been formed in this collision zone (Stampfli et al., 2013). The formation of its modern complex structure is associated with the evolution of the Neotethys Ocean and its margins (e.g., Ben-Avraham and Ginzburg, 1990; Robertson et al., 1991; Ben-Avraham et al., 2002). The EMM was formed during the initial phase of the Neotethys in the Early and Late Permian (Golonka and Ford, 2000; Stampfli et al., 2013).

The EMM region has attracted increasing attention in connection with the recent discoveries of significant hydrocarbon deposits in this region (Eppelbaum and Katz, 2011; Eppelbaum et al., 2012). Currently seismic prospecting is the main tool used in hydrocarbon deposit discovery. However, even sophisticated seismic data analysis (e.g., Roberts and Peace, 2007; Gardosh et al., 2010; Marlow et al., 2011), fails to identify the full complex structural-tectonic mosaic of this region, and more importantly, is unable to clarify its complex tectonic evolution. This highlights the need for combined analysis of geophysical (first of all, magnetic and gravity (Eppelbaum, 2006)) data associated with the paleomagnetic and paleobiogeographic conditions that can yield deep paleotectonic criteria for unmasking the complex geodynamic pattern of this region (Eppelbaum and Katz, 2015a).

Ben-Avraham et al. (2002) have proved an existence of oceanic crust in the Levant Basin (in the middle of EMM) and continental crust under the Eratosthenes Seamount on the basis of integrated seismic-gravity-magnetic (with thermal data utilization) analysis. Extensive geological-geophysical investigations have been carried out in this region, and a significant number of deep boreholes have been drilled (Eppelbaum and Katz, 2011; 2014b). Geophysical-geological evolution of the EMM in terms of the modern geodynamics (first of all, plate tectonics) is reflected in (Ben-Avraham and Ginz-

burg, 1990; Ben-Avraham et al., 2002, 2006; Robertson et al., 1998; Jimenez-Munt et al., 2006; Le Pichon and Kreemer, 2010). Integrated geological-geophysical zonation of the deep structure of this region was triggered in (Eppelbaum and Katz, 2011; Eppelbaum and Katz, 2012, 2014b; Eppelbaum et al., 2012, 2014b).

Results of 3D combined gravity-magnetic modeling

Let's consider a few fragments of the carried combined research. The first Moho map of the EMM was constructed on the basis of gravity and seismic data analysis with application of some tectonic-geodynamic reconstructions (Eppelbaum and Pilchin, 2006; Eppelbaum et al., 2012). The first Curie map of Israel (Eppelbaum et al., 2014a) (developed with utilization of thermal, seismic and gravity data and with 3D magnetic modeling) also correlates with the position of the terranes (e.g., Ben-Avraham et al., 2006). The sources of the two most significant gravity-magnetic anomalies in Israel – Hebron and Carmel – were classified (on the basis of 3D gravity-magnetic fields modeling) as phenomena associated with tectonically weakened zones between the terranes (Eppelbaum et al., 2005, 2006).

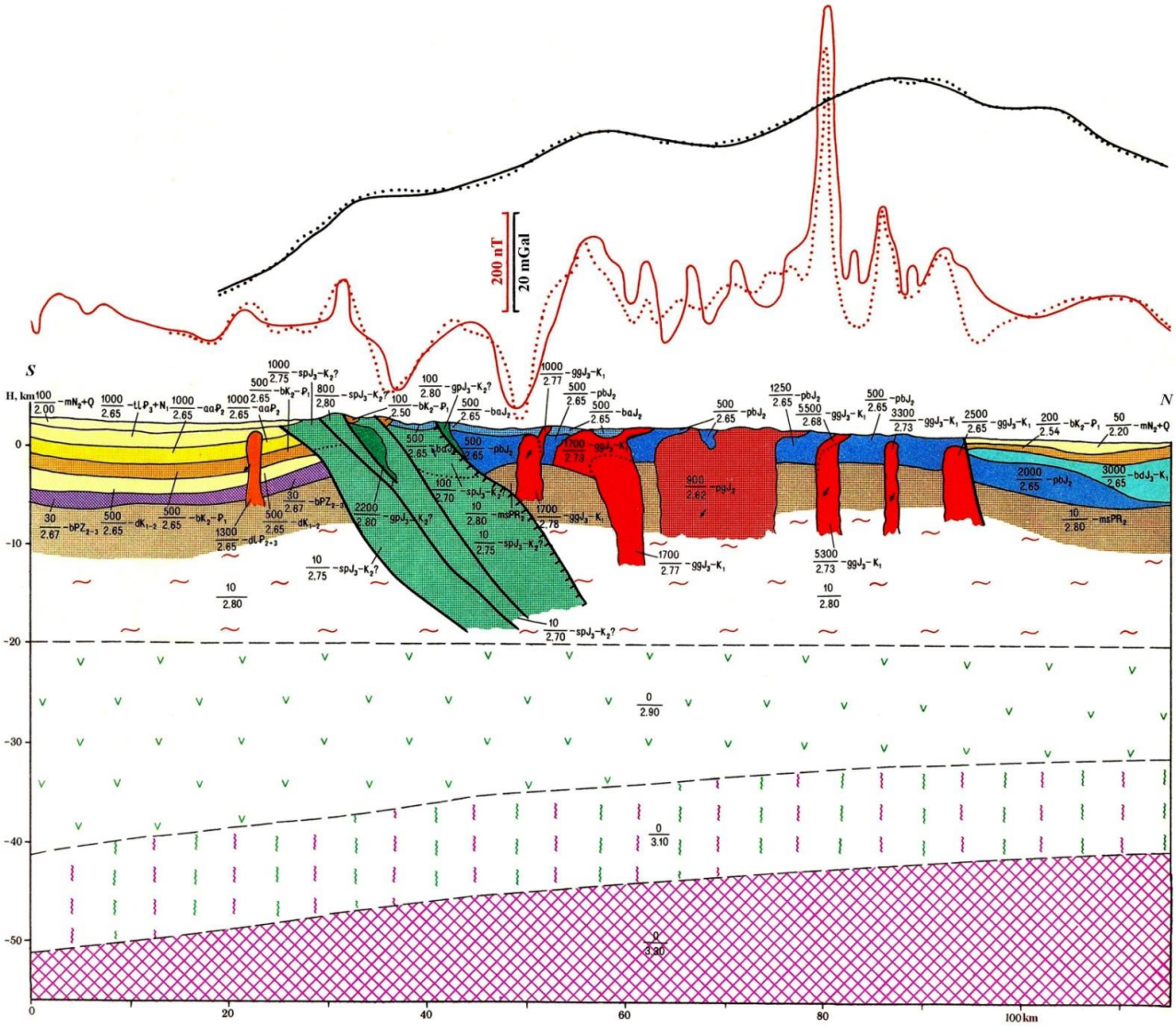
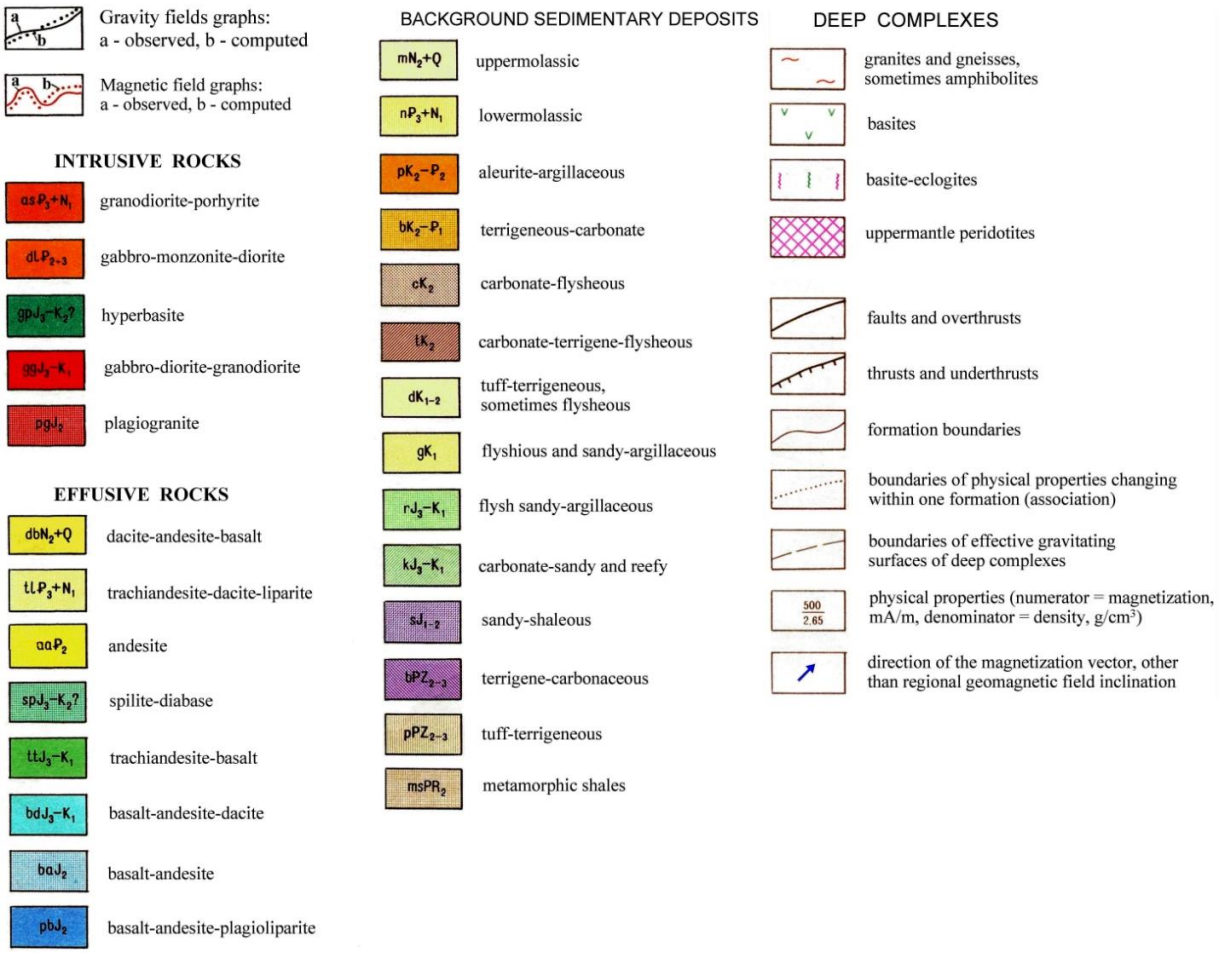


Figure 6. Physical-geological model along Profile 1: Mez-Mazra – Gedabey - Dzegam-Djirdakhan (location of the profile is shown in Figure 4) (after Eppelbaum and Khesin, 2011)

Captions for Figure 6



Studying the EMM deep structure demands a careful attention to the blocks of oceanic (basaltic) crust with reverse magnetization that were discovered (Ben-Avraham et al., 2002; Eppelbaum, 2006). This issue was very briefly explained as paleomagnetic Kiama zone of inverse polarity (Eppelbaum and Katz, 2012) and a rather more detailed description was given in (Eppelbaum et al., 2014b; Eppelbaum and Katz, 2015a, 2015b), which demands separate consideration. 3D magnetic analysis conducted along three interpretation profiles supported by gravity-seismic examination along the same lines (location of profiles is shown in Figure 8A) unambiguously indicates the presence of blocks of the Earth's crust with reverse magnetization (Ben-Avraham et al., 2002). By other words, in the mentioned research for a first time combined seismo-magnetic-gravity models for three crossing profiles (Profiles II – II and III – III are shown in Figures 8B and 9, respectively) were developed. It should be noted that the most difficult process was the 3D magnetic field modeling (hundreds of iterations were applied) taking into account very complex and magnetically variable media and requiring the necessity to create a common 3D geometrical model for three geophysical fields. Integrated interpretation of three independent geophysical fields (assuming that each field is characterized by three anomalous points) increases the reliability of interpretation by the use of error function in three times (Eppelbaum, 2014a). In our case the number of anomalous points is many times larger, consequently the reliability of interpretation is greater.

Results of 3D combined magnetic-gravity modeling along Profile I – I are presented in Figure 9. It is obvious that in this ***PGM*** magnetic field modeling is much more complex problem than gravity field modeling. The main peculiarities of this ***PGM*** are discovered crystal block of oceanic crust with inverse magnetization (about -120°) in the center of profile (Ben-Avraham et al., 2002) (faintly yellow colored) and a crystal block of continental crust with inverse magnetization in the eastern part of this profile (about -45°) (brightly yellow colored). A reconstruction of

the position of a reverse magnetized block of the Earth's crust enabled us to obtain a magnetization zone with a S – N orientation with a width reaching 70 km and length of about 200 km (Eppelbaum et al., 2014b; Eppelbaum and Katz, 2015a). Such a large, thick (about 10 km) zone (the total volume of this zone exceeds 120,000 km^3) of inverse magnetization must correspond to a significant and prolonged effect of inverse polarity in the Earth's magnetic field history. The Early Cretaceous or Early Jurassic, as was supposed in (Ben-Avraham et al., 2002), do not contain sufficiently prolonged periods of the Earth's magnetic field inverse polarity (Figure 10). It was suggested that this is the Kiama zone of inverse polarity (Eppelbaum et al., 2014b; Eppelbaum and Katz, 2014a) with duration of about 50 mln years (see Figure 10) that was first detected in the Late Carboniferous and Permian in Australia (Irving, 1966).

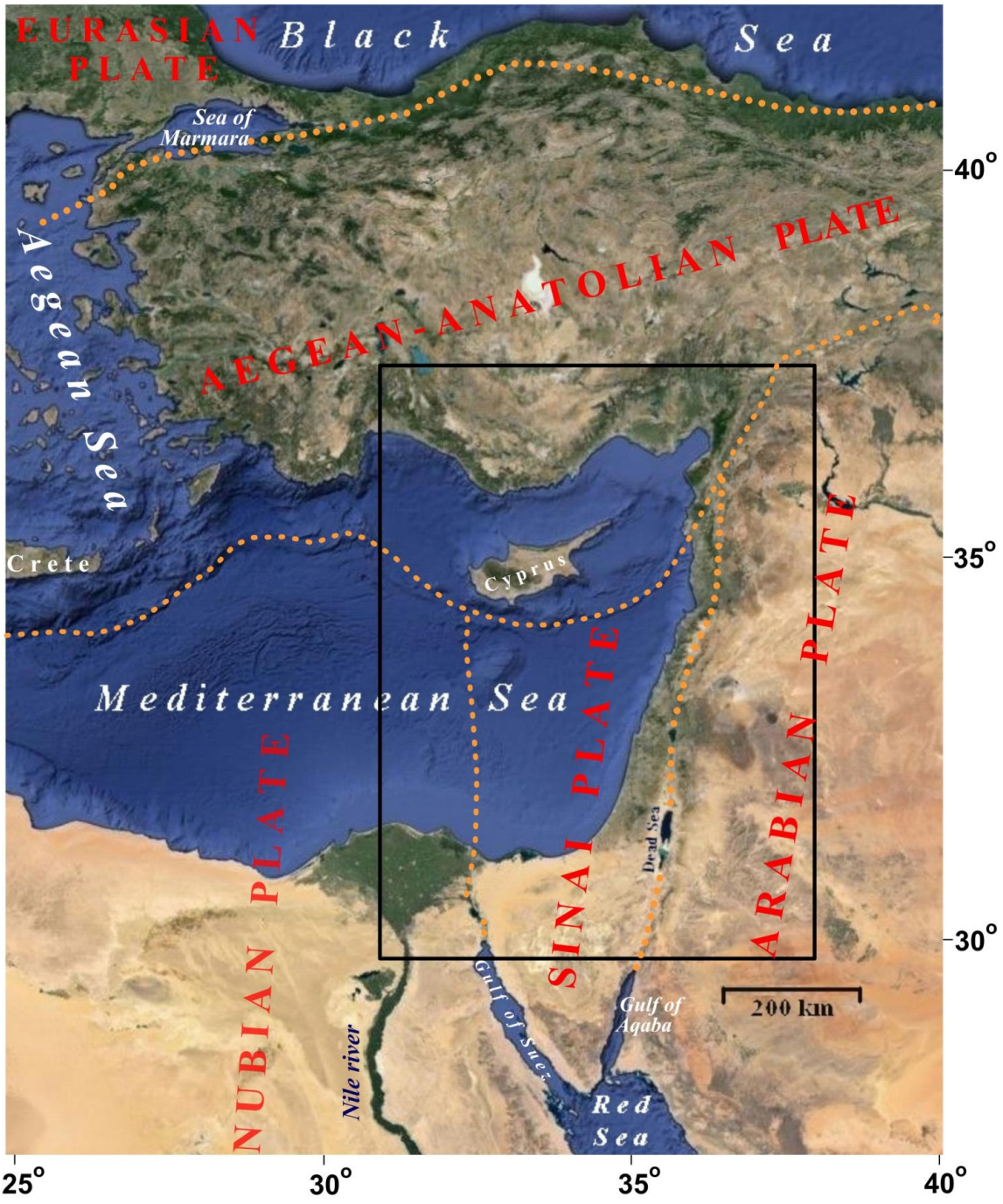


Figure 7. Overview map of the region. The study area is outlined by a black rectangle. Orange dot lines indicate boundaries between tectonic plates

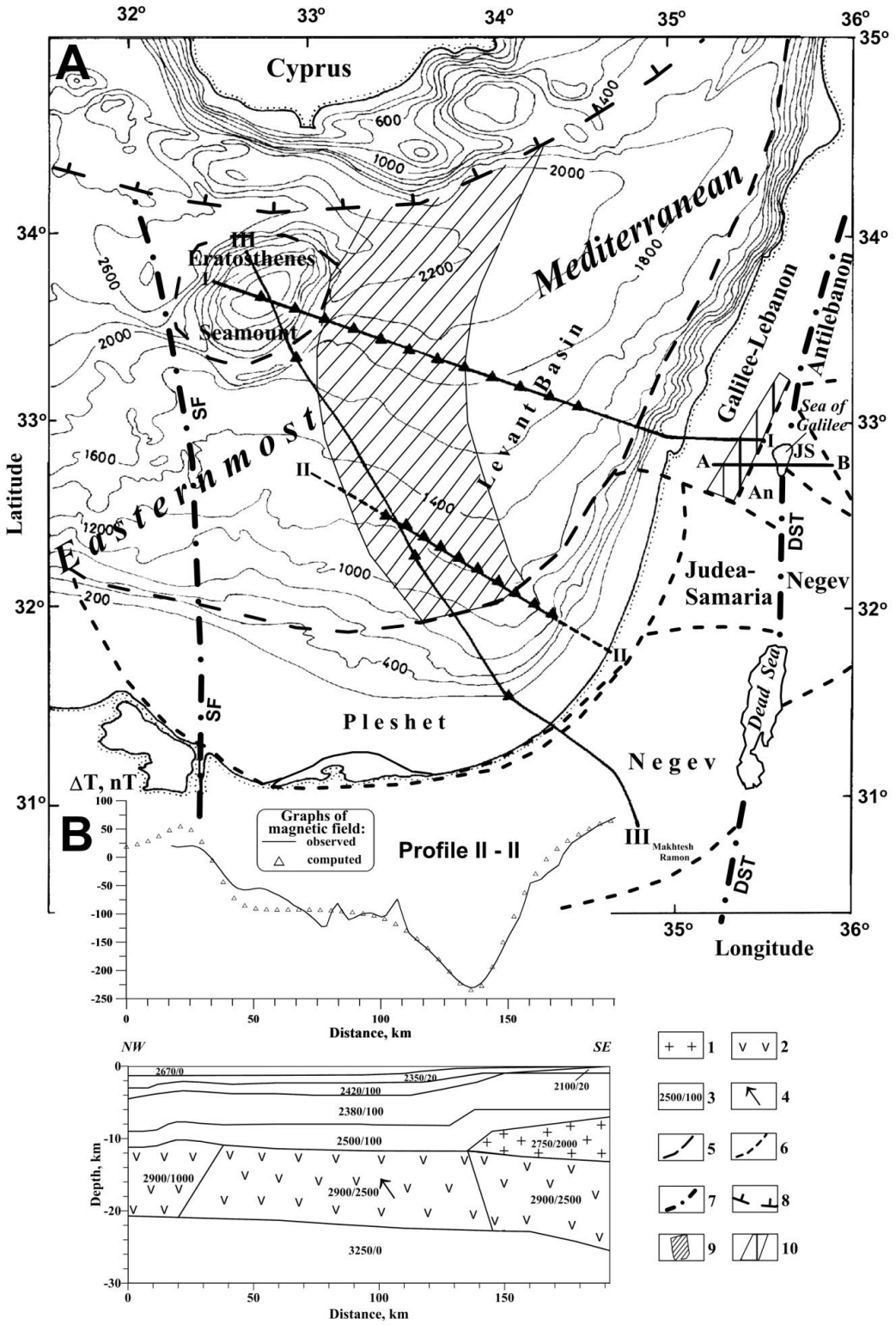


Figure 8. A: Tectono-paleomagnetic map of the region with location of seismic-gravity-magnetic profiles, B: Results of 3D magnetic field modeling along profile II – II

(1) granitic layer, (2) basaltic layer, (3) physical properties (numerator=density, kg/m^3, denominator=magnetization, mA/m), (4) direction of the magnetization vector other than the geomagnetic field inclination of the region, (5) boundary discovered between the continental and oceanic crust within the Sinai plate, (6) faults limiting terrane location, (7) interplate deep faults of the Eastern Mediterranean: SF, Sinai Fault and DST, Dead Sea Transform, (8) deep fault separating the Alpine Belt and oceanic depression of the Easternmost Mediterranean, delineated paleomagnetic zones of inverse polarity: (9) Kiama, (10) Neoproterozoic. JS, Judea-Samaria, An, Antilebanon. (1-5) generalized after Ben-Avraham et al. (2002).

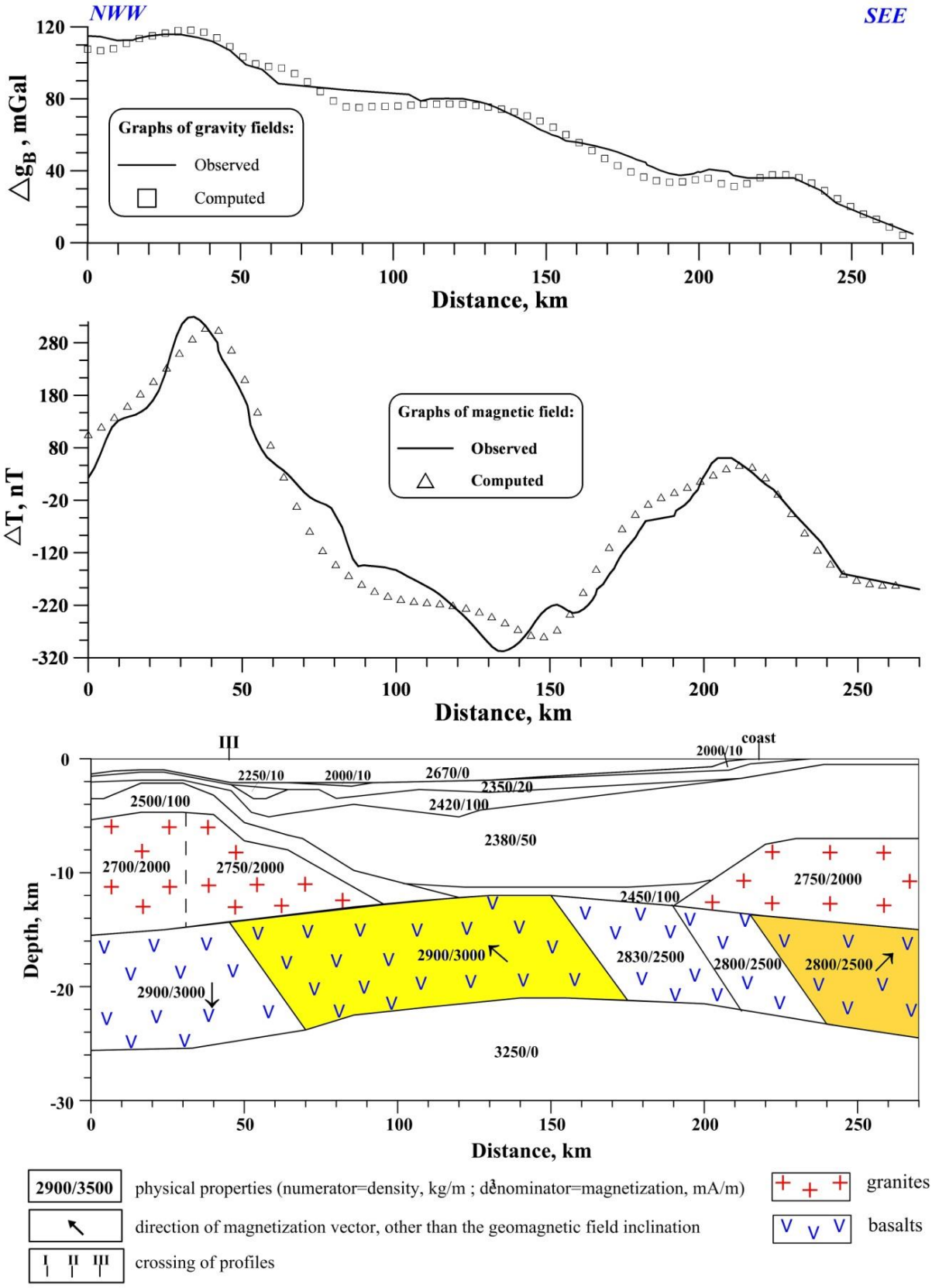


Figure 9. Combined ***PGM*** constructed on the basis of seismic analysis and 3D gravity-magnetic modeling along Profile I – I (location of Profile I – I is shown in Figure 8) (modified after Ben-Avraham et al., 2002)

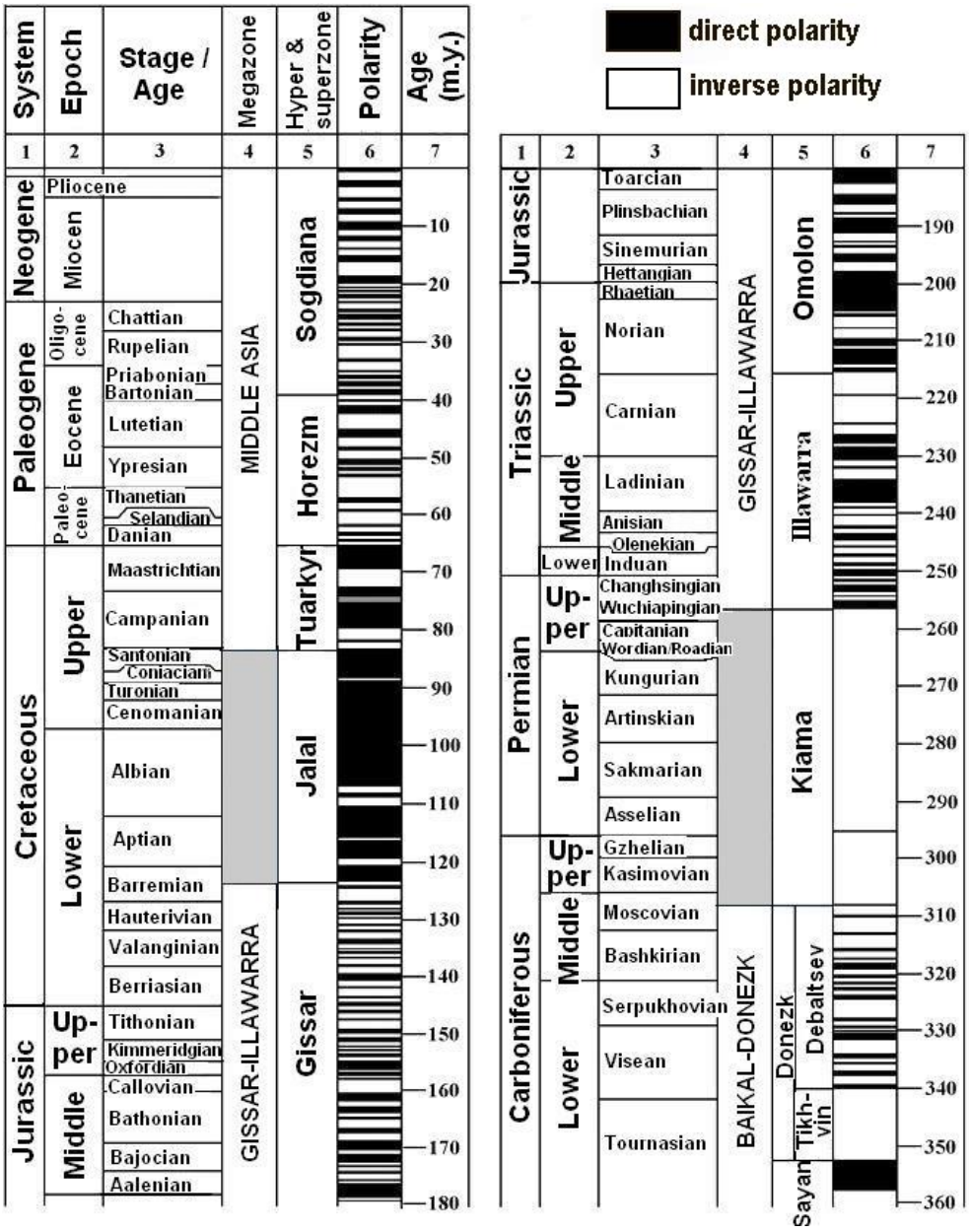


Figure 10. The combined Paleomagnetic Scale – Chronostratigraphic Chart of the most part of the Phanerozoic (compiled on the basis of Molostovsky et al. (1998) and Molostovsky et al. (2007) and Molostovsky (2009) paleomagnetic reconstructions and International Chronostratigraphic Chart (International Commission on Stratigraphy, 2014)

Another example displays the final ***PGM*** along profile crossing the Dead Sea Transform (DST) within the Sea of Galilee (Profile A – B) obtained by use of 3D combined gravity-magnetic field modeling (Figure 11) (location of this profile is presented in Figure 8A). A preliminary ***PGM*** of this profile was constructed on the basis of Rotstein and Bartov (1989), Rotstein et al. (1992), Ben-Avraham et al. (1996), Eppelbaum and Pilchin (2006), Eppelbaum et al. (2007), Meiler et al. (2011), Ben-Avraham et al. (2014).

Negative gravity anomaly along Profile A – B (Figure 11) is caused mainly by the low dense sedimentary deposits and salt accumulated in the DST zone. At the same time comprehensive analysis of magnetic field behavior indicates that it cannot be explained by subsurface basalts effects (and by effects from any basaltic plates occurring at low depth). Such a behavior may provide in these physical-geological conditions only a deep crystal block with an inverse magnetization. A similar crystal block with the same direction of magnetization was

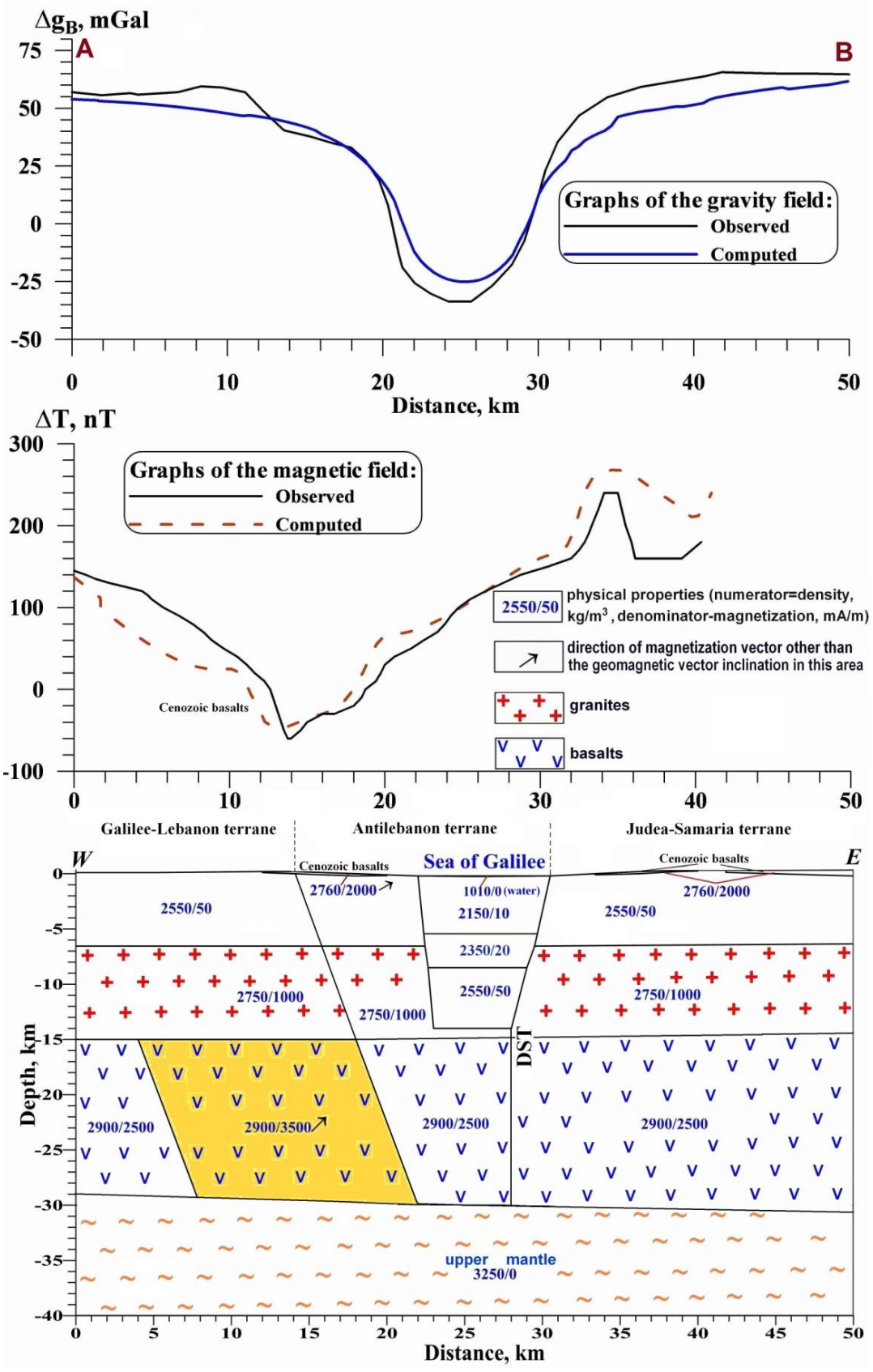


Figure 11. Combined ***PGM*** constructed on the basis of 3D gravity-magnetic modeling and seismic data analysis along profile A – B (location of profile A – B is shown in Figure 8)

discovered in the eastern part of Profile I – I (see Figure 9). Petrographic and radiometric analyses of the Sinai and Arabian shields (see Figure 7) indicate that here occur various complexes of Middle and Upper Precambrian among which dominate Neoproterozoic associations with a radiometric age of 600 – 1000 Ma (e.g., Stern et al., 2004; Johnston and Kattan, 2008). Numerous paleomagnetic examinations of Neoproterozoic display that in these rocks an inverse magnetization is prevailing (Gurevich, 1981; Molostovsky et al., 1998). A generalized paleomagnetic scale of Neoproterozoic (reconstructed by Y. Katz on the basis of numerous paleomagnetic determinations analysis) is presented in Figure 12. Simple visual analysis of this scale indicates that the most intervals of magnetic field inverse polarization relate to 605 – 815 Ma. Thus, we can relate the discovered zone of inverse magnetization (on the basis of Profile I – I (Figure 9) and Profile A – B (Figure 11)) (see the brightly yellow colored blocks) to Neoproterozoic (interval about 210 My, between 605 and 815 Ma). The delineated Neoproterozoic paleomagnetic zone of inverse polarity is contoured in Figure 8A.

Undoubtedly, application of different transformation procedures (upward and downward continuation, calculation of difference anomalies, wavelet, entropy, self-adjusting filtering, etc.) may help to obtain some additional parameters of geological sections which may be useful for 3D gravity-magnetic modeling and ***PGMs*** development. For instance, recently developed new integrated wavelet approaches (e.g., Eppelbaum et al., 2011) enable to join results of geophysical methods based on different physical principles (for instance, magnetics and seismics). However, presentation of such examples is beyond of the goal of this article.

It should be noted that for solving different tectonic and geodynamic problems both in the South Caucasus and EMM can be effectively applied the satellite observed gravity and magnetic data (measured with the same grid and accuracy and having an important property of repetition). A successful example of the tectono-geodynamic examination of satellite derived gravity data for the EMM was demonstrated in Eppelbaum and Katz (2015b). Exploration of satellite observed magnetic data for studying deep structure in the considered above scale is more complex problem. For this aim, apparently, complex Gaussian function and advanced wavelet transform (i.e., Alperovich et al., 2013) may be employed.

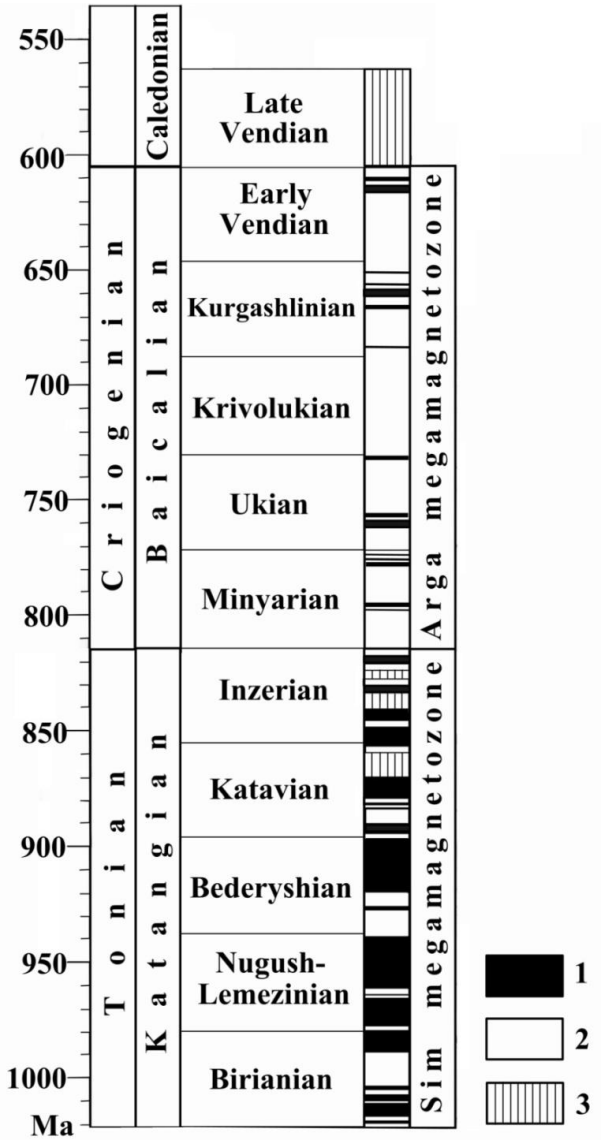


Figure 12. A generalized paleomagnetic scale of Neoproterozoic (complied by Y. Katz, Tel Aviv University).
(1) direct polarity, (2) inverse polarity, (3) alternating polarity

Comparison of results of 3D combined gravity-magnetic field modeling in the South Caucasus and EMM indicate that in both regions characterized by different tectono-structural and other peculiarities the skillful modeling may provide important results that can be used for construction of geodynamic models, searching economic deposits and long-term seismological prognosis.

Conclusions

It can be concluded that 3D combined gravity-magnetic field modeling is a powerful interpretation tool for recognizing deep structure of complex geological regions. Application of this methodology

together with petrophysical and paleomagnetic examination, seismic, magnetotulliric, thermal and other investigations allowed to unmasking deep geological structure of such complex regions as the South Caucasian and Easternmost Mediterranean segments of the Alpine-Himalayan tectonic belt. The process of 3D modeling, taking into account a constant necessity of interrelation between the physical, mathematical, tectonic, structural and some other factors, supposes a high qualification level of the interpreter (interpreters). A further evolution of this methodology will consist not only in analysis and application of modern tectonic-geodynamic conceptions, but and in wide attraction and of different geological-geophysical data, including comprehensive utilization of satellite observed (constantly renewing) gravity and magnetic arrays.

Acknowledgements

Author would like to thank Prof., Academician of the Georgian Acad. of Sci. T. Chelidze and Dr. S. Gongadze as well as anonymous reviewers, who thoroughly reviewed the manuscript, and whose critical comments and valuable suggestions were very helpful in preparing this paper. The research leading to these results has received funding from the Ministry of Energy, National Infrastructures and Water Resources of Israel under Grant Agreement No. 212-17-018.

REFERENCES

ALEXEYEV, V.V., GADJIEV, T.G., KARKOSHKIN, A.I., KHESIN, B.E., ISMAIL-ZADEH, T.A. 1988. Gravity and magnetic anomalies in Azerbaijan and their geological interpretation. Map Printing Factory. Leningrad (in Russian).

ALEXIDZE, M.A., GUGUNAVA, G.E., KIRIA, D.K., CHELIDZE, T.L. 1993. A three-dimensional stationary model of the thermal and thermoelastic fields of the Caucasus. *Tectonophysics*, **227**, 191-203.

ALLEN, M.B., VINCENT, S.J., ALSOP, G.I., ISMAIL-ZADEH, A., FLECKER, R. 2003. Late Cenozoic deformation in the South Caspian region: effects of a rigid basement block within a collision zone. *Tectonophysics*, **366**, 223-239.

ALIZADEH, AK.A. (Ed.). 2005. Geology of Azerbaijan. Vol. **5**: Physics of the Earth. Nafta Press. Baku (in Russian).

ALI-ZADEH, AK.A. (Ed.). 2012. Modern problems of geology and geophysics of the Caucasus. Nafta Press. Baku.

ALPEROVICH, L., EPPELBAUM, L., ZHELUDEV, V., DUMOULIN, J., SOLDOVIERI, F., PROTO, M., BAVUSI, M., LOPERTE, A. 2013. A new combined wavelet methodology applied to GPR and ERT data in the Montagnole experiment (French Alps). *Journal of Geophysics and Engineering*, **10**, 2, 025017, 1-17.

AZIZBEKOV, SH.A., AGABEKOV, M.G., GRIGORYANTS, B.V., SHIKALIBEYLI, E.SH., MAMEDOV, A.V. 1972. The history of the geological evolution. In: Azizbekov Sh.A. (Ed.), *Geology of the USSR*, *Azerbaijan*, Vol. **XLVII**, Nedra, Moscow, 441-503 (in Russian).

ARTYUSHKOV, E.V., MÖRNER, N.-A., TARLING, D.H. 2000. The cause of loss of lithospheric rigidity in areas far from plate tectonic activity. *Geophysical Jour. International*, **143**, 752-766.

BARTON, P.J. 1986. The relationship between seismic velocity and density in the continental crust – A useful constraint? *Geophys. Jour. Royal. Astr. Soc*., **87**, 195-208.

BEN-AVRAHAM, Z., GINZBURG, A. 1990. Displaced terranes and crustal evolution of the Levant and the eastern Mediterranean. *Tectonics*, **9**, 613-622.

BEN-AVRAHAM, Z., GINZBURG, A., MAKRIS, J., EPPELBAUM, L. 2002. Crustal structure of the Levant basin, eastern Mediterranean. *Tectonophysics*, **346**, 23-43.

BEN-AVRAHAM, Z., ROZENTHAL, M., TIBOR, G., NAVON, H., WUST-BLOCH, H., HOFSTETTER, R., RYBAKOV, M. 2014. Lake Kinneret, ecology and management. In: *Structure and Tectonic Development of the Kinneret Basin* (Ed. T. Zohary et al.), Aquatic Ecology Series, **6**, Springer, 19-38.

BEN-AVRAHAM, Z. SCHATTNER, U., LAZAR, M., HALL, J.K., BEN-GAI, Y., NEEV, D., RESHEF, M. 2006. Segmentation of the Levant continental margin, eastern Mediterranean. *Tectonics*, TC5002, **25**, 1-17.

BEN-AVRAHAM, Z., TEN-BRINK, U., BELL, R., REZNIKOV, M. 1996. Gravity field over the Sea of Galilee: evidence for a composite basin along a transform fault. *Jour. Geophys. Res*earch, **101**, 533-544.

BRUNET, M.-F., KOROTAEV, M.V., ERSHOV A.V., NIKISHIN, A.M. 2003. The South Caspian Basin: a review of its evolution from subsidence modelling. *Sedimentary Geology*, **156**, 119-148.

EPPELBAUM, L.V. 2006. Methodology of 3-D combined modeling of magnetic and gravity fields in the Eastern Mediterranean. *Proceed. of the 3rd EUG Meeting*, Vienna, Austria, **8**, 02057, 1-4.

EPPELBAUM, L.V. 2014a. Four color theorem and applied geophysics. *Applied Mathematics*, **5**, 358-366.

EPPELBAUM, L.V. 2014b. Estimating informational content in geophysical observations on example of searching economic minerals in Azerbaijan. *Izv. Acad. Sci. Azerb. Rep., Earth Sciences*, 3-4, 31-40.

EPPELBAUM, L.V., ALPEROVICH, L., ZHELUDEV, V., PECHERSKY, A. 2011. Application of informational and wavelet approaches for integrated processing of geophysical data in complex environments. *Proceed. of the 2011 SAGEEP Conference*, Charleston, South Carolina, USA, **24**, 24-60.

EPPELBAUM, L., BEN-AVRAHAM, Z., KATZ, Y. 2005. Does mantle diapir produce Hebron magnetic anomaly? *Trans. of the Conf. of the Israel Geol. Soc. Ann. Meet*., Moshabim Country Logging (Negev), Israel, 26 p.

EPPELBAUM, L.V., BEN-AVRAHAM, Z., KATZ, Y.I. 2007. Structure of the Sea of Galilee and Kinarot Valley derived from combined geological-geophysical analysis. *First Break*, **25**, 1, 21-28.

EPPELBAUM, L., KATZ, Y. 2011. Tectonic-Geophysical Mapping of Israel and eastern Mediterranean: Implication for Hydrocarbon Prospecting. *Positioning*, **2,** 1, doi: 10.4236/pos.2011.21004, 36-54.

EPPELBAUM, L.V., KATZ, Y.I. 2012. Key features of seismo-neotectonic pattern of the Eastern Mediterranean. *Proceedings of Azerb. Nat. Acad. of Sci., Earth Sciences*, 3, 29-40.

EPPELBAUM, L.V., KATZ, Y.I. 2014a. First paleomagnetic map of the Easternmost Mediterranean derived from combined geophysical-geological analysis. *Trans. of the 10th EUG Meet.*, *Geophysical Research Abstracts*, **16**, EGU2014-2424, Vienna, Austria, 1-5.

EPPELBAUM, L.V., KATZ, Y.I. 2014b. First maps of Mesozoic and Cenozoic structural-sedimentation floors of the Easternmost Mediterranean and their relationship with the deep geophysical-geological zonation. *Proceed. of the 19th Intern. Congress of Sedimentologists*, Geneva, Switzerland, 1-3.

EPPELBAUM, L.V., KATZ, Y.I. 2015a. Newly developed paleomagnetic map of the Easternmost Mediterranean unmasks geodynamic history of this region. *Central European Jour. of Geosciences*, **7**, 1, 95-117.

EPPELBAUM, L.V., KATZ, Yu.I. 2015b. Eastern Mediterranean: Combined geological-geophysical zonation and paleogeodynamics of the Mesozoic and Cenozoic structural-sedimentation stages. *Marine and Petroleum Geology*, **65**, 198-216.

EPPELBAUM, L., KATZ, Y., BEN-AVRAHAM, Z. 2006. Mt. Carmel structure as a plate tectonics phenomenon. *Trans. of the Conf. of the Israel Geol. Soc., Ann. Meet*., Beit-Shean, Israel, 31.

EPPELBAUM, L.V., KATZ, Y.I., BEN-AVRAHAM, Z. 2012. Israel – Petroleum Geology and Prospective Provinces. *AAPG European Newsletter*, 4, 4-9.

EPPELBAUM, L.V., KHESIN, B.E. 2004. Advanced 3-D modelling of gravity field unmasks reserves of a pyrite-polymetallic deposit: A case study from the Greater Caucasus. *First Break*, **22**, 11, 53-56.

EPPELBAUM, L.V., KHESIN, B.E. 2012. Geophysical studies in the Caucasus. Springer.

EPPELBAUM, L.V., KUTASOV, I.M., PILCHIN, A.N. 2014a. Applied geothermics. Springer.

EPPELBAUM, L.V., ITKIS, S.E., KHESIN, B.E. 2000. Optimization of magnetic investigations in the archaeological sites in Israel. In Special Issue of Prospezioni Archeologiche*: Filtering, Modeling and Interpretation of Geophysical Fields at Archaeological Objects*, 65-92.

EPPELBAUM, L.V., NIKOLAEV, A.V., KATZ, Y.I. 2014b. Space location of the Kiama paleomagnetic hyperzone of inverse polarity in the crust of the eastern Mediterranean. *Doklady Earth Sciences* (Springer), **457**, 6, 710-714.

EPPELBAUM, L.V., PILCHIN, A.N. 2006. Methodology of Curie discontinuity map development for regions with low thermal characteristics: An example from Israel. *Earth and Planetary Sciences Letters*, **243**, 3-4, 536-551.

ETIRMISHLI, G.D., KAZIMOVA, S.E. 2013. Velocity model of crust of Azerbaijan from the data of digital seismic stations. *Geology and Geophysics of South of Russia*, 1, 59-74.

FORTE, A.M., COWGILL, E., MURTUZAYEV, I., KANGARLI, T., STOICA, M. 2013. Structural geometries and magnitude of shortening in the eastern Kura fold-thrust belt, Azerbaijan: Implications for the development of the Greater Caucasus Mountains. *Tectonics*, **32**, 688-717.

GADJIEV, R.M. 1965. Deep geological structure of Azerbaijan. Azgosizdat. Baku (in Russian).

GAMKRELIDZE, I.R., SHENGELIA, D.M. 2007. Pre-Alpine geodynamics of the Caucasus, suprasubduction regional metamorphism and granitoid magmatism. *Bull. of the Georgian National Acad. of Sci*., **175**, 1, 57-65.

GARDOSH, M.A., GARFUNKEL, Z., DRUCKMAN, Y., BUCHBINDER, B. 2010. Tethyan rifting in the Levant Region and its role in Early Mesozoic crustal evolution. *Geological Society*, London, **341**, 9-36.

GASANOV, A.G. 2001. Deep structure and seismicity of Azerbaijan in relation to hydrocarbons prognosis. Elm. Baku (in Russian).

GOLONKA, J., FORD, D. 2000. Pangean (Late Carboniferous – Middle Jurassic) paleoenvironment and lithofacies. *Palaeogeography, Paleoclimatology, Paleoecology*, **161**, 1-34.

GULIYEV, I., PANAHI, B. 2004. Geodynamics of the deep sedimentary basin the Caspian sea region: paragenetic correlation of the seismicity and mud volcanism. *Geo-Marine Letters*, **24**, 3, 169-176.

GUREVICH, E.L. 1981. Paleomagnetism of Upper Precambrian rocks of Irkutian amphitheatre; Problems of their correlation and paleogeographic location. In: *Paleomagnetism and Problems of Paleogeography*, *Transactions of VNIGRI*, 11-22 (in Russian).

IRVING, E. 1966. Paleomagnetism of some carboniferous rocks from New South Wales and its relation to geological events. *Jour. of Geophysical Research*, **71**, 24, 6025-6051.

JIMENEZ-MUNT, I., SABADINI, R., GARDI, A. 2006. Active deformation in the Mediterranean from Gibraltar to Anatolia inferred from numerical modeling and geodetic and seismological data. *Jour. of Geophysical Research*, **108**, B1, doi: 10.1029/2001JB001544, 1-24.

JOHNSON, P.R., KATTAN, F.H. 2008. Lithostratigraphic revision in the Arabian shield: The impacts of geochronology and tectonic analysis. *The Arabian Jour. for Science and Engin*., **33**, 1, 3-16.

KADIROV, F.A. 2000. Gravity field and models of deep structure of Azerbaijan. Nafta Press. Baku (in Russian).

KADIROV, F.A. 2006. Nature of gravitational anomaly in the South Caspian Basin. *Trans. of the EAGE 68th Conference*, Vienna, P325, 1-4.

KADIROV, F.A., GADIROV, A.H. 2014. A gravity model of the deep structure of South Caspian Basin along submeridional profile Alborz–Absheron Sill. *Global and Planetary Change*, **114**, 66-74.

KABAN, M.K. 2002. A gravity model of the north Eurasia crust and upper mantle: 2. The Alpine-Mediterranean fold belt and adjacent structures of the southern former USSR. *Russian Journal of Earth Sci*., **4**, 1, 19-33.

KHAIN, V.E. 1975. Structure and main stages in the tectonic-magmatic development of the Caucasus: An attempt at geodynamic interpretation. *American Jour. of Science*. **275A**, 131-156.

KHAIN, V.E. 1984. Regional geodynamics. Alpine Mediterranean Belt. Nedra. Moscow (in Russian).

KHAIN, V.E. 2000. Tectonics of continents and oceans. Nauchnyi Mir. Moscow (in Russian).

KHAIN V.E. 2007. Mesozoic–Cenozoic Accretionary complexes of the Greater Caucasus. *Doklady Earth Sciences*, **413A**, 3, 376-379.

KHAIN, V.E., ALIZADEH, AK.A. (Eds.). 2005. Geology of Azerbaijan. Vol. 4: Tectonics. Nafta Press. Baku (in Russian).

KHALAFLY, A.A. 2006. Paleomagnetism and some problems of shear deformations of the Lesser Caucasus. Takhsil. Baku (in Russian).

KHESIN, B.E., ALEXEYEV, V.V., EPPELBAUM, L.V. 1993. 3-D modelling of gravity and magnetic fields as a final stage of application of effective interpretation system of geophysical data under difficult geological conditions. *Geoinformatics*, **4**, 3, 177-188.

KHESIN, B.E., ALEXEYEV, V.V., EPPELBAUM, L.V. 1996. Interpretation of geophysical fields in complicated environments. Kluwer Academic Publisher (Springer). Ser: Modern Approaches in Geophysics. Boston – Dordrecht – London.

KOULAKOV, I., ZABELINA, I., AMANATASHVILI, I., MESHKINA, V. 2012. Nature of orogenesis and volcanism in the Caucasus region based on results of regional tomography. *Solid Earth*, **3**, 327-337.

LE PICHON, X., KREEMER, C. 2010. The Miocene-to-present kinematic evolution of the Eastern Mediterranean and Middle East and its implications for dynamics. *Annu. Rev. Earth Planet. Sci*., **38**, 323-351.

LEONOV, Yu.G. (Ed.), 2008. The Greater Caucasus in the Alpine Epoch. Geos. Moscow (in Russian).

MARLOW, L., KORNPIHL, K., KENDALL, C.G.ST.C. 2011. 2-D basin modeling study of petroleum systems in the Levantine Basin, Eastern Mediterranean. *Geoarabia*, **16**, 2, 17-42.

MAMEDOV, P.Z. 2009. Sedimentation models in the SCMB and their seismostratigraphic characteristics. *Stratigraphy and Sedimentology of Oil-Gas Basins*, 3, 70-85.

MEDERER, J., MORITZ R., ULIANOV A., CHIARADIA, M. 2013. Middle Jurassic to Cenozoic evolution of arc magmatism during Neotethys subduction and arc-continent collision in the Kapan Zone, southern Armenia. *Lithos*, **177**, 61-78.

MEILER, M., RESHEF, M., SHULMAN, H. 2011. Seismic depth-domain stratigraphic classification of the Golan Heights, central Dead Sea Fault. *Tectonophysics*, **510**, 354-369.

MOLOSTOVSKY, E.A., MOLOSTOVSKY, I.I., MINIKH, M.G. 1998. Stratigraphic correlations of the Upper Permian and Triassic beds from the Volga-Ural and Cis-Caspian. In: (Crasquin-Soleau, S. and Barrier, E´., Eds.) *Peri-Tethys memoir 3: Stratigraphy and Evolution of Peri-Tethyan platforms*. *Me´moires du Muse´um national d'histoire naturelle*, Paris, **177**, 35-44.

MOLOSTOVSKY, E.A., PECHERSKY, D.M., FROLOV, I.Yu. 2007. Magnetostratigraphic timescale of the Phanerozoic and its description using a cumulative distribution function. *Izvestiya*, *Physics of the Solid Earth*, **43**, 10, 811-818.

MOLOSTOVSKY, E.A. 2009. An improved magnetostratigraphic scale of Phanerozoic. *A report prepared for the Russ. Acad. of Sci*. (in Russian).

MOSAR, J., KANGARLI, T., BOCHUD, M., GLASMACHER, U.A., RAST, A., BRUNET M.-F., SOSSON, M. 2010. Cenozoic–Recent tectonics and uplift in the Greater Caucasus: A perspective from Azerbaijan. *Geological Society*, London, *Special Publications*, 340, 261-280.

MUMLADZE, T., FORTE, A.M., COWGILL, E.S., TREXLER, C.C., NIEMI, N.A., YIKILMAZ, M.B., KELLOGG, L.H. 2015. Subducted, detached, and torn slabs beneath the Greater Caucasus. *Geores J.*, **5**, 36-46.

PAVLENKOVA, G.A. 2012. Structure of the Caucasus' earth crust along the deep seismic sounding profiles Stepnoe-Bakuriani and Volgograd-Nakhchevan (results of initial data re-interpretation). *Izvestiya*, *Physics of the Earth*, 5, 16-25.

PILCHIN, A.N., EPPELBAUM, L.V. 1997. Determination of magnetized bodies lower edges by using geothermal data. *Geophysical Journal International*, **128**, 1, 167-174.

RAPPEL, C., McNUTT, M. 1990. Regional compensation of the Greater Caucasus mountains based on an analysis of Bouguer gravity data. *Earth and Planetary Science Letters,* **98**, 360-379.

REILINGER, R., McCLUSKY, S., VERNANT, P. LAWRENCE, S., ERGINTAV, S., CAKMAK, R., OZENER, H., KADIROV, F., GULIEV, I., STEPANYAN, R., NADARIYA, M., HAHUBIA, G., MAHMOUD, S., SAKR, K., ARRAJEHI, A., PARADISSIS, D., AL-AYDRUS, A., PRILEPIN, M., GUSEVA, T., EVREN, E., DMITROTSA, A., FILIKOV, V., GOMEZ, F., AL-GHAZZI, R., KARAM, G. 2006. GPS constraints on continental deformation in the Africa-Arabia-Eurasia continental collision zone and implications for the dynamics of plate interactions. *Jour. of Geophysical Research,* **111**, B05411, 1-26.

RICKETTS, J.W., TAKEDATSU, R., MELLORS, R.J., SANDWELL, D., GOK, R., YETIRMISHLI, G. 2008. Crustal structure of the Caucasus and Caspian Region using gravity and receiver functions. *Proceed. of the American Geophysical Union Fall Meet*., abstract #T21A-1922.

RIORDAN, J. 2014. An Introduction to Combinatorial Analysis. Princeton Univ. Press.

ROBERTS, G., PEACE, D. 2007. Hydrocarbon plays and prospectivity of the Levantine Basin, offshore Lebanon and Syria from modern seismic data. *GeoArabia*, **12**, 3, 99-124.

ROBERTSON, A.H.F., CLIFT, P.D., DEGNAN, P.J., JONES, G. 1991. Palaeogeographic and palaeotectonic evolution of the Eastern Mediterranean Neotethys. *Palaeogeography, Palaeoclimatology, Palaeoecology*, **87**, 289-343.

ROTSTEIN, Y., BARTOV, Y. 1989. Seismic reflection across a continental transform: An example from a convergent segment of the Dead Sea rift. *Jour. of Geophys. Research*, **94**, 2902-2912.

ROTSTEIN, Y., BARTOV, Y., FREISLANDER, U. 1992. Evidence for local shifting of the main fault and changes in the structural setting, Kinarot basin, Dead Sea transform. *Geology*, **20**, 251-254.

RUBAN, D.A. 2013. The Greater Caucasus – A Galatian or Hanseatic terrane? Comment on "The formation of Pangea" by G.M. Stampfli, C. Hochard, C. Vérard, C.Wilhem and J. von Raumer [*Tectonophysics*, **593** (2013), 1-19]. *Tectonophysics*, **608**, 1442-1444.

SAINTOT, A., BRUNET, M.-F., YAKOVLEV, F., SEBRIER, M., STEPHENSON, R., ERSHOV, A., CHALOT-PRAT, F., MCCANN, T. 2006. The Mesozoic-Cenozoic tectonic evolution of the Greater Caucasus. *The Geological Society of London*, Memoirs, **32**, 277-289.

SARKER, G., ABERS, G.A. 1998. Deep structures along the boundary of a collision belt: attenuation tomography of P and S waves in the Greater Caucasus. *Geophysical Jour. International*, **133**, 326-340.

SHARKOV, E., LEBEDEV, V., CHUGAEV, A., ZABARINSKAYA, L., RODNIKOV, A., SERGEEVA, N., SAFONOVA, I. 2015. The Caucasian-Arabian segment of the Alpine-Himalayan collisional belt: Geology, volcanism and neotectonics. *Geosciences Frontiers*, Vol. **6**, No. 4, pp. 513-522.

SHEKINSKY, E., RADZHABOV, M., TIMUKYAN, G., LEVI, V., RIGER, R. 1967. Study of the Earth's crust structure in Azerbaijan using deep seismic sounding. *Izv. Akad. Nauk Azerb. SSR*, Nauki o Zemle, 5, 41-50 (in Russian).

SHIKHALIBEYLI, E.SH. 1972. Location of Azerbaijan in general structure of the Caucasus and surrounding folded region, In: AZIZBEKOV, SH.A. (Ed.), Geology of the USSR, Azerbaijan, Vol. XLVII. Nedra, Moscow, 286-290 (in Russian).

SPICHAK, V.V. 2006. Comparative analysis of hypotheses of the geoelectric structure of the Transcaucasian region from magnetotelluric data. *Izvestiya, Physics of the Solid Earth*, **42**, 1, 60-68.

STAMPFLI, G.M., HOCHARD, C., VÉRARD, C., WILHEM, C., VON RAUMER, J. 2013. The formation of Pangea. *Tectonophysics*, **593**, 1-19.

STERN, R.J., JOHNSON, P.R., KRONER, A., YIBAS, B. 2004. Neoproterozoic ophiolites of the Arabian-Nubian shield. *Developments of in Precambrian Geology*, **13**, 95-128.

STRAKHOV, V.N. 1976. Main ideas and methods for deriving information from gravitational and magnetic observations. Nedra. Moscow (in Russian).

TZIMELZON, I.O. 1965. Deep structure of the Earth's crust and tectonics of Azerbaijan on the geophysical data analysis. *Soviet Geology*, 4, 103-111 (in Russian).

TZIMELZON, I.O. 1970. Relation between the tectonics of sedimentary deposits of Azerbaijan and earth's deep structure. *Geotectonics*, 5, 69-81 (in Russian).

© F.F.Altinoğlu, A.Aydin, 2015

INTERPRETATION OF DEEP CRUSTAL STRUCTURE AND LINEAR FEATURES OF WESTERN ANATOLIA BY USING BOUGUER GRAVITY DATA

F.F.Altinoğlu, A.Aydin

Pamukkale University,
20017 Kınıkli, Denizli, Turkey
faltinoglu@pau.edu.tr,
aaydin@pau.edu.tr

Western Anatolia is an important region with its' complex tectonic history, the horst-graben system progressed under this regime and high seismic activity take place in Aegean Extension Region. The most important tectonic structures of this system are E-W trendly Gediz and Büyük Menderes grabens. Our study area is involving the western part of Büyük Menderes and Gediz grabens. The Bouguer gravity data was used to investigate topography of the deep crust layers and the tectonic structure of the basins. Bouguer gravity anomalies values of western Anatolia increase from east to west direction. Parker-Oldenburg algorithm has been used to obtain 3D Moho and basement topography and horizontal gradient, analytic signal and tilt angle methods has used to delineate linear features. As a result of 3D modelling process, we determined the maximum depth of Moho and basement is in Büyük Menderes graben as 35 km and 12.5 km, respectively. By detection of lineaments, new lineament map of study area is given in this study. The study area also, has been investigated by the seismic activity. The most of the earthquakes have been occurred in study area in depth to the basement.

Introduction

Western Turkey is tectonically complex high-deformed continental region that specified by N-S trendly extension and E-W trendly parallel grabens and their normal faults (Le Pichon et al., 1995; Reilinger et al., 1997; McClusky et al., 2000). The crustal deformation in the region comprises many geothermal systems, volcanism and high seismic activity.

The most common one of many different theories have been suggested about the development of this complicate tectonic structure is suggested by Şengör (1979) that the tectonic regime shaped by the effect of compression then extension regimes. The region is bounded from the east by Anatolian plate and North Anatolian Fault Zone and from the south by African plate (Fig. 1). By the western direction movement of Anatolian plate western Anatolia was compressed and western escape have taken placed and African plate subducted under Anatolian plate on the south, with this effect compression and extension regime occurred. Moreover, with the total effect of this regime the complicated tectonism developed. The most remarkable structures of this tectonic regime are the grabens, which were developed under the compression and extension regimes (Bozkurt, 2001).

The objective of this article is to determine the crustal structure and tectonical features of the region. The area between 27.00°-28.25° eastern longitudes and 37.50°-38.50° northern latitudes was selected as the study area including the main important graben structures of western Anatolia shown in Figure 1. We used the gravity data of the study area and obtained the three dimensional (3D) Mohorovicic discontinuity (Moho) and the basement topography, the undulation of crust layers within the grabens and the linear features of the region.

Tectonic setting

The Anatolian plate is a continental belt between the Eurasian, African and Arabian plates, it is bounded by the North Anatolian Fault and East Anatolian Fault in the east and the Northern Aegean Trench in the west has been moving westward (Şengör, Yılmaz, 1981; McClusky et al., 2000). The extension in western Anatolia is related to the northward movement of the Arabian plate in the east, this movement pushed Anatolia westwards through the North Anatolian Fault Zone and East Anatolian Fault Zone (Dewey, Şengör, 1979). African Plate was subducting northwards under the south Anatolian Plate along the Aegean-Cyprean subduction zone (Şengör and Yılmaz, 1981; Bozkurt and Mittwede, 2005). Four different shemas have been proposed as the cause of extension in the region (Bozkurt, 2001): **(i)** subduction rollback along the Aegean–Cyprian trench (McKenzie,

1972; 1978; Le Pichon, Angelier, 1979; Le Pichon et al., 1995; Mercier et al., 1989; Jackson, McKenzie, 1984; Meulenkamp et al., 1988; Thomson et al., 1998); **(ii)** westward escape of the Anatolian plate along North Anatolian and East Anatolian fault systems (Dewey, Şengör, 1979; Şengör, Yilmaz, 1981); **(iii)** post-orogenic collapse of the crust over thickened during the closure of the northern branch of Neotethys (Dewey, 1988; Seyitoğlu, Scott, 1991); and **(iv)** different convergence rates along the Aegean–Cyprian subduction zone (Reilinger et al., 2006).

The result of this regime caused the formation of mainly E-W trending horst-graben system. The mainly tectonic structures in the western Anatolia are E-W trending grabens and the most important of these grabens are Büyük Menderes and Gediz grabens. Akçığ (1988) recommended that E-W elongated graben regions in the Western Anatolia was the result of uplift on the upper mantle, and rift systems which were developed parallel to the N-S directional strain tectonic.

Bouguer gravity anomaly data

Bouguer gravity anomaly data of the study area was achieved from General Directory of Mineral Exploration and Research Company of Turkey (MTA) and Turkish Petroleum Corporation (TPAO). The surveys were obtained by 250-500 meters intervals and the data are gridded with 10 mGal intervals, Bouguer gravity anomaly map is given in Figure 2.

Bouguer gravity anomalies of Western Anatolia are generally decreased from east to west direction related to the thinning of the crust from E to W direction and high negative Bouguer gravity anomalies are shown in the grabens related to the thick sediment cover of the graben area.

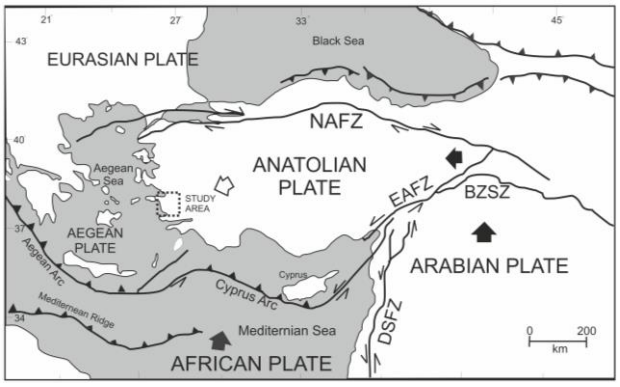


Figure 1. Location map of the study area

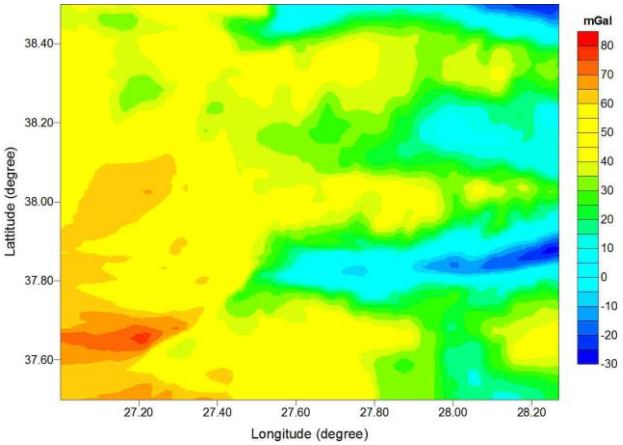


Figure 2. Bouguer gravity anomaly map of study area (Contour interval is 10 mGal)

The methods

One of the main tasks of geophysical study is to determine the geometry of the interface from gravity anomaly, Parker-Oldenburg algorithm was used to obtain the 3D geometry of interface topography from the relationship between the Fourier transform of gravity data and the sum of the interface topography's Fourier transformation. This algorithm is given as equation (1) iteratively from the given depth and density of an interface by Parker (1973), to calculate the gravity anomaly of uneven homogeneous layer by using the Fourier transform where, $F[\Delta g]$ represents Fourier transform of the gravity anomaly; G is the gravitational contrast; g represents the density contrast within the interface; k is wave number; z_1 is depth to the interface; z_0 is the average depth of horizontal interface. Oldenburg (1974) rearranged this equation to calculate the undulating interface depth.

$$F[z_1(x)] = -\frac{F[\Delta g(x)]e^{|k|z_0}}{2\pi G g} - \sum_{n=2}^{\infty} \frac{|k|^{n-1}}{n!} F[z_1{}^n(x)]. \quad (1)$$

The present equation (1) is a useful tool for calculation of density interface topography iteratively from Δg and z_0. From the beginning of the iteration, assignment of $z_1=0$ or an approximated value is assigned to the right part of the equation. Its inverse Fourier transform provides the first estimation of the topography. This topography value was used in calculation of the right hand sight of the equation to achieve the second topography ap-

proach. Until the convergence criterion is achieved; or until reaching the determined iteration number; or until the difference between successive steps is smaller than the convergence criterion, the iteration process continues. 3DINVER.M MATLAB program, developed by Gomez-Ortiz and Agarwal (2005) to compute 3D density geometry of the interface's from gridded gravity anomaly was used.

The horizontal gradient, analytic signal and tilt angle methods has been used to determine the lineaments. The horizontal gradient method has been used to locate the lateral changes in the density of near surface bodies. The horizontal gradient anomalies of the gravity data, give the maximum value over the edge of the body, if the edge is vertical (Cordell, Grauch, 1985). Its mathematical equation is presented in equation (2):

$$h(x,y)=\sqrt{\left(\frac{\partial g(x,y)}{\partial x}\right)^2+\left(\frac{\partial g(x,y)}{\partial y}\right)^2}\,. \qquad (2)$$

The analytic signal method was firstly used by Gabor (1946), than by Nabighian (1972) for interpretation of the potential field data. The analytic signal value of a potential field anomaly is defined as a magnitude of the total gradient of the field anomaly. Its mathematical equation is presented as Equation 3:

$$A(x,y)=\sqrt{\left(\frac{\partial g}{\partial x}\right)^2+\left(\frac{\partial g}{\partial y}\right)^2+\left(\frac{\partial g}{\partial z}\right)^2} \qquad (3)$$

The ratio of the vertical gradient ratio's arctangent to the total field horizontal gradient composes tilt angle. Miller and Singh (1994) then firstly introduce it; Verduzco et al. (2004) publicized it. The equation of tilt angle can be given as Equation 4:

$$\phi=\arctan\left[\frac{\left(\frac{\partial g}{\partial z}\right)}{\left[\left(\frac{\partial g}{\partial x}\right)^2+\left(\frac{\partial g}{\partial y}\right)^2\right]^{\frac{1}{2}}}\right]= \qquad (4)$$

$$=\arctan\left[\frac{\text{Vertical Derivative}}{\text{TotalHorizontalDerivative}}\right].$$

Results and discussion

3D Modeling of Moho and basement topography

With the aim of determining the tectonical structure of western part of Western Anatolia by using Bouguer gravity anomaly data the 3D Moho and basement topography by using the MATLAB 3DINVER.M program were modeled and the linear features were determined by using data processing methods with the POTENSOFT.M program**.** The enhanced Moho topography map is given in Fig.3. Moho topography is increased from east to west direction, it can be easily seen on the obtained Moho topography map, and there is an uprising on Moho undulations out of the graben areas. The crust depth of study area was determined as 35 km on the eastern side and rise to 24 km towards to west and 20 km towards to SW of study area. The maximum Moho depth indicates the grabens, which are the main important tectonic structures of the region, the determined maximum depth is 33-34 km in Büyük Menderes and Gediz grabens and the minimum depth is defined as 20-22 km in W and SW part of the study area. The Moho depth under the Menderes massive that is the one of most important geological structure of the region, is decreased. These results are similar with the recent studies; Riad et al. (1981) reported that the crust thickness was changed in range between 28-36 km in Western Anatolia, Akçığ et al. determined on their study in 1988 that there was uplift on upper mantle from Aegean region to Aegean Sea, it was averagely 30 km on Aegean Sea and crust thickness averagely 32 km on Aegean Sea side and reported that it reached 40 km on west to east direction inner side of Anatolia. The crust thickness of Aegean region reported as 30 km by Saunders et al. (1998), 33 km by Horasan et al. (2002), 29 km by Akyol et al. (2006) for Aegean region. Tezel et al. (2010) determined the Moho depth along a profile, which lies from Aegean Sea to Middle Anatolia, is 25 km to 35 km. And Cianetti et al. (2011) determined the Moho depth is 30 km for Western Anatolian region.We can say with the light of the other studies, there is uplift on Moho depth from east to the west direction in the study area.

The obtained basement topography map of study area is given in Fig.4. The maximum basement level is 12.5 km in Büyük Menderes and Gediz grabens similarly. Minimum depth value is 5.5 km in the SW of the study area. These basement levels are coinciding with the value determined by Çiftçi, Bozkurt, (2010). In the determined basement topography map, the topography undulation is on match with the main fault system directions, which are on NW-SE and E-W direction.

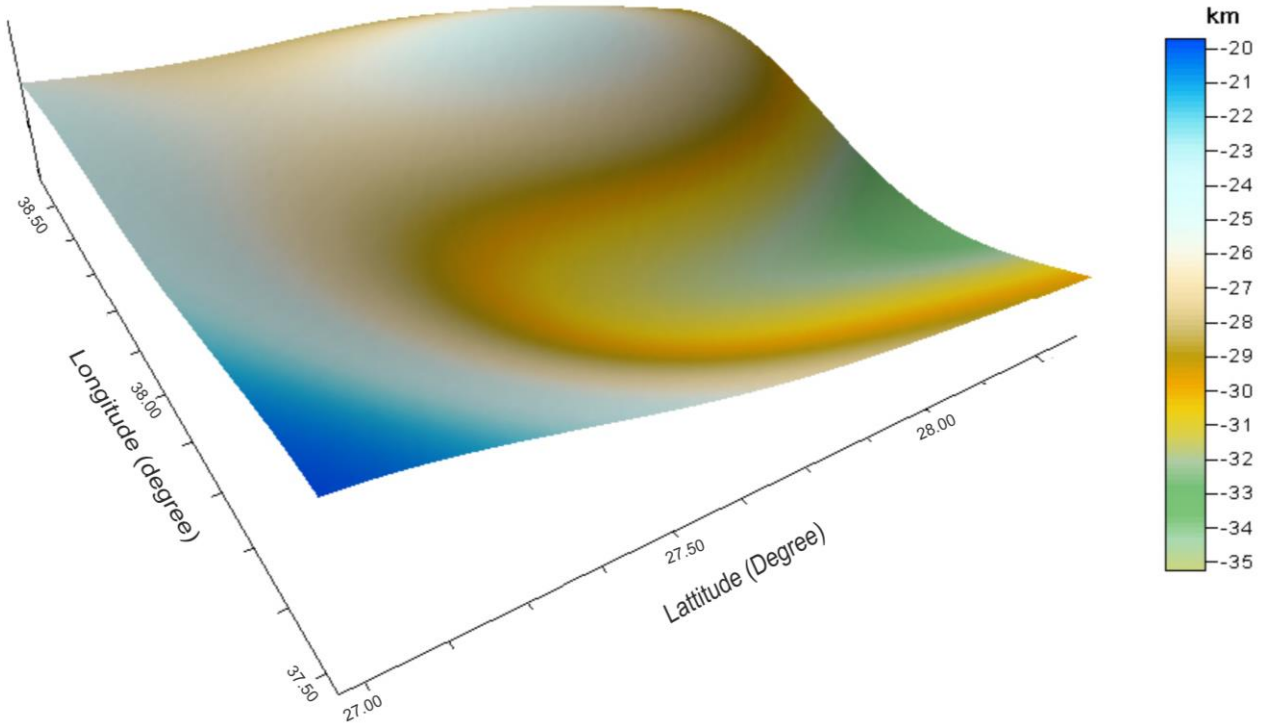


Figure 3. Moho topography map of study area derived from inversion of Bouguer gravity anomalies using Parker-oldenburg's algorithm

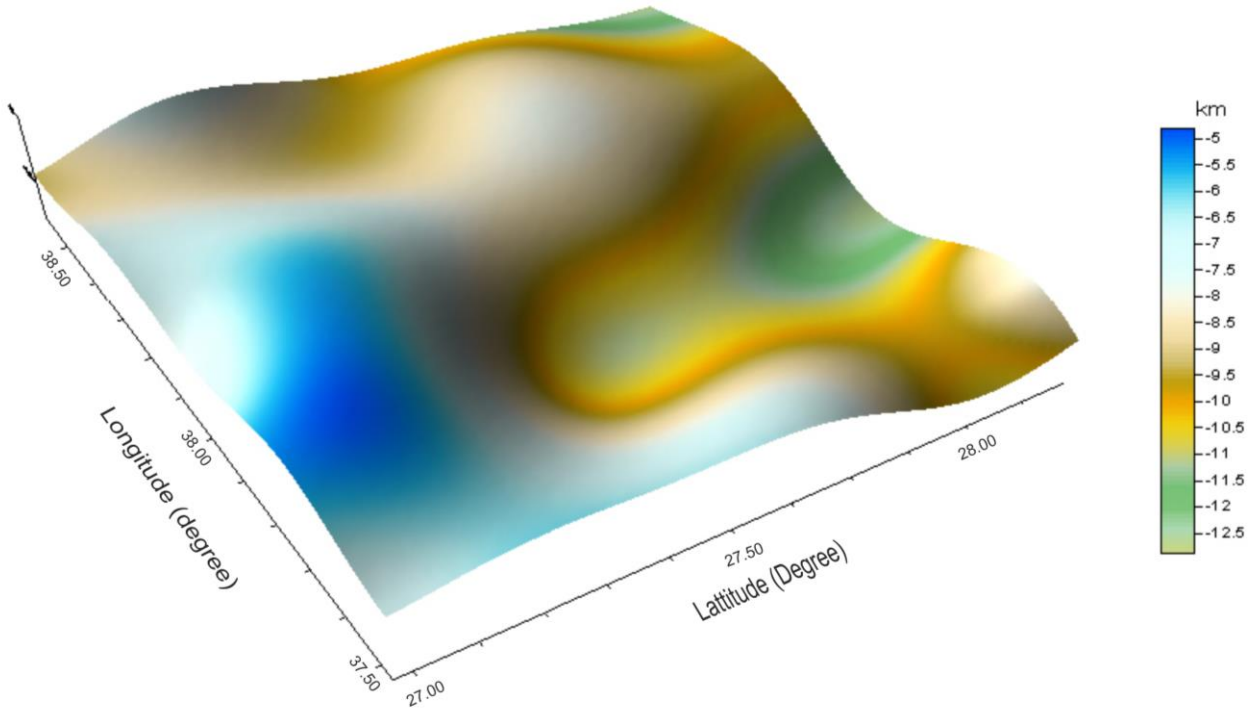


Figure 4. Basement topography map of study area derived from inversion of Bouguer gravity anomalies using Parker-oldenburg's algorithm

Detection of lineaments

To detect the linear features of the study area, the horizontal gradient, and analytic signal and tilt angle methods have been used to Bouguer gravity anomaly data of the study area, the produced maps are given in Fig.5. In the horizontal gradient map of the study area, the maximum values indicate the areas represented by high negative values on Bouguer gravity anomaly map and those areas indicate the highest depth in graben areas (see Fig.5a). The strong gradient values of horizontal gradient correspond to boundaries of Büyük Menderes and Gediz grabens lie on E-W direction.

In the analytic signal map of Bouguer gravity anomaly data (Fig. 5b), the strongest gradient values are seen on E-W trendily in the graben area of Büyük Menderes graben and in the northern side of the study area in Gediz graben. Figure 5c shows the results of tilt angle map of the study area, the zero values on the tilt angle maps indicate the boundaries of grabens, the positive values represent Menderes massive and negative values represent the graben fillings.

These three maps lead us to determine the tectonical lineaments of the study area. The common area with maximum horizontal gradient and analytic signal values and the zero values of tilt angle indicates the existence of a lineament. By this way, we have determined the new lineaments map given in Figure 6 and compared with the active fault map given by MTA.

To interpret the lineaments with seismic activity, the earthquakes have been occurred between the times period 2005-2015 have been used. The region has a high seismic activity; the western part of the area is more active than the eastern part. The epicentral distribution of these earthquakes is given in Fig.7. Most of the earthquakes have been occurred below the basement level as seen in Fig.8.

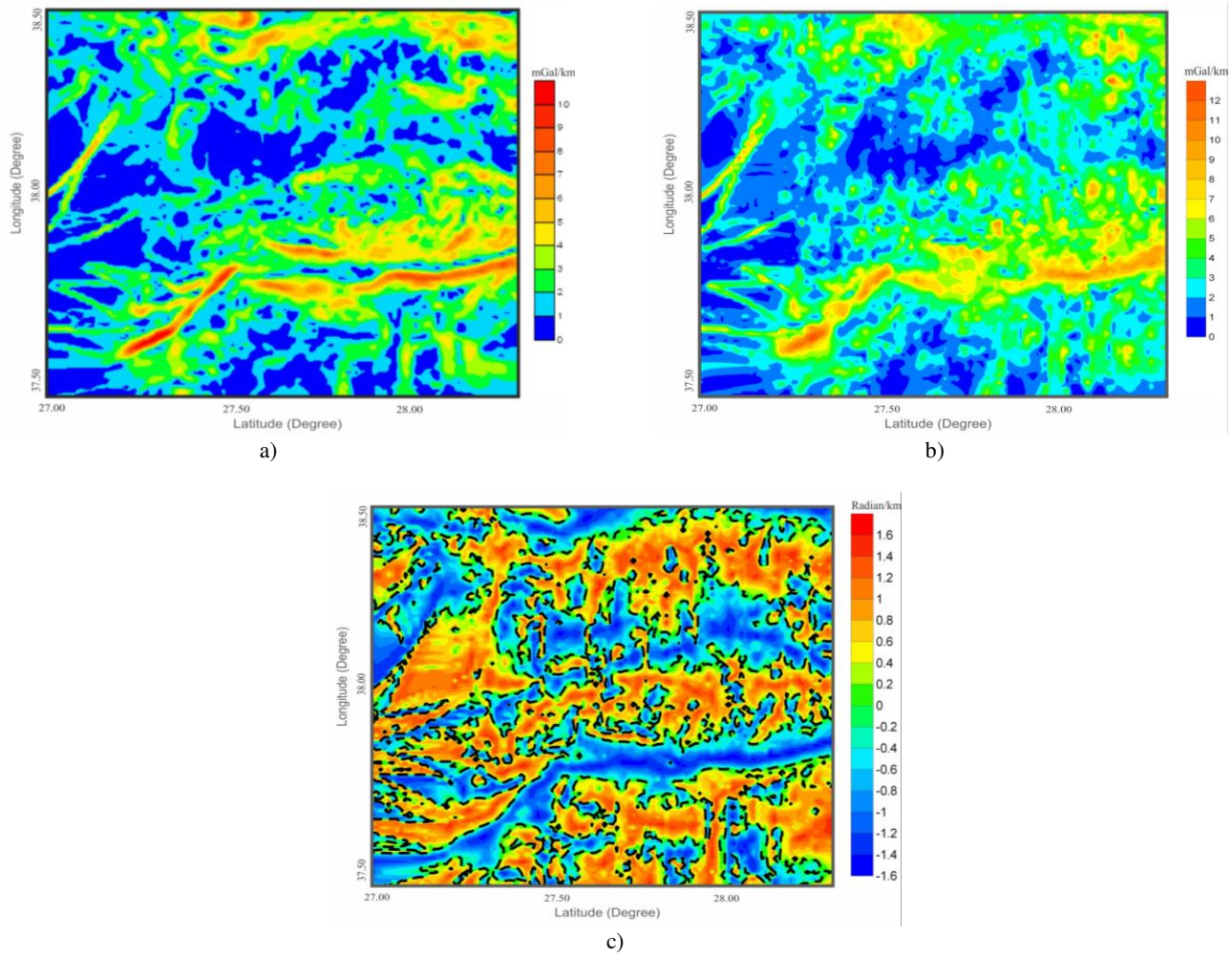


Figure 5. a) Horizontal gradient b) Analytic signal c) Tilt angle maps of study area

Conclusions

In this study, the undulations of the deep crust layers in western Anatolia have been presented. The maximum Moho depth is determined as 34-35 km in the east and minimum Moho depth is 20-22 km in the west. There is uplift on Moho level on Western Anatolia region from east to west direction and it decreases on the Menderes massive, this is a result of strain, which released to the compression of Hellenic subduction. This strain caused a decant on the region and graben areas occurred as a result of this. The basement level is range 5 km to 12 km. The most of the earthquakes have been occurred in depth to the basement. Beside this there are also, deep epicentral earthquakes have taken place beneath the basement in the region.

The other contribution of this study is the new upgraded lineaments map the west of western Anatolia. This study result may shed light on the future tectonical studies in the Western Anatolia.

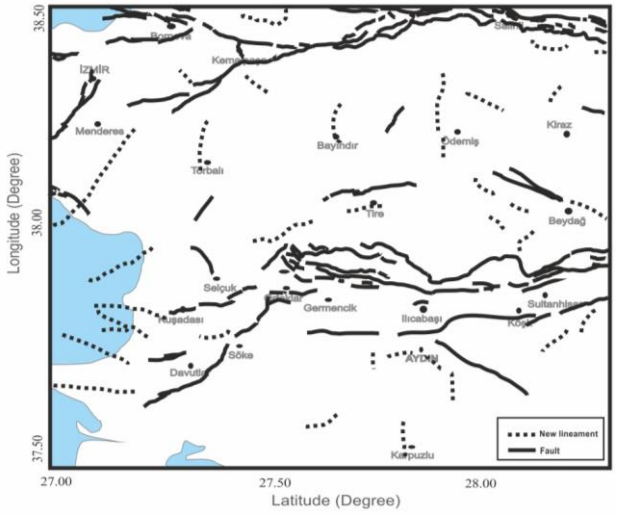


Figure 6. New lineaments map of the study area

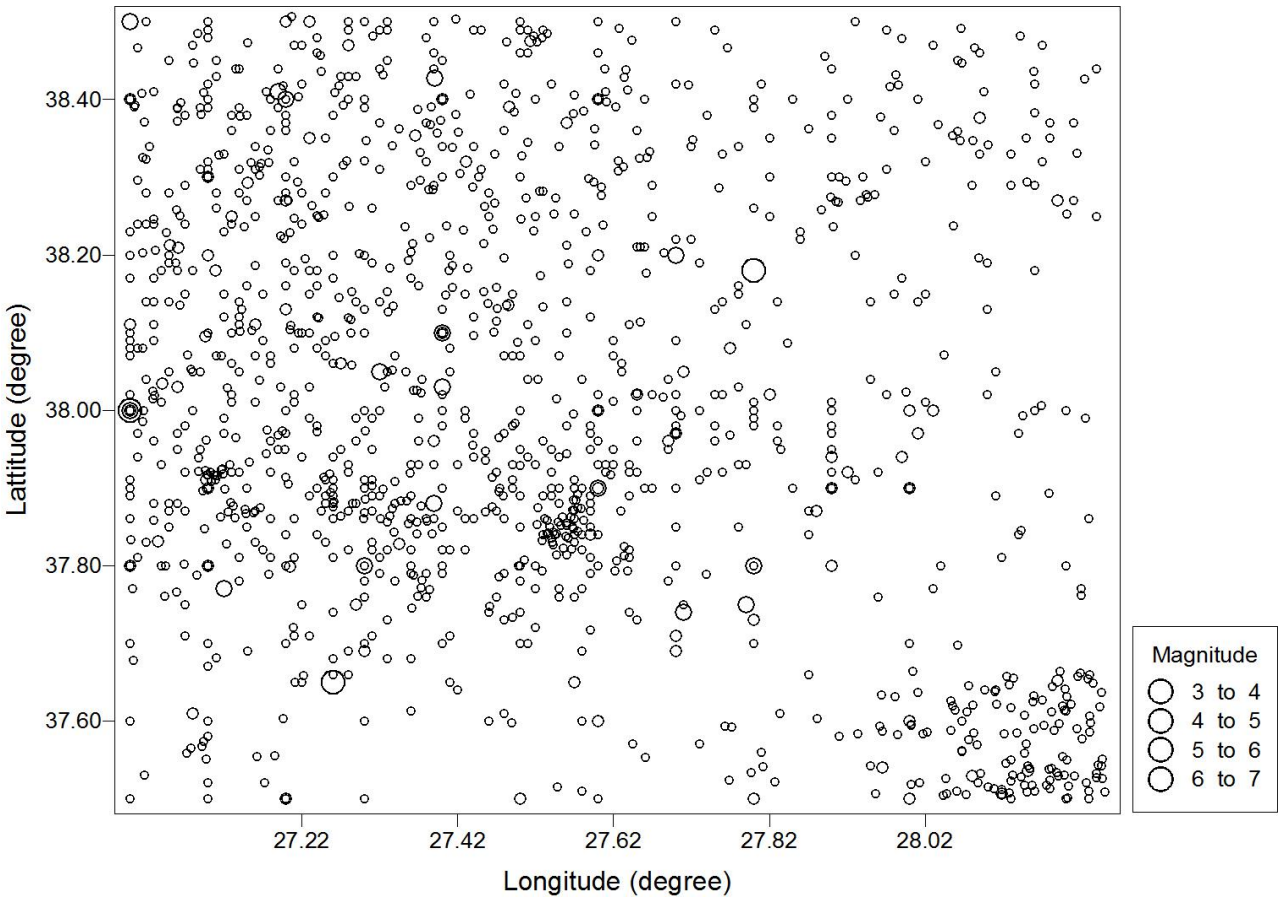


Figure 7. Epicentral distribution of the eartquakes occured in the study area.

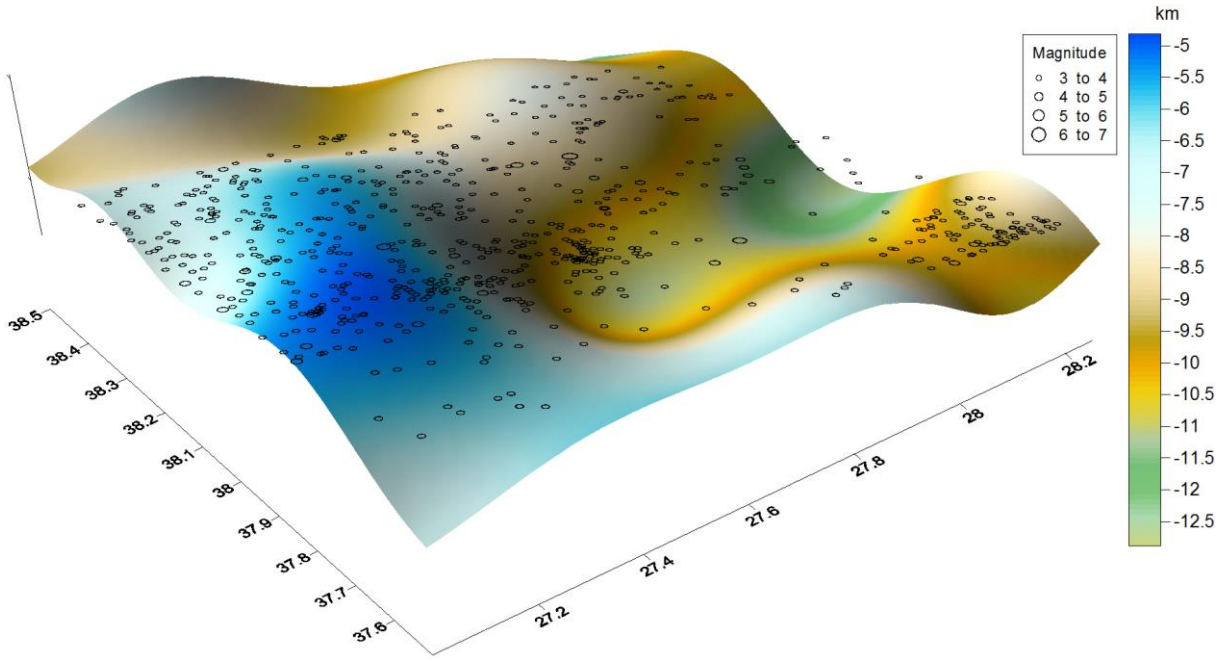


Figure 8. Epicentral distribution of the eartquakes occured below the basement level

REFERENCES

AKÇIĞ, Z. 1988. Batı Anadolu'nun yapısal sorunlarının gravite verileriile irdelenmesi. *TJK Bült.* 31, 63-70.

AKYOL, N., ZHU, L., MITCHELL, B.J., SÖZBİLİR, H., KEKOVALI, K. 2006. Crustal structure and local seismicity in western Anatolia. *Geophysical Journal International,* 166, 1259-1269.

BOZKURT, E. 2001. Neotectonics of Turkey – a Synthesis. *Geodinamica Acta,* 14, 3-30.

BOZKURT, E., MITTWEDE, S.K. 2005. Introduction: Evolution of neogene extensional tectonics of Western Turkey. *Geodinamica Acta,* 18, 153-165.

CIANETTI, S., GASPARINI, P., GIUNCHI, C., BOSCHI, E. 2011. Numerical modelling of the Aegean–Anatolian region: geodynamical constraints from observed rheological heterogeneities. *Geophys. J. Int.,* 146, 760-780.

CORDELL, L., GRAUCH, V.J.S. 1985. Mapping basement magnetization zones from aeromagnetic data in the San Juan Basin, New Mexico. (Ed. Hinze, W.J.) The utility of regional gravity and magnetic anomaly maps. Soc. Explor. Geophys.181-197.

ÇIFTÇI, N.B., BOZKURT, E. 2010. Structural evolution of the Gediz Graben, SW Turkey: temporal and spatial variation of the graben basin. *Basin Research*, 22, 846-873.

DEWEY, J.F. 1988. Litospheric stress, deformation and tectonic cycles: the description of Pangaea and the closure of the Tethis. In Audley-Charles M.G., Hallam A., eds. Gondwana and Tethis: Geological Society, London, Special publication, 37, 23-40.

DEWEY, J.F., ŞENGOR, A.M.C. 1979. Aegean and surrounding regions: complex multiplate and continuum tectonics in a convergent zone. *Geol. Soc. Am.*, B, 90, 84-92.

GABOR, D. 1946. Theory of communication. *Journal of the Institute of Electrical Engineers*, 93, 429-457.

GÓMEZ-ORTIZ, D., AGARWAL, B.N.P. 2005. 3DINVER.M: A MATLAB program to invert the gravity anomaly over a 3-D horizontal density interface by Parker-Oldenburg's algorithm, *Computer Geoscience*, 31, 513-520.

HORASAN, G., GÜLEN L., PINAR A., KALAFAT D., OZEL N., KULELI H.S., IŞIKARA A.M. 2002. Lithospheric structure of the Marmara and Aegean regions, Western Turkey. *Bull. Seism. Soc. Am.,* 92, 332-329.

JACKSON, J.A., McKENZIE, D.P. 1984. Active tectonics of Alpine–Himalayan Belt between western Turkey and Pakistan. *Geophys. J. R. Astron. Soc*., 77, 185-265.

Le PICHON, X., ANGELIER, J. 1979. The Hellenic arc and trench system: a key to the neotectonic evolution of the Eastern Mediterranean area. *Tectonophysics,* 60, 1-42.

Le PICHON, X., CHAMOT-ROOKE, C., LALLEMANT, S., NOOMEN, R., VEIS, G. 1995. Geodetic determination of the kinematics of central Greece with respect to Europe: implications for Eastern Mediterranean tectonics. *J. Geophys. Res.,* 100, 12675-12690.

MEULENKAMP, J.E., WORTEL, M.J.R., VAN WAMMEL, W.A., SPAKMAN, W., HOOGERDUYN STRATING, E. 1988. On the Hellenic subduction zone and the geodynamic evolution of Crete since the late middle Miocene. *Tectonophysics,* 146, 203-215.

McCLUSKY, S., BALASSANIAN, S., BARKA, A.A., DEMIR, C., ERGINTAV, S., GEORGIEV, I., GURKAN, O., HAMBURGER, M., HURST, K., KAHLE, H.G. et al. 2000. Global Positioning System constraints on plate kinematics and dynamics in the Eastern Mediterranean and Caucasus. *J. Geophys Res.,* 105, 5695-5720.

McKENZIE, D.P. 1972. Active tectonics of the Mediterranean Region. *Geophys. J. Royal Astro. Soc*., 30, 109-185.

McKENZIE, D.P. 1978. Active tectonics of the Alpine-Himalayan belt: The Aegean Sea and surrounding regions. *Geophys J. Royal Astro. Soc*., 55, 217-254.

MERCIER, J.L., SOREL, D., VERGELY, P., SIMEAKIS, K. 1989. Extensional tectonic regimes in the Aegean basins during the Cenozoic. *Basin Res*., 2, 49-71.

MILLER, H.G., SINGH, V. 1994. Potential field tilt -a new concept for location of potential field sources. *Journal of Applied Geophysics*, 32, 213-217.

NABIGHIAN, M.N. 1972. The Analytic Signal of two dimensional magnetic bodies with polygonal cross section: Its properties and use for automated anomaly interpretation. *Geophysics,* 37, 507-517.

PARKER, R.L. 1973.The rapid calculation of potential anomalies. *Geophys. J., R. Astr.Soc.,* 31, 447-455.

REILINGER, R.E., MCCLUSKY, S.C., ORAL, M.B., KING, W., TOKSOZ, M.N. 1997. Global Positioning System measurements of present-day crustal movements in the Arabian-Africa-Eurasia plate collision zone. *J. Geophys. Res.,* 102, 9983-9999.

REILINGER, R.E., McCLUSKY, S., VERNANT, P., LAWRENCE, S., ERGINTAV, S., CAKMAK, R., OZENER, H., KADIROV, F., GULIEV, I., STEPANYAN, R., NADARIYA, M., HAHUBIA, G., MAHMOUD, S., SAKR, K., ArRAJEHI, A., PARADISSIS, D., AL-AYDRUS, A., PRILEPIN, M., GUSEVA, T., EVREN, E., DMITROTSA, A., FILIKOV, S.V., GOMEZ, F., AL-GHAZZI, R., KARAM, G. 2006. GPS constraints on continental deformation in the Africa-Arabia-Eurasia continental collision zone and implications for the dynamics of plate interactions. *J. Geophys. Res.,* BO5411, doi:10.1029/2005JB004051.

RIAD, S., REFAI, E., GHALIB, M., 1981. Bouguer anomalies and crustal structure in the Eastern Mediterranean. *Tectonophysics,* 71.

SAUNDERS, P., PRIESTLEY, K., TAYMAZ, T. 1998. Variations in the crustal structure beneath western Turkey. *Geophys. J. Int.,* 134, 373-389.

SEYITOĞLU, G., SCOTT, B.C. 1991. Late Cenozoic crustal extension and basin formation in west Turkey. *Geol. Mag*., 128, 155-166.

ŞENGÖR, A.M.C., YILMAZ, Y. 1981.Tethyan evolution of Turkey: a plate tectonic approach. *Tectonophysics,* 75, 181-241.

TEZEL, T., SHIBUTANI, T., KAYPAK, B. 2010. Crustal structure variation in western Turkey inferred from the receiver function analysis. *Tectonophysics,* 492, 240-252.

THOMSON, S.N., STOCKHERT, B., BRIX, M.R. 1988. Thermochronology of the high-pressure metamorphic rocks of Crete, Greece. Implications for the speed of tectonic processes. *Geology,* 26, 259-262.

VERDUZCO, B., FAIRHEAD, J.D., GREEN, C.M., MACKENZIE, C. 2004. New insights into magnetic derivatives for structural mapping. *The Leading Edge*, 23, 116-119.

© A.Sh.Mukhtarov, R.S.Nadirov, A.V.Mammadova (Asadova), V.A.Mammadov, 2015

GEOLOGICAL CONDITIONS AND BUSINESS OPPORTUNITIES FOR GEOTHERMAL ENERGY DEVELOPMENT IN AZERBAIJAN

A.Sh.Mukhtarov[1], R.S.Nadirov[2], A.V.Mammadova (Asadova)[1], V.A.Mammadov[1]

1 – Institute of Geology and Geophysics, Azerbaijan National Academy of Sciences, 119, H.Javid ave., Baku, Azerbaijan

2 – Azerbaijan National Academy of Sciences, 30, Istiglaliyyat str., Baku, Azerbaijan, abdulvahab.mukhtarov@gmail.com

The territory of Azerbaijan is rich in thermal waters. Sources of thermal water can be found in the Greater and Lesser Caucasus, on the Absheron Peninsula and Talysh. Also in the vast territory of the Kur basin and the Precaspian-Guba area numerous wells drilled for oil and gas discovered aquifers with thermal water. The highest initial temperature of thermal water 96°C was registered in Jarly-3 well. Currently temperature of water is 92°C and mineralization is 50 g/l at the well head. Flow rate of the well exceeds 20000 m^3/day. According to estimates based on the set of parameters, currently the capacity of the well is approximately 70 MW if water is cooled down to 20°C. Another high-potential well is located in the Daridagh thermal area of Nakhchivan with the power potential about 10 MW.

Introduction. Geological and geothermal conditions

Recently control of carbon dioxide concentration in atmosphere is very important because of the global warming problem. As CO_2 is the result of the fuel burning processes, we should reduce usage of the energy of conventional fuels and look for solution of this problem in alternative energy sources globally. Alternative energy sources are actively used in the world recently and it will be one of the priorities in the near future.

Azerbaijan Republic does not stand idle in this area. The President of the country has repeatedly mentioned the importance of development and use of various forms of alternative energy in Azerbaijan. As Azerbaijan possesses vast potential of the alternative energy, this issue must be investigated in detail. Research and development should comply with the requirements of modern industry.

Geothermal energy is one of the most promising sources of alternative energy. There are different forms of outcrops of the Earth heat to the surface, e.g. volcanoes, geysers, mud volcanoes, thermal water wells, etc. There are no active volcanoes and geysers in Azerbaijan, however we have enough exploration wells where temperatures of thermal water in aquifers are higher than 100°C.

The most interesting area is western part of the South Caspian basin along the Talysh-Vandam maximum (Надиров, 1985). This gravitation maximum reflects buried fragment of Mesozoic island arc where local volcanic uplifts were explored in detail, as Muradkhanli oil field was discovered here in 70-s within the weathered and fractured volcanic rocks. The area is characterized by high fluid activity, which promotes formation of local abnormally high heat flows. Jarly-3 well is still flowing to the earth surface with high production rate. Temperature of volcanic rocks penetrated here at 2800-3000 m depth in some places is higher than 100°C (Алиев и др., 2002).

Sources of geothermal energy: Some results of research

Thermal waters

Thermal water resources in Azerbaijan are found mainly in the mountainous regions. In Lesser Caucasus, especially famous regions are Istisu and Bagirsag. Measurements in Bagirsag region have shown that water temperature there is 80°C at 100 m depth; in Istisu region temperature is 62°C at 70 m depth and 75°C at 300-350 m depth. Flow rate of water in Higher Istisu is 800-900 m^3/day, and in Lower Istisu it is 25 m^3/day.

As Azerbaijan is an oil country, there was no need in alternative energy in the past; geothermal energy potential was not studied separately, except researches targeted thermal waters. Another reason

is that Azerbaijan has a lot of thermal water sources with relatively low temperatures (<80°C), while technologies using low potential geothermal energy were developed recently. At present, such technologies are developing rapidly following growing demand for alternative energy. The Global warming problem targets the humanity to the direction of low-carbon technologies. As examples of the most perspective objects in Azerbaijan we can list thermal water sources in Lyankaran, Astara and Masally regions, Jarly, Sarisu, etc. E.g. water temperature in Donuzuten spring is 64°C and flow rate up to 1.5 million l/day.

A number of thermal springs and thermal water wells are available in Azerbaijan. The highest temperature (initial temperature 96°C) of thermal water flowing to the surface is from Jarly-3 well, which was drilled between the villages Jarly and Mollakend on the left bank of the Kur River. Currently water temperature is 92°C, mineralization is 50 g/l at the well head (Fig.1). Flow rate from the well is more than 20000 m^3/day. According to the parameters obtained during the recent period, initial potential power of the well is approximately 70 MW (if 100% efficiency is achieved by cooling water down to 20°C).

Another well in the same region exposed thermal water with the flow rate 10000 m^3/day and temperature at the wellhead 82°C. Thermal capacity (on cooling to 40°C) is 20.4 MW.

In the Precaspian-Guba zone (Fig.2, south-eastern slope of the Greater Caucasus) eight wells specially drilled to aquifers with thermal water flowed with calcium-sodium bicarbonate type of water, mineralization 0.8-1.9 g/l and total production rate 20470 m^3/day (Aliyev et al., 2002) with temperature 50-84°C. Overall capacity (provided that water is cooled only by 20°C) is about 20 MW. In Khachmaz region one well exposed thermal water with the flow rate 1228 m^3/day and temperature 58°C. In Yalama one well exposed thermal water with the flow rate 500 m^3/day and temperature 95°C. Minimum thermal capacity of these wells is respectively 1.2 and 0.5 MW.

Total energy capacity of thermal waters for hydrogeological areas determined on the basis of their commercial reserves is presented in Table 1 (Мухтаров, Хаммедов, 2003; Тагиев и др., 2001).

Nakhchivan (Fig.2) is one of the less investigated regions of Azerbaijan from the geothermal point of view. Besides well-known sources of mineral water, such as Sirab, Badamli, Vaykhir, etc., there is also thermal spring Daridagh. Thermal spring Daridagh with its sodium bicarbonate type of water is one of the most important resources in Nakhchivan, because of its mineral content (up to 20% arsenic and antimony). Temperature of thermal spring reaches 26.5°C. Wells drilled to the 137-665 m depth produced water with temperature 41-53°C. The water is highly mineralized (14.3-21.3 g/l). Flow rate of some wells is 25-34 l/sec. Energy potential power of wells in this area is 10 MW. Table 2 shows energy potential of water flowing from those wells.



Figure 1. Jarly-3 thermal water well

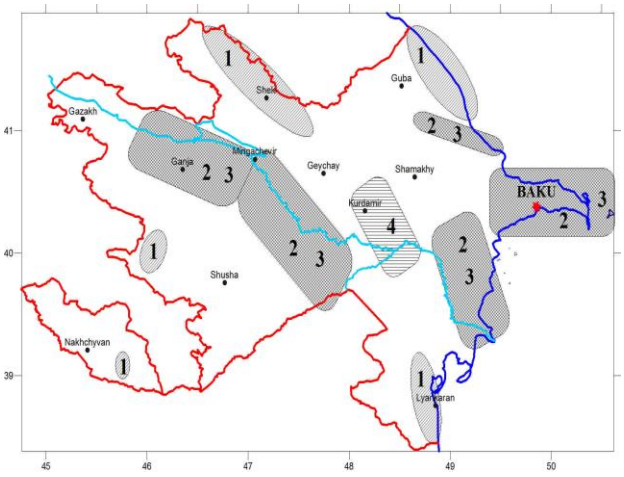


Figure 2. Schematic map of thermal fields of Azerbaijan
1 – Regions with thermal waters; 2 – Regions with mud volcanoes; 3 – Regions with oil and gas fields; 4 – Regions with petro-thermal systems

Table 1

Hydrogeological areas	Water T, °C	Water flow rate, m^3/day	Energy potential, MW
Absheron Peninsula	20-90	20000	up to 504
Kur depression	22-95	172466	up to $47 \cdot 10^3$
Greater Caucasus	30-50	2000	up to 168
Lesser Caucasus	30-74	4171	up to 771
Gusar foothill lowlands	30-97	21654	up to 609
Nakhchivan	40-53	3000	126-290
Talysh	31-64	14405	605-778
Lyankaran	42-84	7908	399-1129
Total		245604	Up to $51 \cdot 10^3$

Table 2

Well number	Mineralization, g/l	pH	T, ºC	Flow rate, l/sec	Energy potential, MW	
					ΔT=10ºC	ΔT=T-20°C
16	18.9		20	0.34	0.01	0
32	14.3		22	0.51	0.02	0
7/64	19.0		42	29.9	1.26	2.76
8/64	19.5	7	42	25.5	1.07	2.36
9/64	17.4	6.8	28	5.5	0.23	0.18
10/64	21.3		52	33.4	1.40	4.49
28	15.7		21	0.17	0	0
			Total	95.3	3.72	9.75

Mud volcanoes

Mud volcanism is one of the most interesting natural phenomena encountered in many countries of the world. A number of geological factors promoted development of mud volcanism in the South Caspian basin. The thickness of the sedimentary layer reaches 30 km, the upper 10 km being composed of the Pliocene-Quaternary predominantly clayey rocks deposited at extremely high sedimentation rates (up to 1300 m/my). Among the special features of the basin are low heat flow, abnormally high formation pressure, high degree of dislocation and seismicity, etc. In the South Caspian Basin, both onshore and offshore of Azerbaijan, there are over 300 mud diapirs and mud volcanoes. These mud structures are associated with the production of oil and gas field, because here production wells were drilled on the flanks of many onshore mud diapir structures.

For the first time temperatures of mud volcanoes in Azerbaijan were measured in 1904-1905. It was established that water temperature of mud volcanoes could be compared with the average annual temperature at this location.

Various anomalies of geothermal field were established in the area of mud volcanism development (Fig. 2). Against the overall low heat flow backgrounds across the basin, mud volcano sites stand out by comparatively high values of the parameter. Temperature gradients defined in the depth interval 0.3-1.5 m are very high and vary in the range of 0.02-21.25 K/m; it was established that temperature gradient declined with depth (Mukhtarov, 2003).

More extensive study of geothermal aspect regarding mud volcanoes was carried out in the course of oil and gas fields' development. As a result of these studies various anomalies of thermal field were identified, including decline of regional geothermal gradient with depth, and in the area of mud volcanism development (Мехтиев и др., 1971; Якубов, Атакишиев, 1973). Mud volcanoes are characterized by high values of heat flow density. At the same time in the areas of mud volcanism the regional values of heat flow density were below medium continental ones (Кашкай, Алиев, 1974; Алиев, 1988). Besides, Lower Kur depression is characterized by the lowest heat flows in the same

region. However, in all these cases the abnormal heat flow exceeds the medium value across the structure approximately twice and reaches just about 100 mW/m^2 at mud volcanoes.

Geothermal studies and the results of experimental determinations of rocks' thermal conductivity also allow evaluating the magnitude of thermal flows in wells at a number of fields on the Absheron Peninsula. Thus, at the Lokbatan field, thermal flows at 23 sites, evenly arranged along the structure, have been determined. Geothermal investigations were undertaken near the neck of mud volcano at two wells.

Maximum values of thermal flow were registered on these wells at the Lokbatan mud volcano field, 2.6 and 1.96 HFU (Heat Flow Unit, 1HFU = 42 mW/m^2), which is quite credible provided that the roots of mud volcano are located within the Upper Cretaceous deposits at a large depth (>6-12km). Also, the eruptive process promotes intensive heat transmission from the root horizons along with observed rock fragments of the same age.

Heat flow density was determined using drilled well temperature gradients and thermal conductivity of core samples. The offshore heat flow density through the Caspian Sea bottom was determined with the marine thermal probe. (Алиев и др., 2002; Nadirov et al., 1997).

It is necessary to note that mud volcanoes are distributed in a zone of minimum of thermal field (the thickness of the sedimentary layer reaches 20 km).

It turned out, that mud volcanoes are known by the high values of heat flow density. At the same time in districts of mud volcanism development regional values of heat flow density occurred below medium continental ones.

Other interesting places are crater fields of continuously erupting mud volcanoes in Azerbaijan, where local abrupt anomalies of temperature gradients and heat flows exceed and three magnitudes higher than regional background values of respective parameters. E.g. this fact was confirmed by measurements of heat flow in the area of a Haakon Mosby mud volcano in the Barents Sea, reaching 1045 mW/m^2. Similar local anomalies of a heat flow (210-600 mW/m^2) were found in the Caspian Sea.

These data demonstrate disintegrated character of the crust and high fluid-dynamic activity in the boundaries of tectonically active areas. In the boundary zones processes of heat-transportation are described by the equations of heat-mass transportation in porous media. As a result, abnormally high heat flows can be formed locally.

The results can hardly be explained in the context of the theory of thermal conductivity. So the process of simultaneous transportation of substance and heat through the channels of mud volcanoes should be considered. This process can be simulated as a thermal jet or as pressure filtration of fluids. That is described by the system of differential equations. The solution of this system shows the dependence of temperature from the depth.

Taking into consideration thermal features of fluids and rocks, and the temperature along the channel gives us an opportunity to explain the high temperature gradients on the surface and decrease of gradient with depth. It is similar to temperature distribution on the contours of the area of mud volcano; zones of hydrocarbons' formation are accordingly displaced upwards.

Thus, within the neck of mud volcano, in its deeper parts there are high temperatures and low gradient. With approach to the surface the gradient is sharply increased, and temperature falls down. It is necessary to take into consideration these conditions for estimation of parameters for formation of hydrothermal minerals (temperature dependence of depth and age) along the neck of the volcano.

Estimation of heat flow density shows that during eruption heat flow via the neck of mud volcano might be very high (10^8-10^{10} W/m^2).

Oil-gas fields and geothermal wells

There are thermal water wells at the Absheron oil fields (Fig.2). The most interesting one was drilled in Shikh field. This well (depth 2400 m) produced mineralized water with temperature 68°C, and this mineral water is being used for the balneo-therapy. Potential power of the well reaches 1.3 MW.

At the Absheron Peninsular thermal water was discovered by drilled wells at various depths and as natural outcrops. At the Absheron Peninsular, to the east from Hovsan village temperature of mineralized water from drilled wells reaches 100-135°C. Overflowing thermal waters are found in various places of the Absheron Peninsula. At Bibi-Eibat, near Baku, wells flow with chloride-hydrocarbonate sodium water, with mineralization 16.5 g/l, temperature 71°C and flow rate more than 450 m^3/day. In Gyuzdek well flowed with water with temperature over 50-65°C. Hot water also flows from wells in Gara-Eibat, Chilov Island and other places. With depth temperature of thermal water increases and mineralization falls down.

It is interesting to note that in many countries of the world, potential energy of each unit of low

potential geothermal energy sources varies between 1-4 MW. These types of sources are successfully used and this area is developing rapidly. Therefore, usage of this kind of geothermal energy sources has wide perspectives in Azerbaijan.

In exploration wells near Barda area within the depth interval 1500-1600 m thermal water was produced from Sarmatian deposits with the flow rate up to 1500 m^3/day and temperature 45°C. Thermal water with similar parameters also flowed from wells at Sorsor, Karajally, Beylagan, Sovetlar areas, etc (Fig.2).

It should be noted that at all Azerbaijan oil-gas fields numerous oil and gas exploration wells produced thermal water with temperature 100°C and above in relatively deep drilled intervals (Fig. 3).

Petro-thermal energy systems

To assess full energy accumulated within the Earth, all geothermal energy, including petro-thermal energy accumulated within the solid rock and formation fluids must be evaluated (Fig.2). Various methods of the assessment of geothermal resources are available. In this work new methods developed in the countries of Western Europe were used. For the evaluation of density of geothermal resources they represent restorable part of geothermal energy that could be recovered and used. In the countries of Western Europe researchers use the model of volume content of heat in porous reservoirs.

Based on geothermal data of deep wells from various regions density of geothermal resources in Pliocene deposits in Azerbaijan per unit of area (1 m^2) was calculated, and map of distribution of geothermal resources in the Pliocene deposits has been plotted on the base of these data. It was found that density of geothermal resources in Pliocene deposits per unit of area varied within the range of 10-75 MW (Асадова, Мухтаров, 2013).

Business opportunities

It is known that in the Earth concentrated significant amount of thermal energy (geothermal energy) and within certain conditions it is possible to use this energy. In some cases (when the eruption of volcanoes, hot springs, pressure of thermal water wells, etc.), this energy is delivered to the surface of the Earth by natural ways, with increasing ways of geothermal energy using. In other cases, despite the presence in the bowels of the earth a significant amount of geothermal energy that falls on each square meter of surface, its use is accompanied by a host of problems, chief among which is the delivery of geothermal energy from the depths to the surface. This, in turn, is one of the important factors responsible for the profitability and efficiency of geothermal energy. From this point of view beneficial objects (except for the natural output of geothermal energy) are oil and gas fields, which from the earth

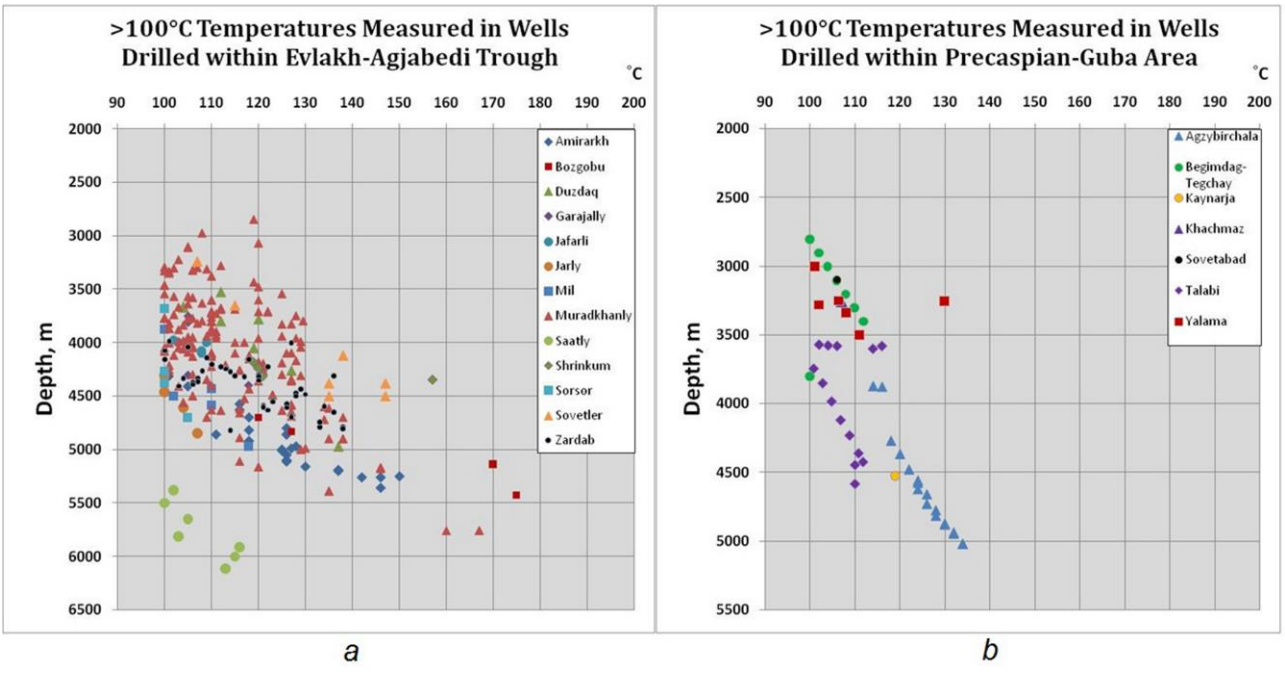


Figure 3. Temperature vs Depth graphs based on data > 100°C from drilled wells in Evlakh-Agjabedi and Precaspian-Guba areas

to the surface derived substrates (water, oil, gas) - carriers of geothermal energy by technical ways. It should be noted that this issue is still not fully understood and its value is scientifically not justified. Therefore, in this project, the task of a comprehensive science-based study of the issue and assessment of geothermal energy resources that are brought to the surface in the oil fields, and a study of the prospects for its use.

Recently, efficiency of the use of thermal energy depended mainly on drilling deep wells. However there are many plugged and abandoned exploration wells in Azerbaijan and these wells could be restored and used for the production of geothermal energy with less investments. Main objective now is the identification of optimal locations of drilled wells with higher geothermal potential and use of this energy. Institute of Geology and Geophysics of the Azerbaijan National Academy of Sciences has vast database with the geothermal data. At present we analyse these data in order to identify optimal sites for the construction of geothermal stations, efficient heat pump unit and also sites for hybrid installations.

State plans envisage increasing several folds volumes of energy produced from alternative sources to 2020. The primary task of specialists involved in research and development is to support implementation of these plans and propose the best sites for effective investments. The purpose of this paper is to summarize and to present a key information about geothermal sources (such as hot springs, mud volcanoes, thermal wells, etc.) in Azerbaijan and adjust results with the opportunities of modern thermal technologies and business opportunities.

Underground water, oil, gases are an example of fluids, actively involved in the process of heat transfer in the Earth's crust convective means. If we consider that in Azerbaijan every year from the bowels of the earth are extracted millions of tons of oil, and this oil carries with it the heat from the interior to the surface, then we get up an interesting problem in connection with geothermal energy. This question has remained without a study and only recently, after the problem of shortage of energy in the world has become urgent, researchers began to pay attention to it (Muxtarov, 2004; Sanyal, 2011). Recently, in connection with the problem of energy shortage and global warming, how to search and use alternative forms of energy have become urgent. Therefore, the assessment of associated geothermal energy carried by the produced oil, and the study of the prospects of using this energy came to the fore as an important task of the day.

REFERENCES

MUKHTAROV, A.SH. 2003. Geothermal energy discharge from mud volcano Channel. In: *Energy – Our Monumental Task* AAPG Annual Meeting Abstract book, May 11-14, Salt Lake City, Utah.

NADIROV, R.S., LERCHE, I., BAGIROV, E., TAGIYEV, M. 1997. Geohistory, thermal history and hydrocarbon generation history of the north-west South Caspian Basin. *Marine and petroleum geology,* 14, 4, 363-382.

SANYAL, S.K. 2011. Geothermal power capacity of petroleum wells. In: *Geothermal Energy Utilization Associated with Oil & Gas Development* abstracts. June 13-15, Dallas, Texas, http://smu.edu/geothermal/Oil&Gas/Oil&GasPresentations.htm

MUXTAROV, A.Ş. 2004. Neft və qaz mədənlərinin istismarı zamanı səmt geotermal enerjisi. *Azərbaycanın geotermal resursları və onların xalq təsərrüfatında istifadə edilməsi* Respublika seminarının materiallarında. Baku, 31.

АЛИЕВ, С.А., МУХТАРОВ, А.Ш., АЛИЕВА, З.А., БАГИРЛИ, Р.Дж. и др. 2002. Геотермические исследования в Азербайджане. В кн.: *Геология Азербайджана. Том V –Физика Земли*. Баку, Nafta-Press, 259-261.

АЛИЕВ, С.А. 1988. Геотермические поля депрессионных зон Южно-Каспийской впадины и их связь с нефтегазоносностью. Дис. док. геол.-мин. наук. Баку. 324 с.

АСАДОВА, А.В., МУХТАРОВ, А.Ш. 2013. Ресурсы геотермальной энергии по республике Азербайджан. *Мониторинг, наука и технологии,* 2(15), 24-28.

КАШКАЙ, М.А., АЛИЕВ, С.А. 1974. Тепловой поток Куринской депрессии. В сборнике: *Глубинный тепловой поток Европейской части СССР.* Киев, Наукова думка, 95-108.

МЕХТИЕВ, Ш.Ф., МИРЗАДЖАНЗАДЕ, А.Х., АЛИЕВ, С.А. 1971. Геотермические исследования нефтяных и газовых месторождений. Москва. Недра. 215 с.

МУХТАРОВ, А.Ш., ХАММЕДОВ, А.М. 2003. Геотермальные ресурсы Азербайджана. В сб*: Проблемы развития геотермальной энергии в странах СНГ и деятельность международного Геофонда, Материалы Международного Семинара*. Москва. 27-32.

НАДИРОВ, Р.С. 1985. Геология и нефтегазовый потенциал зоны Талыш-Вандамского гравитационного максимума. Дис. док. фил. по геол.-мин. наук. Баку.

ТАГИЕВ, И.И., ИБРАГИМОВА, И.Ш., БАБАЕВ, А.М. 2001. Ресурсы минеральных и термальных вод Азербайджана. Чашыоглу. Баку. 168 с.

ЯКУБОВ, А.А., АТАКИШИЕВ, И.С. 1973. Геотермические исследования нефтегазовых месторождений Апшерона. Баку. 86 с.

THEORY AND PRACTICE OF OIL AND GAS FIELDS DEVELOPMENT

© Z.Y.Abbasov, V.F.Fataliyev, 2015

PHYSICAL EXPLANATION OF THE RETROGRADE CONDENSATION PROCESS IN THE GAS-CONDENSATE RESERVOIR CONDITION

Z.Y.Abbasov, V.F.Fataliyev

Institute of Geology and Geophysics, Azerbaijan National Academy of Sciences
119, H.Javid ave., Baku, AZ1143

The paper studied the phase behavior of the gas-condensate systems in the porous media. Special experimental investigations and theoretical analyses have been conducted for learning the colloidal characteristics of the gas-condensate systems and its importance in reservoir condition. Using this obtained information a new explanation about the nature of the condensation process was given and also some theoretical aspects were detailed differently. The conclusions were tested and proven on the natural gas-condensate reservoir in accordance with analysis of real gas-condensate producing well performance.

Introduction

Gas-condensate reservoirs exhibit complex phase and flow behaviors during the depletion of the reservoirs. It associates a loss of valuable condensate fluid in the reservoir and also results in appearance of condensate banking in the near well region. A good understanding of the effect of the changing composition on the flow and phase behavior properties of these reservoirs is essential for carrying out accurate forecasts of the performance of gas condensate reservoirs (Raghavan, Jones, 1996; Katz, Kurata, 1940). Usually the phase transitions of gas-condensate systems are studied in PVT cells which are free from porous media and may affect the quality of results (Chatenever, Calhoun, 1952). Also the dew point pressure of the system which is very important for projecting the exploitation of the gas-condensate pool could be determined incorrectly.

Investigation the effect of porous media on gas-condensate phase behavior or dew point pressure has been studied since middle of last century (Chatenever, Calhoun, 1952; Razamat, Mardakhaev, 1976; Sigmund et al., 1973). Most of the obtained experimental data have proved that the phase behavior of the gas-condensate systems in the reservoir model is entirely different from the PVT cell which is porous media free vessel. In other words, the retrograde dew point pressure of gas condensate system is higher in the porous media than in the porous free media PVT cell (Trebin, Simako, 1977).

Researchers confirm that there are many aspects: condensate/gas ratio, condensate density, thermodynamic condition, lithological properties of the formation etc, should be considered for deeper investigation this phenomenon. Also, connate water in the porous media, it's physical and chemical feature, porosity and the specific surface of the formation granular could be very important factors (Abasov et al., 2013; Abbasov, Fataliyev, 2015; Trebin, Zadora, 1968).

In recent years, there are many papers have been published which related to this subject. All of them emphasize the importance of this phenomenon regarding the gas-condensate field exploitation and development (Abasov et al., 2013; Abbasov, Fataliyev, 2015; Li Mingjun et al., 2008; Mirzadzhanzade et al., 2003). One of the detailed investigation was carried out by us which covered in these papers (Abasov et al., 2013; Abasov et al., 2009). We analyzed all effected parameters and selected those parameters (pressure, temperature, specific surface and porosity of porous media, amount of connate water and condensate density) which have significant role in this exercise. Rational mathematical methods were used for modeling gas-condensate reservoir condition, depletion process of the gas-condensate reservoir and also for planning experiments. The advantage of this study is a mathematical equation was obtained which presented the correlation between the effected parameters. However, this investigation could not explain the physical or thermodynamic nature of the effect.

In the paper (Abbasov, Fataliyev, 2015), we tried to explain the mechanism of the depletion process in the porous media. Experimental investigations on groups of gas-condensate samples from Azerbaijan natural gas-condensate reservoir confirmed that two phases-gas and condensate can be flowing to the well even when reservoir pressure is higher than retrograde dew point pressure of reservoir fluid. This phenomenon can cause condensate blockage or condensate banking on the early stage of reservoir development, results from a combination of different factors. Theoretical and experimental data was summarized, the gas-condensate system was analyzed as a colloidal-dispersion solution and identified that retrograde condensation in porous media can be caused by break off the Brownian motion due to absorption process between sub-micron-sized condensate particles and formation rock granular surfaces.

Summarizing all results of existing works show that the phase behavior of gas-condensate fluid in the reservoir condition plays a significant role in the deliverability evaluation and in the forecasting of gas condensate fields. If neglecting its effect on the deliverability, gas and condensate production rates could not be accurately predicted. In this sense it is very important to understand the mechanism of the retrograde process in the reservoir conditions (Abasov et al., 2005; Ke-Le Yan et al., 2013). Some valuable points related to this issue have been explained in works (Abasov et al., 2009; Razamat, Mardakhaev, 1976) however full explanation has never been given and in-depth study is required.

In this work, a new approach is displayed to explain the physical features of the retrograde condensation process in the porous media. The issue is analyzed base on experimental and theoretical investigations. Using this obtained information a new explanation of the process was given and some theoretical aspects were detailed differently. Also the theoretical conclusions were tested and proven on the natural gas-condensate reservoir in accordance with analysis of real gas-condensate well performance.

Experimental apparatus and procedure

Experiments have been carried out on УГК-3 type of PVT bomb which is standard apparatus designed for determining thermodynamic characteristics and phase behavior of gas condensate systems (Zotov, Aliev, 1980). Maximum working pressure is 45MPa, maximum working temperature is 80^0C and cell volume is $3x10^{-3}$ m^3. The PVT cell is composed of an efficient magnetic fluid mixer mounted on the piston, a dedicated visual head, two sampling valves, an accurate pressure transducer and an electric heater for homogeneous temperature control. In addition, the original design has been slightly modified within the safe operating limits. In order to perform or to model reservoir depletion process and constant composition expansion test in the high temperature range, a heat exchanger was installed to increase working temperature of the bomb up to 110^0 C. Also this unit linked with nitrogen bottles and vacuum pumps which are used for purging, cleaning and preparing the cell for preservation or next operation.

An eyeglass permits observation of the fluid behavior through the cell windows. During Constant Composition Expansion-CCE or Differential Condensation-DC testes, the changes of the gas and liquid phases are observed by the full visibility of the gas/condensate interface through the window of the cell. CCE and DC test procedures are stated in the work (Zotov, Aliev, 1980).

The reservoir model was designed in accordance with mathematical criteria. Porous media composition and other aspects were comprehensively described in the paper (Abasov et al., 2013).

Results and discussions

The colloidal feature of the gas-condensate system

The study of the phase behavior of fluid at high pressure has been mainly restricted to mixtures containing either two or three components. Our understanding of fluid phase equilibria has almost exclusively relied on experimental observation and calculations have only played a relatively minor supporting role. This is likely to change when ternary and other multicomponent mixtures are considered. The most fascinating aspect of high pressure equilibria is perhaps the diversity of critical transitions (Sadus, 1992). It is a common knowledge that a thermodynamic state of fluid is specified by thermodynamic parameters or variables e.g. pressure, temperature, volume, the mole fraction of one of its components (Deiters, Kraska, 2012). If one of these parameters changes in equilibrium condition the system moves to next thermodynamic state. If this change results in phase transition then at first micro embryos of the new phase appears and then they slowly growth as accordance leading parameters. This phase transition mecha-

nism was studied and confirmed by many famous scientists (Mirzadzhanzade et al., 2003). That means, this process is applicable for gas-condensate systems as well. In order to learn the forming of the liquid phase in the gas-condensate mixture near the retrograde condensation region, specific experiments were carried out. УГК-3 type of PVT bomb was used for that. Samples were taken from Azerbaijan gas-condensate field "Bulla-deniz". The reservoir fluids were then prepared in the laboratory by recombining the separator condensate with the separator gas according to the gas/condensate ratio data, based on a standard analytical method for condensate gas properties (Abasov et al., 2013; Zotov, Aliev, 1980). The composition of the gas is C_1-91.61, C_2-4.79, C_3-1.41, C_4-1.64, C_5-0.53, C_6-0.02% and gas density is 0.7322kg/m^3. Condensate density is 745.7kg/m^3 and condensate/gas ratio of recombined gas-condensate system is 250g/m^3.

A constant composition expansion (CCE) test was performed to determine the retrograde dew point-RDP pressure and liquid dropout behavior of the fluid. In this work, similar experimental phenomena for the CCE test monitored through the windows of the PVT cell for gas-condensate systems. As an example, here is the description of our observations when we introduced the process at a temperature of 100^{0}C during the CCE test.

The prepared sample was pressurized to above the dew point pressure-28MPa in isothermal condition. The fluid was a single phase that was transparent and pale yellow in color. As the CCE test proceeded and the pressure dropped, the color of the reservoir fluid also changed gradually from pale yellow to pale red. When the pressure was decreased to close to 24.6MPa the fluid began to fog up. This pressure accepted as a fog up pressure-FUP. Then the fog thickened with decreasing pressure. The convective phenomenon of the thick fog was observed by the naked eye through the PVT cell window. With a continuous drop in pressure, a tiny liquid drop precipitated, at the corresponding pressure-22.68MPa which was the retrograde dew point pressure-RDPP of the gas-condensate system. In this group of experiments, the FUP and RDPP were determined at the different temperatures. These data allowed us to define the correlation between FUP, RDPP and temperature which is presented in fig. 1.

As shown in the Fig. 1, there is a significant difference between FUP and RDPP, also the deference is increasing with the increase of temperature. It is known that microscopic particles of one phase dispersed in another are generally called colloidal solutions or dispersions (Pashley, Karaman, 2004). It means that the fog which we observe in gas-condensate system is colloidal state of system. In this case the gas is dispersion medium and condensate is dispersed phase. If pressure decreases at a constant temperature, surface energy of dispersed phase increases and creates an environment for coalescing fine condensate particles.

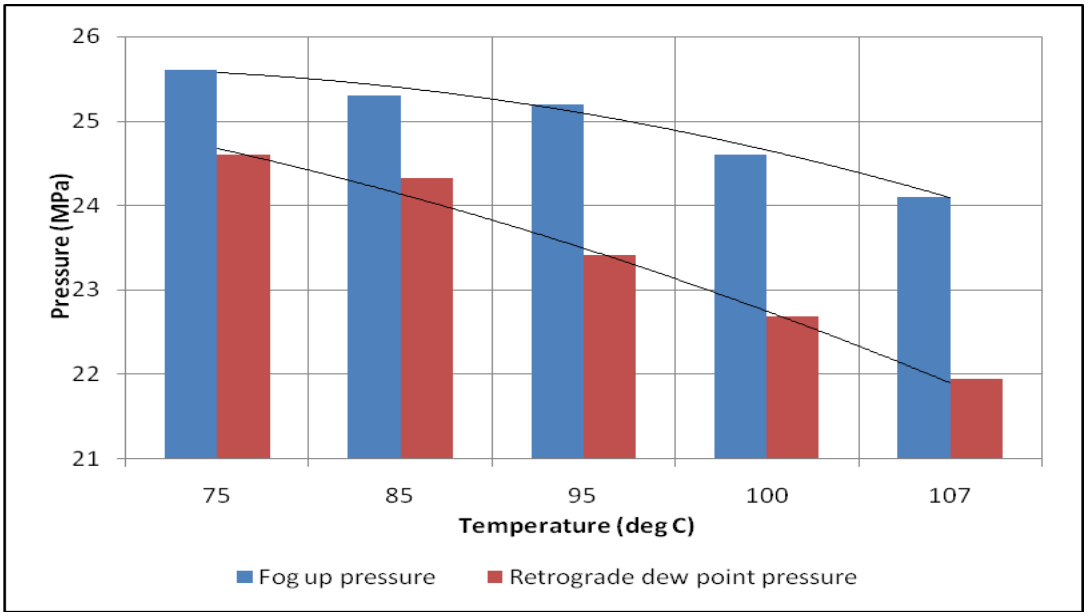


Figure 1. Variation of the fog up and retrograde dew point pressures during constant composition expansion test on gas-condensate systems at different temperatures.

These sub-micron-sized particles grow following pressure drop and turns into aerosol-colloidal state which can be seen as the fogging up process. Also increasing the deference between FUP and RDPP with the increase of temperature can be considered well-matched with the properties of colloidal substances.

In line with this conclusion, it can be assumed that it is the reason why a given constant temperature retrograde dew point pressure of the gas-condensate system in the porous media is higher than in the free cell. In other words retrograde condensation can happen even the liquid phase is in the early or embryo state (Abbasov, Fataliyev, 2015; Razamat, Mardakhaev, 1976). Fog state of the system could be a very suitable condition for intermolecular forces around a molecule in the liquid embryos and formation granular surfaces to dominate liquid to be dropped out at the pressure higher than it was identified in the porous media free PVT cell.

The physical nature of the phase transition in reservoir condition

Understanding the physical nature of this process can play a particularly vital role in gas-condensate reservoirs. Condensate liquid saturation can build up near a well because of early condensation and the near-well choking can cause unstable operation. For more learning this proposition, we used an experimental data which provided in the paper (Abasov et al., 2009). Their intention was to identify the impact of porous media on condensate recovery factor, however some useful information was there that allows a comparison of a couple of experiments that were carried out in parallel on reservoir model and free PVT cell.

Samples were taken from Azerbaijan gas-condensate field "Bulla-deniz". The reservoir fluid was then recombined in the laboratory environment. The composition of the gas was C_1-93.5, C_2-4.2, C_3-1.24, C_4-0.65, C_5-0.14, C_6-0.05, CO_2-0.22%, C_{5+}-6.02 g/m^3 and gas density was 0.7243 kg/m^3. Condensate density was 737.9 kg/m^3 and condensate/gas ratio of recombined gas-condensate system was 200 g/m^3.

The prepared sample was pressurized up above the RDP pressure-30 MPa at a temperature of 100^{0}C as per procedure. The fluid was a single gas phase state. Same temperature and pressure were maintained in the reservoir model using heat exchanger and high pressure nitrogen bottle. In the thermodynamic equilibrium condition, the gas-condensate system was squeezed from PVT cell to the reservoir model and nitrogen replaced slowly. It was continued until same fluid composition was confirmed in the model. Then reservoir model was isolated from PVT cell without disturbance of equilibrium condition. Depletion regime was modeled on both vessels using differential condensation-DC procedure. The amount of gas and condensate which were removed from the system, were measured in the separator. Separation pressure-5MPa and temperature-22^{0}C were maintained during the experiments. These set points were identified as a maximum liquid drop out condition as per special experimental trials which had been carried out before this experimental study. It is required depletion rate to be maximum 8.33-16.67x10^{-6} m^3/sec for two reasons: to maintain thermodynamic equilibrium condition in the PVT cell/reservoir model and to maintain optimal separation condition in the separator. Gas chromatography was used to analyze hydrocarbon compositions. FUP and RDPP were identified 26.4MPa and 24.3MPa respectively in the PVT bomb. Results are given in the fig. 2.

As it is shown in the fig. 2 retrograde condensation pressure in the reservoir model is higher than in the PVT bomb. After applying empirical and graphical analyses the gas-condensate system RDPP has been identified 29MPA in the reservoir model (Abasov et al., 2009). It proves that retrograde condensation of gas-condensate system can start above the aerosol/fog state of the system in porous media condition.

One of the interesting points in this fig.2 is we can see that retrograde condensation process accelerates in the reservoir model when pressure is below RDPP which was identified in the PVT bomb. That evidences that in this pressure interval gravitational force starts to lead the retrograde condensation progress.

The properties of colloidal solutions are intimately linked to the high surface area of the dispersed phase, as well as to the chemical nature of the particle's surface. How it can happen, we can see from simple physics. Three fundamental forces operate on fine particles in solution: 1) a gravitational force, tending to settle or raise particles depending on their density relative to the solvent; 2) a viscous drag force, which arises as a resistance to motion, since the fluid has to be forced apart as the particle moves through it; 3) the 'natural' kinetic energy of particles and molecules, which causes Brownian motion (Pashley, Karaman, 2004). However, the situation can change dramatically if colloidal substance is located in very tiny pores and directly contacts with large solid granular surfaces. Surface energy and force between granular surface and dispersed phase leads to the adsorption process.

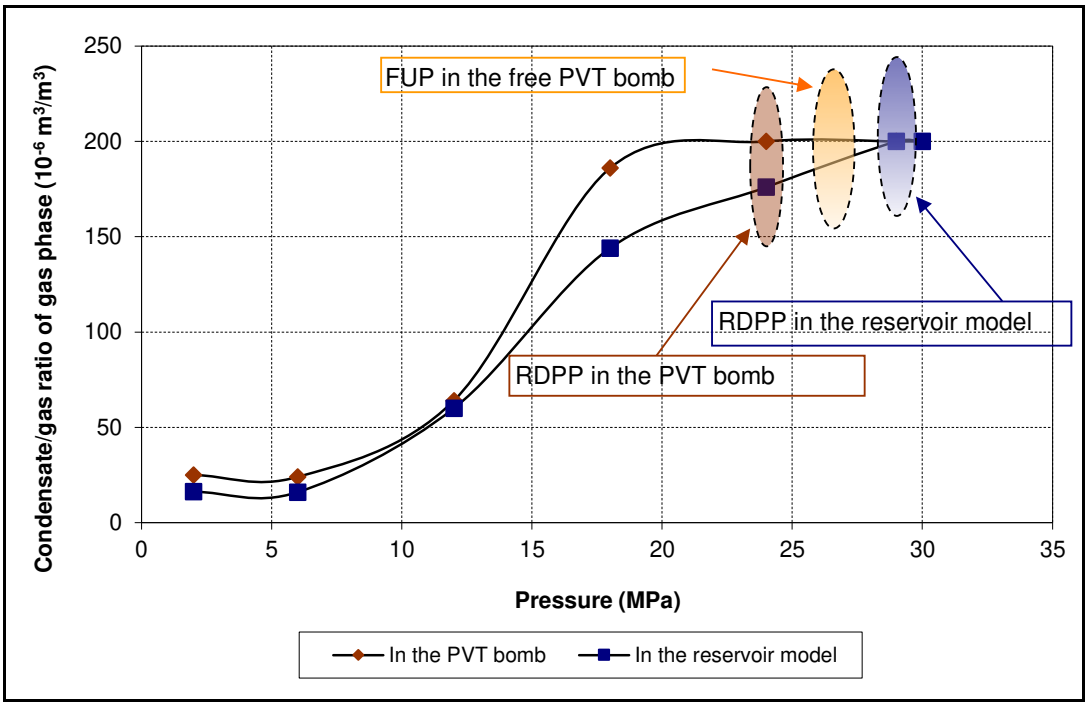


Figure 2. Differential condensation isotherms of gas-condensate fluid at temperature of 100 deg. C in the free PVT bomb and reservoir model.

Exactly this adsorption process between submicron-sized condensate particles and formation rock granular surfaces in the porous media causes early condensation when even gas-condensate system is above FUP which is identified in the PVT bomb. This will progress until then porous media saturated with hydrocarbon condensate. If pressure continuously depletes, then the condensate particles grow larger. When pressure is around RDPP (identified in the PVT cell) region the gravitation force will dominate the process and at some stage, break off the Brownian motion and will correspond to the maximum weight of the drop that can hang in the dispersion medium which is gas. That is reason why retrograde condensation was accelerated at this pressure point in the fig. 2. Also vertical filtration can occur due to gravity force being larger than the surface force in the reservoir condition at some stage when pressure is around or below RDPP (which was identified in the PVT bomb). However, this conclusion is obtained as the results of the experimental and theoretical studies. There is a need this conclusion to be tested in real reservoir condition because of some toleration on the modeling of formation condition and reservoir depletion process.

For this purpose, we analyzed the performance of a couple of wells on "Bulla-deniz" gas-condensate field. These wells are first drilled wells and that is why we could get some relevant information about formation flow characteristics in the downhole zone of the wells at early stage of field development. Well No20 average daily condensate/gas ratio per month in first two years was presented in the work (Abbasov, Fataliyev, 2015). For more detailed analyses, we included well No25 information as well (fig. 3).

Well No20 was drilled in April 1976, depth is 5443 m. Well No25 was drilled in June 1977, depth is 5757 m. Both wells belong to horizon VII which initial reservoir pressure – 71MPa, reservoir temperature –102^{0}C and condensate density – 800kg/m^3 were determined. Retrograde dew point pressure obtained 62.5MPa in the УГК-4 type of PVT bomb as per thermodynamic analyses on well No20 in 1976 (Abasov et al., 2013).

As it is shown in the fig. 3 condensate/gas ratio was increasing in the first 5 months since the well No20 started. In this period of time the factor even exceeded the condensate/gas ratio of this reservoir which was 362 g/m^3. It evidences that, two phases were flowing to the well in this period of time however reservoir pressure (71MPa) was above the retrograde dew point pressure (62.5MPa). It can be assumed that this was just stabilization period after drilling. There is a visible decrease over the next few months but then this continues in a cyclic trend. Same cyclic trend is presented for well No25 however during this time, reservoir pressure (65Mpa) was still above the fluid RDPP.

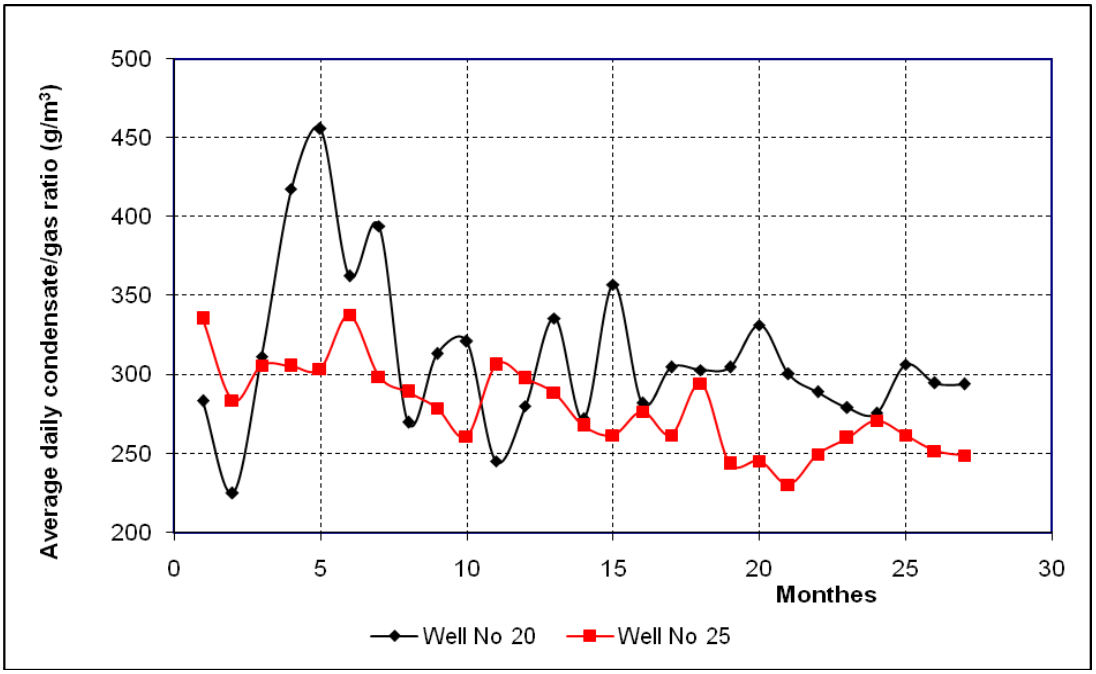


Figure 3. Average daily condensate/gas ratio characteristic of well No20 and No25 in first two years on "Bulla-deniz" gas-condensate field of Azerbaijan.

Reason for this phenomenon was explained that there are free condensate pools existing at some areas in the reservoir. These condensate pools can take part in the hydrodynamic processes and flow to the well under pressure gradient (Mirzadzhanzade et al., 2003). This explanation can answer some questions but it is well known that the field has been forming for many years under the influence of gravity. In this circumstance it looks unlikely that moveable condensate pools to be exist in some areas of the single gas phase region of the reservoir. Taking into account the results obtained above, we tried to explain the route differently.

At the time of discovery, a typical gas-condensate reservoir pressure might be above or close to the retrograde dew point pressure. If reservoir pressure is above system RDPP, then at this time there only single-phase gas exists. However, as the production is carried out, there is isothermal pressure decline and as the downhole pressure in a flowing well falls below a certain point of reservoir pressure which can be higher than FUP a liquid hydrocarbon phase is formed. In other words retrograde condensation starts at an earlier stage because of surface forces between sub-micron-sized condensate particles in the dispersed phase with formation rock granules. This condensate formation results in buildup of a liquid phase around the downhole, leading to a decrease in the effective permeability to gas into the wellbore. The productivity loss associated with condensate buildup can be substantial. The liquid dropout first occurs near the wellbore and propagates radially away from the well along with the pressure drop. Closer to the well, in the vicinity of the downhole where the liquid saturation reaches a critical value and the effluent travels as two-phase flow under pressure gradient. That repeats from time to time, so downhole zone washes periodically.

Conclusion

The colloidal feature of the gas-condensate system was investigated base on group of gas-condensate samples from Azerbaijan gas-condensate field "Bulla-deniz". It was confirmed that gas-condensate fluid is in dispersed condition when pressure is above the retrograde dew point pressure. If pressure decreases at a constant temperature, surface energy of dispersed phase increases and creates an environment for coalescing fine condensate particles. These sub-micron-sized particles grow following pressure drop and turns into aerosol-colloidal state which can be seen as the fogging up process. This transition pressure is defined as a fog up pressure-FUP. Also, confirmed that increasing the deference between FUP and RDPP with the increase of temperature can be considered well-matched with the properties of colloidal systems.

Furthermore, detailed analyses of experimental and theoretical studies, it was concluded that the surface energy and force between granular and dispersed phase surfaces leads to the adsorption process. Exactly this adsorption process between sub-micron-sized condensate particles and formation rock granular causes early condensation when even gas-condensate system is above FUP which is identified in the PVT bomb. This means that, if these factors are not analyzed or studied correctly at the beginning of the field development sooner or later production performance can suffer

This phenomenon was verified in real situation. For that, the flow behavior of the couple of wells on "Bulla-deniz" gas-condensate field was examined. Reason for flowing two phases when even reservoir pressure is above fluid retrograde dew point pressure stated differently using basic knowledge about colloidal substances

Acknowledgements

The authors wish to thank PhD Hamidov N.N. (lead researcher) for encouragement and guidance throughout the experimental investigation, PhD Mamedova G.H. and Salimova T.A. for the manufacture and maintenance of the experimental facilities.

REFERENCES

ABASOV, M.T., ABBASOV, Z.Y., FATALIYEV, V.M., HAMIDOV, N.N. 2005. A new phenomenon in phase transformations of gas-condensate systems and its experimental study. *Doklady (Earth Sciences) of Russian Academy of Sciences,* 403A, 6, 858-860.

ABASOV, M.T., ABBASOV, Z.Y., FATALIYEV, V.M., HAMIDOV, N.N., MAMMADOVA, G.H. 2013. Applied thermodynamic aspects in oil and gas production. Nafta Press. Baku, 212 p. (in Russian).

ABASOV, M.T., ABBASOV, Z.Y., FATALIYEV, V.M., HAMIDOV, N.N., MAMMADOVA, G.H. 2009. Phase transformations in condensate pool development. *Doklady (Earth Sciences) of Russian Academy of Sciences,* 427A, 6, 939-942.

ABBASOV, Z.Y., FATALIYEV, V.M. 2015. About the physical nature of the retrograde condensation pressure of gas-condensate systems in the porous media condition. *The Reports of National Academy of Sciences of Azerbaijan,* LXXI, 1, 60-65.

CHATENEVER, A., CALHOUN, J.C. 1952. Visual examination of fluid behavior in porous media. *Pet. Trans AIME (Petroleum Div.),* 195, 149-156.

DEITERS, U.K. KRASKA, T. 2012. High-pressure fluid phase equilibria. Elsevier. 370 p.

KATZ, D.L., KURATA, F. 1940. Retrograde condensation. *Ind. Eng. Chem.,* 32 (6), 817-827.

KE-LE YAN, HUANG LIU, CHANG-YU SUN, QING-LAN MA, GUANG-JIN CHEN, DE-JI SHEN, XIANG-JIAO XIAO B., HAI-YING WANG. 2013. Measurement and calculation of gas compressibility factor for condensate gas and natural gas under pressure up to 116 MPa. *J. Chem. Thermodynamics,* 63, 38-43.

LI MINGJUN, DU JIANFEN, BIAN XIAOQIANG. 2008. Advances on condensate oil-gas phase behavior research in porous medium. *Fault-Block Oil & Gas Field,* 01, 618.

MIRZADZHANZADE, A.Kh., KUZNETSOV, O.L., BASNIEV, K.S., ALIEV, Z.S. 2003. Foundation of gas recovery technology. Nedra. Moscow. 880 p. (in Russian).

PASHLEY, R.M. KARAMAN, M.E. 2004. Applied colloid and surface chemistry. John Wiley & Sons Ltd. 190 p.

RAGHAVAN, R., JONES, J.R. 1996. Depletion performance of gas-condensate reservoirs. *JPT*, 725-731.

RAZAMAT, M.S., MARDAKHAEV, I.M. 1976. On the mechanism of the influence of a porous media on phase transformation of gas-condensate mixtures. *Doklady, AN Az SSR,* 6, 24-27 (in Russian).

SADUS, R.J. 1992. High pressure phase behavior of multicomponent fluid mixture. Elsevier. Amsterdam-London-New York-Tokyo. 392 p.

SIGMUND, R.M., NORROW, N.R., PURVIS, R.A. 1973. Retrograde condensation in porous media. *Soc. Petrol Eng. J.*, 2, 93-104.

TREBIN, G.F., SIMAKO, V.A., 1977. About the phase transformation of the reservoir fluid in porous media. *Trudi, VNII neft*, 37, 75-82 (in Russian).

TREBIN, G.F., ZADORA, G.I. 1968. Experimental study of influence of porouse media on phase transformation in gas-condensate system. *Izv. Vyssh. Uchebn. Zaved., Ser. Nefti Gaza*, 8, 37-41 (in Russian).

ZOTOV G.A., ALIEV Z.S. 1980. Instructions for integrated study of gas and gas condensate reservoirs and wells. Moscow, Nedra, 301p (in Russion).

© F.Gümrah, A.Aliyev, O.Ozavci, 2015

EVALUATION OF DRIVE MECHANISMS ON OFFSHORE OIL RESERVOIRS BY ANALYTICAL METHODS

F.Gümrah[1], A.Aliyev[2], O.Ozavci[3]

1 – *Genel Energy,*
Dumlupinar Bulvarı, No 3A-10, Ankara, Turkey

2 – *BP Caspian, 153, Neftchiler ave., Baku, AZ1010*

3 – *Bahar Energy Operating Company,*
Zig shossesi, Gum Adası, Baku, AZ1011
email: fevzi.gumrah@genelenergy.com
ala6ju@bp.com
omur.o@baharenergy.az

Gum Deniz Oil Field played the important role in energy production from Caspian Region. The Field is still under production and needs further engineering studies to recover more energy from the remaining reserves by controlling environmental issues. Therefore, the reservoir performance and drive mechanisms of an oil reservoir in Gum Deniz Oil Field, Azerbaijan, were determined by material balance and simulation studies. The oil in place, average reservoir pressure, amount of water encroachment, fluid saturations, recovery factor and the type of reservoir drive mechanisms were estimated based on field production data. The estimated oil in place was 35.4 MMstb. Initially, the dominant reservoir drive mechanism was depletion drive together with compaction drive and fluid expansion mechanisms. After water encroachment, both water drive and depletion drive mechanisms played important roles on fluid production. The current and ultimate recovery factors were obtained as 25 and 37% of OOIP, respectively.

FIELD AND RESERVOIR DESCRIPTION

Gum Deniz (GD) was one of the important oil fields of Azerbaijan at Caspian Sea. The GD Oil Field lies in shallow water approximately 20 km southeast of Baku immediately off the coast of Azerbaijan. Following discovery in the early 1950's, production began from the GD oil Field in 1955. As of the end of 2009, ~32.9 million m^3 (207 million bbls) of oil and ~16.5 Bm^3 (581Bcf) of gas were reported as having been produced from the field. The company reported that 484 wells have been drilled historically, with 61 wells reported on production at the end of September 2010 using gas lift. The GD Oil Field is a faulted anticline (16 fault blocks) located up dip from the Bahar Gas Field. Of the fault blocks, 11 are reported as having established commercial production. 12 separate pay zones over ~1525 m (IV, V, VI, VII, VIII, IX, X, SP, NKP, KS, PK, KaS) have been identified in the field, with three to four found (on average) in each of the productive fault blocks. These intervals are composed of alternating sandstones and shales. Average crude from the field has 36° API gravity; although this ranged from 30° API to 45° API. Similar to the Bahar gas field, the reservoir rocks (sandstone and siltstones) are of good quality, with 10% to 22% porosity and most of the producing zones display permeability in the 100 mD to 230 mD range. Historical peak production from the field was achieved to 7.378 m^3/d (46,400 bpd) in 1964.

The primary reservoir sands are contained in the upper and middle parts of the Productive Sequence – the Surakhany, Sabunchi, Balakhany and Pereryva suites. The lower parts of the Middle Miocene consist primarily of mudstone with thin impersistent sandy units. Reservoir quality in the Productive Sequence is a function of three main criteria – reservoir facies, the provenance of the sands and burial depth. Sandstone and siltstone reservoirs of the Productive Sequence are sealed by numerous intra-formational mudstones and shales (Abreu, Nummedal, 2007).

Rock and fluid data

Permeability-porosity relationship

The wells on the field have been logged using various Russian logging tools. Permeability was estimated from routine porosity and permeability measurements performed on cores. From the avail-

able data, the following relationship between permeability and porosity was established.

$$k = 0.1615e^{0.3387\phi} \quad (1)$$

Where k (permeability) in mD and ϕ (porosity) is in percentage.

Pore compressibility

Rock strength is estimated from two common laboratory techniques; unaxial compressive strength (UCS) tests, and triaxial or confined compressive strength tests. UCS tests is used to determine the ultimate strength of a rock, i.e., the maximum value of stress attained before failure (Fjaer et al., 1992). UCS (Bruce, 1990) was calculated for unconsolidated (loose) sand. The correlation between the formation compressibility and porosity was developed by using Newman's study (1973). The properties can also be used for estimating sand failure problem during production (Collins, 2002).

PVT Data

The PVT properties can be obtained from a laboratory experiment using representative samples of the crude oils. However, the values of reservoir liquid and gas properties must be computed when detailed laboratory PVT data is not available. Correlations on PVT which is commonly used in the oil industry are important tools in reservoir-performance calculations. For developing PVT correlation, the chemical composition of crude oil must be considered (Mahmood, Al-Marhoun, 1996). Because of the availability of a wide range of correlations, it is beneficial to analyze them for a given set of PVT data belonging to a certain geological region. Therefore, PVT correlations need to be modified prior to their applications to account for regional characteristics. PVT correlations were modified for Gum-Deniz Field's SP reservoir oil (Gumrah et al., 2012).

RESULTS AND DISCUSSION

The hydrocarbon in place for SP oil horizon in Block 7 was estimated. The volumetric method based on area, porosity, saturation and thickness was conducted. Then, the material balance method was applied with the use of field production data. The reservoir simulation model was constructed. The fluid productions and pressures were matched. The results were compared with that of material balance analysis.

Estimating hydrocarbon in place by volumetric method

The average reservoir parameters for SP horizon are given in Gumrah et al. (2012). The bulk volume was determined from the isopach map of the reservoir, average porosity and oil saturation values from log and core analysis data, and oil formation volume factor from correlations. The volumetric initial oil in place was 38.5 MMstb and the recovery factor was 23.1 % of OOIP (181.4 stb/acre-ft). In volumetric method, the net pay (30.9 m), areal extent (483.7 Acre), water saturation (0.24) and porosity (0.17) data were taken as average values and there are many uncertainties with regard to these parameters.

Estimating hydrocarbon in place by material balance analysis

One tool the reservoir engineer uses to monitor field/well performance quickly and accurately is the material-balance plots. The material balance method for solution gas drive reservoir is given below in a linear from. In this type of reservoir, the principal source of energy is a result of gas liberation from the crude oil and the subsequent expansion of the solution gas as the reservoir pressure is reduced. As pressure falls below the bubble-point pressure, gas bubbles are liberated within the microscopic pore spaces. These bubbles expand and force the crude oil out of the pore space. As the reservoir pressure declines, the rock and fluids expand due to their individual compressibility.

The summation of production terms (F);

$$F = N_p\left[B_{o2} + \left(R_p - R_{so2}\right)B_{g2}\right] + W_p B_{w2} \quad (2)$$

Oil and Dissolved gas expansion terms (E_o);

$$E_o = (B_{o2} - B_{o1}) + (R_{so1} - R_{so2})B_{g2} \quad (3)$$

Gas cap expansion term (E_g);

$$E_g = B_{o1}\left(\frac{B_{g2}}{B_{g1}} - 1\right) \quad (4)$$

Rock and water compression/expansion terms ($E_{f,w}$)

$$E_{f,w} = -(1+m)B_{o1}\frac{C_r + C_w S_{w1}}{1 - S_{w1}}\Delta P \quad (5)$$

Both of the above two factors are the results of a decrease of fluid pressure within the pore spaces, and both tend to reduce the pore volume through the reduction of the porosity. This driving mechanism is considered the least efficient driving force and usually results in the recovery of only a small percentage of the total oil in place. Abasov et al. (2012) studied the hydrogasdynamics of deep deposited deformable porous media in Caspian region.

The complete material balance equation (MBE) is

$$F = N\left(E_o + mE_g + E_{f,w}\right) + \left(W_i + W_e\right)B_{w2} + G_i B_{g2} \qquad (6)$$

Equation 6 can be modified as equations of straight lines, which can be applied to different types of reservoirs. In our case, without water injection (W_i=0), gas injection (G_i=0) and no initial gas cap (m=0), the equation becomes;

$$F=N(E_o+E_{f,w})+W_eB_{w2} \qquad (7)$$

Figure 1 shows the estimated initial oil in place with rock and water compression/expansion terms. The calculated initial oil in place was 35.4 MMstb that is less than 38.5 MMstb obtained by volumetric estimation. The effect of rock and water expansion on N value was insignificant.

Pressure history matching

Historical data goes back to 1960 and are updated occasionally. Material Balance (MB) study was done based on gas, oil and water production data. The average reservoir and aquifer pressures were predicted through MB analysis by matching the recorded well static pressures. The average reservoir pressures were compared with measured data by changing the water influx rate till getting reasonable match. The aquifer influx rate (J) was obtained as 2 bbl/psi. The total water encroachment was 25.95 MMstb. The cumulative oil production was 8.895 MMstb. The cumulative water production was 7.99 MMstb and the cumulative gas production was 21.04 Bcf. The water production was higher in few wells; this might be attributed to the possible locations of water entry into the SP reservoir. Since the calculated N by MB method is less than that of volumetric method, the fluid production from SP reservoir within the boundaries of Block 7 was verified. The faults or boundaries set for Block-7 were defined well. The current recovery factor (RF) reached to 25% of OOIP. The ultimate oil recovery factor of individual reservoirs under primary and/or conventional recovery methods may range from 5% of OOIP for the poorest reservoir characteristics or for viscous oil, to as high as 55% of OOIP for the best reservoir characteristics or for light oil.

Oil, water and gas saturations

The fluid saturations were calculated with the following equations:

Oil saturation;

$$S_{o2} = \frac{(N - N_p)B_{o2}}{V_{p2}} \qquad (8)$$

Water saturation;

$$S_{w2} = \left[(1+m)NB_{o1}\left(\frac{S_{w1}}{1-S_{w1}}\right)\left(\frac{1}{B_{w1}}\right) + \left(W_i + W_e - W_p\right)\right]\frac{B_{w2}}{V_{p2}} \qquad (9)$$

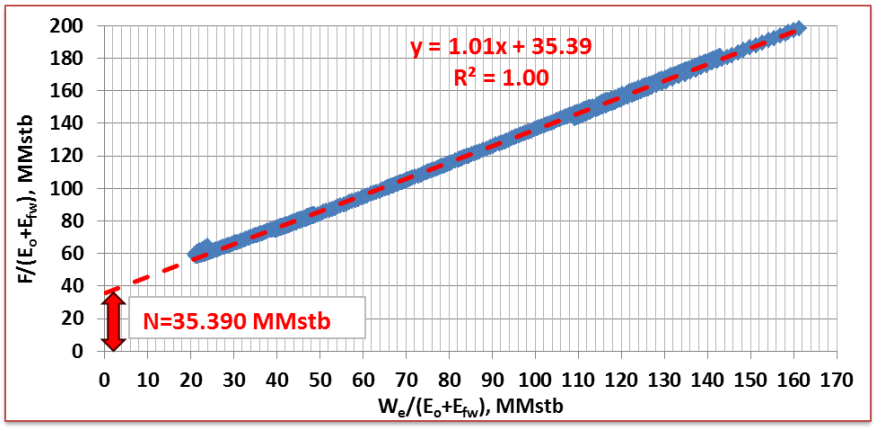


Figure 1. Material balance plot for N with E_{fw} term

Gas saturation;

$$S_{g2}=\left[N\left[\left(R_{so1}-R_{so2}\right)+m\left(\frac{B_{o1}}{B_{g2}}\right)-N_p\left(R_p-R_{so2}\right)+G_i\right]\right]\frac{B_{g2}}{V_{p2}} \quad (10)$$

And

$$S_o+S_w+S_g=1 \quad (11)$$

Reservoir drive mechanisms

Table shows the indices for depletion drive (DDI), segregation drive (SDI), compaction drive (CDI) and water drive (WDI) mechanisms (Smith et al., 1992). The denominator for each index is the same; total cumulative oil-zone production on a reservoir volume basis. This is the factor to normalize the energy (expansion) associated with each of the drive mechanisms. When production begins from a new reservoir, the pressure declines. So, every reservoir operates, in the beginning, predominantly by expansion drive. Whether much water drive occurs depends upon the proximity of water (bottom or edge), the volume of water, and the permeability-area product available to the water. A drive index may be considered as the fraction of total oil zone withdrawals due to a particular drive mechanism.

Rock properties of loose sand (SP Reservoir)

LOOSE SAND					
E,psi	12,000	16,250	21,000	32,000	72,000
v	0.478	0.467	0.456	0.425	0.300
UCS, psi	117	145	178	238	437
TWC, psi	774	867	966	1127	1555
C_f, 1/psi-Eqn 3	1.115E-05	1.218E-05	1.257E-05	1.406E-05	1.667E-05
C_f, 1/psi-Eqn 4	1.143E-05	1.206E-05	1.275E-05	1.388E-05	1.700E-05
C_f, 1/psi-Eqn 7	1.199E-05	1.264E-05	1.334E-05	1.450E-05	1.776E-05
Porosity,%	24.0	22.7	21.3	19.4	15.4
V_{shale},%	34.0	37.0	46.0	55.0	71.5

Since the initial gas cap (m) for SP reservoir is zero, SDI is also zero. The reservoir drive mechanism indices were calculated with production and PVT data. In early production time, depletion drive together with compaction drive and fluid expansion mechanisms were dominant. After water entrance into the reservoir, water drive mechanism played an important role together with depletion drive mechanism. This type of information will be useful for the reservoir development strategies that lead to possible improved oil recovery activities.

The summation of all reservoir drive indices is one.

$$\text{DDI+SDI+CDI+WDI=1} \quad (16)$$

Ultimate recovery factor

The current recovery factor was obtained as 25% of OOIP. The decline curve analyses for the wells were done to estimate the remaining recoverable reserve from SP Horizon in Block 7. The past annual decline rate ranged between 0.11 and 0.25 1/year (average of 0.18 1/year). The project time is 15 years after 2012 and the remaining recoverable reserve was estimated as 4.246 MMstb. Therefore, the ultimate oil production will be around 13.141 MMstb. It corresponds to the ultimate recovery factor of 37.0% of OOIP. The additional production from SP reservoir will be obtained by drilling new wells. This recovery factor is within the recovery range of combined drive mechanisms of solution gas drive and partial water drive.

Reservoir modeling study

The upper and lower flow units of SP reservoir were constructed by using all available data. All rock and fluid properties gathered in material balance analysis were used in reservoir simulation study. Knowledge of reservoir characteristics, which include drainage area size, rock and fluid properties, change in pore volume, amount of water influx and type of reservoir drive mechanisms, gives insight into well spacing efficiency and the need for reservoir development strategies that lead to possible improved oil recovery activities. All the production wells have been drilled on the region having good reservoir quality (Figure 2). The resultant relative permeability curves are given in Figure 3.

The history matching study was done till getting a good match between the simulated and recorded production data (Figure 4). The measured and the calculated average reservoir pressures by material balance analysis and modeling study were in good agreement.

The future production till 2025 was forecasted by producing from 5 new wells. The ultimate recovery factor was obtained as 37% of OOIP. The recoveries and the remaining oil reserve are shown in Figure 5.

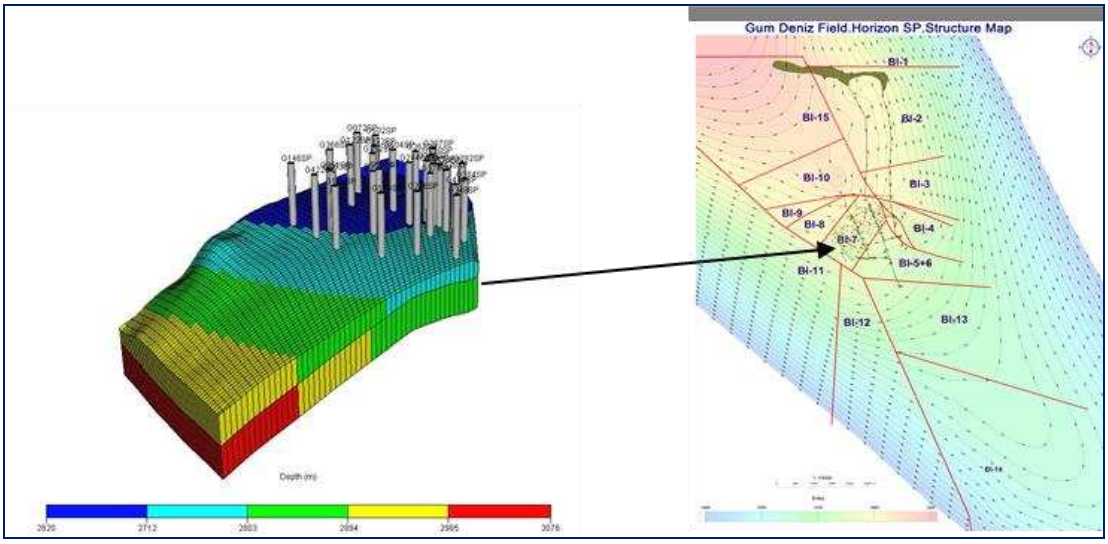


Figure 2. SP structure map with blocks and reservoir model with production wells

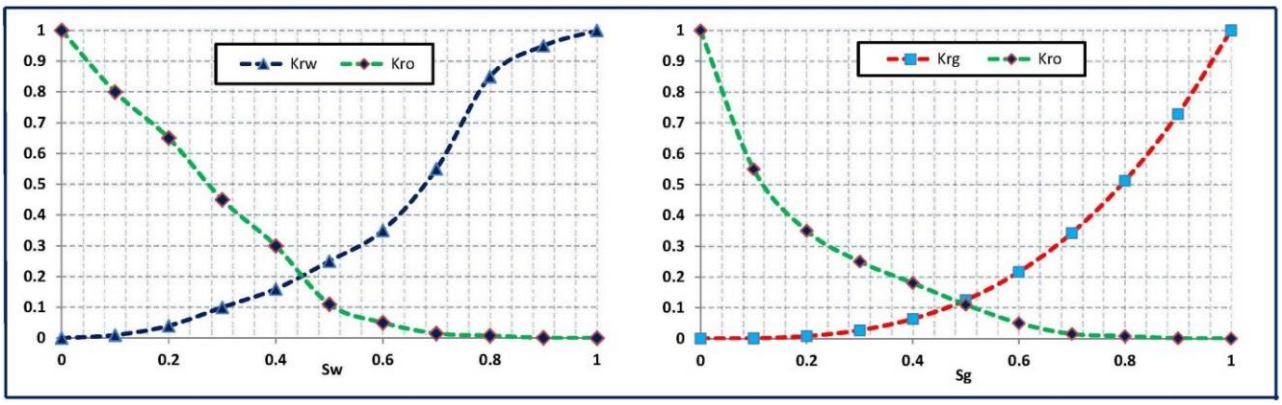


Figure 3. Oil-water & gas-oil relative permeability

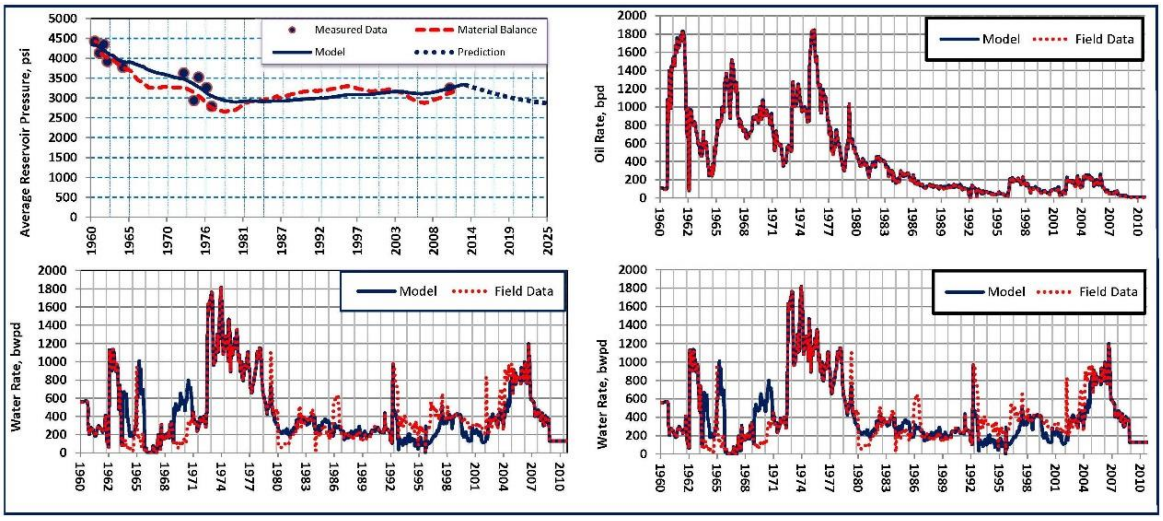


Figure 4. History matching of field data and model results

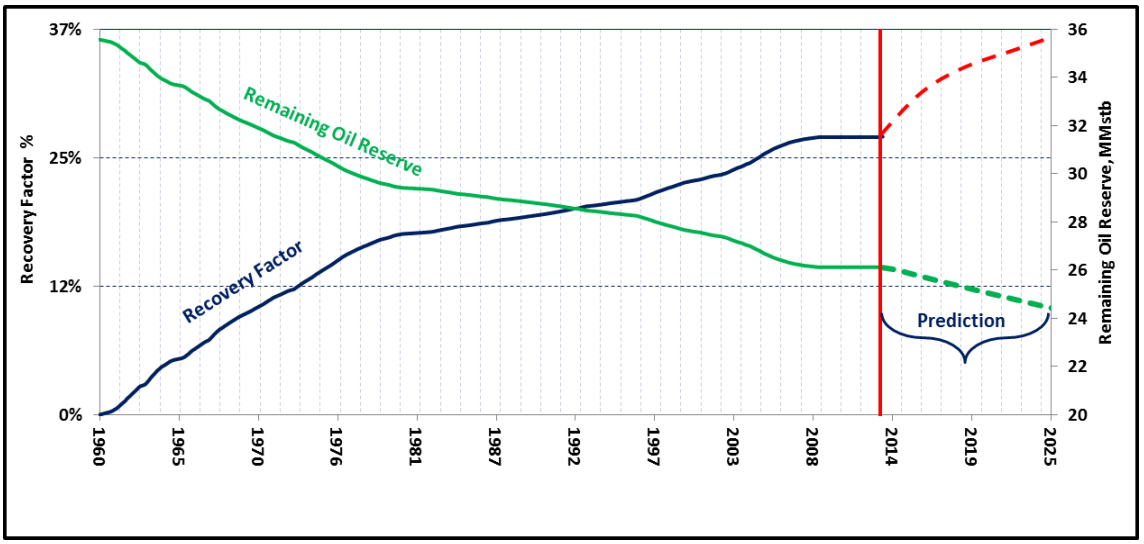


Figure 5. Oil recovery factor &remaining oil reserve (simulation)

CONCLUSIONS

• Since the calculated oil in place (N) by material balance method is 35.4 MMstb which less than that of volumetric method (38.5 MMstb), it was verified that the fluids were mainly produced from SP reservoir within the boundaries of Block 7. The faults or boundaries set for Block-7 were defined well.

• In early production time, compaction drive and fluid expansion mechanisms were dominant. After water encroachment, water drive mechanism played an important role together with depletion drive mechanism. The current recovery factor was obtained as 25.0% of OOIP. The ultimate recovery factor was estimated as 37.5% of OOIP by decline curve analysis of well data.

• The results obtained by material balance and simulation studies are consistent and these models can be used for future plans to develop the reservoir on a field base.

ACKNOWLEDGENMENTS

The authors would like to acknowledge technical support and field data provided for this study and encouragement to publish by Bahar Energy Operating Company, Azerbaijan.

NOMENCLATURE

B_{gi} = Initial gas volume factor at P_i (ft^3/scf)
B_g = Gas volume factor at current pressure P (ft^3/scf)
B_{oi} = Initial oil volume factor at pi (rb/stb)
B_o = Oil volume factor at current pressure P (rb/stb)
B_w = Formation volume factor of water at current pressure P (rb/stb)
B_t = Total volume factor at current pressure P (rb/stb)
c_f = Compressibility of formation (psi^{-1})
c_w = Compressibility of water (psi^{-1})
f_w = Water-cut (fraction)
G_p = cumulative gas produced (scf)
N_p = Cumulative oil produced (stb)
p_i = Initial mean pressure in the reservoir (psi)
p = Current average pressure in the reservoir, (psi)
$R_p = G_p/N_p$ = Cumulative produced gas-oil ratio (scf/stb)
R_{si} = solution gas-oil ratio at initial pressure P_i (scf/stb)
R_s = solution gas-oil ratio at current pressure P (scf/stb)
S_{wc} = Connate water saturation, (fraction)
S_o = Oil saturation, (fraction)
S_g = Gas saturation, (fraction)
W_p = Cumulative water produced (stb)

REFERENCES

ABASOV, M.T., JALALOV, G.J., IBRAHIMOV, T.M., MAMEDOV, A.M., MAMIYEV, V.S. 2012. Hydrogasdynamics of deep deposited deformable porous media. Nafta-Press. Baku. (in Russian).

ABREU, V., NUMMEDAL, D. 2007. Miocene to Quaternary sequence stratigraphy of the South and Central Caspian Basins. In P.O.Yilmaz and G.H.Isaksen, Editors: *Oil and Gas of the Greater Caspian Area: AAPG Studies in Geology.* 55, 65-86.

BRUCE, S. 1990. A Mechanical stability log. IADC/SPE19942. *IADC/SPE Drilling Conf.*, Houston, TX, Feb 27-Mar. 2, 276-281.

COLLINS, P.M. 2002. Geomechanics and wellbore stability design of an offshore horizontal well, North Sea. SPE/Petroleum Society of CIM/CHOA 78975, *SPE ITOHOS/ICHWT Conference*, Calgary, Alberta, Canada.

FJAER, E., HOLT, R.M., HORSUD, P., RAEN A.R., RISNES R. 1992. Petroleum related rock mechanics. 1st Edition. Elsevier Science Publishers BV. Amsterdam. The Netherlands. 338 p.

GEERTSMA, J. 1957. The effect of fluid pressure decline on volumetric changes of porous rocks. *Trans AIME*, 210, 331-339.

GUMRAH, F. ALIYEV A., QULIYEVA, C., OZAVCI, O. 2012. Determining reservoir characteristics and drive mechanisms for an oil reservoir. *SOCAR Proceedings,* ISSN 2218-6867, 4, Oil-Gas Scientific Research Institute, Baku, Azerbaijan, 6-19.

MAHMOOD, M.A., Al-MARHOUN, A. 1996. Evaluation of empirically derived PVT properties for Pakistani crude oils. *J. Pet. Science and Engineering*, 16, 275-290.

NEWMAN, G.H. 1973. Pore volume compressibility of consolidated, friable and unconsolidated reservoir rocks under hydrostatic loading. *Journal of Pet. Tech.* 25, 2, 129-134.

SMITH, C.R., TRACY, G.W., FARRAR, R.L. 1992. Applied reservoir engineering. Oil&Gas Consultants International. Inc.. OK. USA.

© I.R.Guliyev, 2015

EFFECT OF POLYMER COMPOSITIONS ON THE ISOLATION QUALITY OF ABSORPTION AREA OF DRILLING FLUIDS

I.R.Guliyev

General Field Engineer – Schlumberger Logelco Inc., Baku Azerbaijan

The article describes the implementation of experimental research and tests of polymer compositions with drilling fluids under laboratory conditions in order to improve the efficiency of drilling fluid absorption complications and taking into account the permeability characteristics classification analysis of rocks field. The main purpose of this test is to create non-permeable screen or reduce the rock permeability significantly in the areas where mud absorption is observed to reduce mud losses. Key methodology used during the researches and tests were homogeneous model of the formation line composed of flanges welded from both side made from the steel, and at the same time valves allowing connecting the line were built. Modelling the water injection process was the main driver to select adequate length (1m) of the formation. Quartz sand milled during experiments was taken as porous medium model. All lab tests were performed in isometric environment. Based on the results achieved during experimental research, the dependence of remaining resistance factor on polymer composition concentration and permeability coefficient was built. The dependence was achieved of the required polymer composition concentration providing high value of remaining resistance factor from absorber layer permeability allowing finding concentration. This result will significantly improve drilling fluid properties and characteristics in order to avoid mud losses in difficult areas of drilled reservoir.

Introduction

In order to improve the efficiency of drilling fluid absorption complications and taking into account the permeability characteristics classification analysis of rocks field, it is required to create non-permeable screen or reduce the rock permeability significantly in the areas where mud absorption is observed.

Till now, many formation plugging fluids were developed in order to create water-separation screens in the absorption areas and to prevent mud losses into the reservoir. It is almost impossible to review all these formation plugging fluids in practice. Research on the formation permeability characteristics was performed, where formation was divided into several severity levels of absorption categories, chemicals creating waterproof screen in the shortest time and reducing several times formation permeability of well horizontal slice were reviewed. Apart from this and depending on different conditions, chemicals chosen have to be more economical in regards of finance and available in the area where drilling operations were ongoing. Nowadays apart from polymer application for the 2nd oil recovery (Гяллямов, Рахимкулов, 1978) mentioned the above chemicals are used to prevent drilling fluid absorption into the formation (Абасов и др., 2009). In (Абасов и др., 2009) it was determined that, polymer filtering with the low permeability core occurs with the reduction and high differential pressure. During lab tests it was discovered that solution of KMS and PA fluids created the composition with synergistic effect. In comparison with bentonite clay, this composition has higher flocculating characteristics. It was also discovered in the lab test that PAA fluid in the concentration of 0.15-0.20% has hydro filling and stabilizing characteristics, showing flocculating characteristics in other concentrations more clearly. In (Шарипов, 1995) special attention was paid to the change in dynamic viscosity and effect of KMS dynamic viscosity on PAA concentration expression was achieved. Rheological characteristics of KMS and PAA composition was fully analyzed (Агамалиева, 2012). The research showed that polymer based fluids played an important role in the isolation of absorption areas. Their isolation capabilities also depends on formation geological and petro-physical characteristics. That's the main reason to manage polymer based fluid contents.

Problem statement

Lab test was performed in order to study the isolation characteristics of polymer based fluids. Test was carried out with the application of the theory of the five level variations based on two factors. Permeability and polymer fluid concentration were considered as these two factors. **Rrem** resistance characterizing polymer fluid isolation was assumed

as an output parameter. To describe permeability reduction effect after contact of porous medium with polymers, Smith created concept of remaining resistance (**Rrem**) in 1970, defined as ratio of polymer fluids in porous medium with its water permeability development before and after:

$$R_{rem} = \frac{K_w}{K_p} \quad (1)$$

Where K_w is permeability of porous medium to water, K_p is permeability of porous medium to polymer fluids. Remaining resistance factor is important factor showing the permeability reduction porous media interacting with polymer based composition. Known in (Абасов и др., 2009) test equipment was used to perform lab test on remaining resistance factor and its different influencing parameters. This equipment consisted of formation model, is covered with electrical heater, and container for gasified oil, rude oil and fluid and vacuum pumps, gas container with the redactor, separator, gas meter and measurement cylinder.

The methodology of the researches

Homogeneous model of the formation line is composed of flanges welded from both side made from the steel, and at the same time valves allowing connecting the line were built. Modelling the water injection process was the main driver to select adequate length (1m) of the formation. Quartz sand milled during experiments was taken as porous medium model (Эфрос, 1968). The required resistance of porous medium was achieved by quartz sand milled in the round mill in accordance with established factions. Laboratory tests were performed for remaining resistance factor formula, the analysis of different parameters influencing on remaining resistance formulation process via application of polymer based fluids as follows. Formation homogeneous model was put in vacuum and then was saturated with water. Later the resistance of porous medium based on water samples was determined in several pressure drops.

All lab tests were performed in isometric environment.

Formation static temperature was achieved by electrical heater. Later polymer composition was pumped into the formation model in specific pressure drops and kept in static conditions. After that water and polymer composition were pumped into the formation model at the same pressure drop figures, the resistance of porous medium which was worked with polymer composition in stabilized filtering regime at the given pressure drop was determined.

Remaining resistance was determined (Smith, 1970) by formula (1).

Filtering characteristics depend on flow rate, permeability and appraisal are made by the change of remaining resistance factor. The isolation function of polymer composition is determined as following formula:

$$W = \frac{K_{bef} + K_{aft}}{K_{aft}} \cdot 100\% \quad (2)$$

Where K_{bef} is porous medium resistance factor before being filtered by polymer composition, K_{aft} after. mkm^2.

Laboratory test results

Planning matrix and test results completed with output and input numbers were given in the below table:

Planning matrix and test results

№	C	Kbef	Kaft	Rres		Errors		$W = \frac{K_{bef} + K_{aft}}{K_{aft}} \cdot 100\%$
				Actual numbers	Calculated numbers	Certain	Relative	
1	*2*	*3*	*4*	*5*	*6*	*7*	*8*	*9*
1	0.005	0.05	0.005	11	12.06	1.06	9.63	90.91
2	0.1	0.05	0.002	30	27.58	2.42	8.07	96.67
3	0.5	0.05	0.001	95	90.47	4.53	4.77	98.95
4	1	0.05	0.000	200	166.83	33.17	16.59	99.5
5	2	0.05	0.000	350	316.14	33.86	9.67	99.71
6	0.005	0.25	0.031	8	8.01	0.1	0.18	87.50
7	0.1	0.25	0.017	15	18.33	3.33	22.19	93.33

1	2	3	4	5	6	7	8	9
8	0.5	0.25	0.004	60	60.13	0.13	0.21	98.33
9	1	0.25	0.002	120	110.88	9.12	7.60	99.17
10	2	0.25	0.001	250	210.11	39.89	15.96	99.6
11	0.005	0.45	0.075	6	5.33	0.67	11.23	83.33
12	0.1	0.45	0.045	10	12.18	2.18	21.82	90.00
13	0.5	0.45	0.011	40	39.96	0.04	0.09	97.50
14	1	0.45	0.006	80	73.69	6.31	7.89	98.75
15	2	0.45	0.003	130	139.64	9.64	7.42	99.23
16	0.005	0.65	0.163	4	3.54	0.46	11.50	75.00
17	0.1	0.65	0.108	6	8.10	2.10	34.93	83.33
18	0.5	0.65	0.403	22	26.56	4.56	20.72	93.33
19	1	0.65	0.016	40	48.97	8.97	22.44	97.50
20	2	0.65	0.008	80	92.81	12.81	16.01	98.75
21	0.005	1.2	0.800	1,5	1.15	0.35	23.27	33.33
22	0.1	1.2	0.400	3	2.63	0.37	12.26	66.67
23	05	1.2	0.150	8	8.64	0.64	7.94	87.50
24	1	1.2	0.0122	15	15.92	0.92	6.15	93.33
25	2	1.2	0.034	35	30.17	4.83	13.79	97.14

The results shown in table 3-5 are the average cost of each of the pieces repeated in the tests. Graph reflecting the dependence of remaining resistance in the average numbers of permeability coefficient polymer composition from concentration and permeability was built based on the lab test results (fig. 1,2). For this case the average number is taken which suits polymer composition concentration and remaining resistance factor. For example, average number suitable for 0.005% polymer concentration and remaining resistance factor defining 1 single point takes place where with the definition of other numbers of graph for the dependence of remaining resistance factor and polymer concentration can be built. The following graph was given in (fig.1). As it is clearly seen, the analyzed dependence in the graph is straightforward. As a result of the statistical processing the dependence of approximation was as follows:

$$R_{rem} = 82{,}41C + 5{,}3623 \quad (3)$$

At the same time, the graph of remaining resistance and medium permeability dependence was built accordingly (fig.2).

As it is obvious from the picture, the following dependence graph is subjected to exponential law. As a result of statistical processing, following analytical approximation was achieved:

$$R_{rem} = 143{,}88\, e^{-2{,}116 K_{bef}} \quad (4)$$

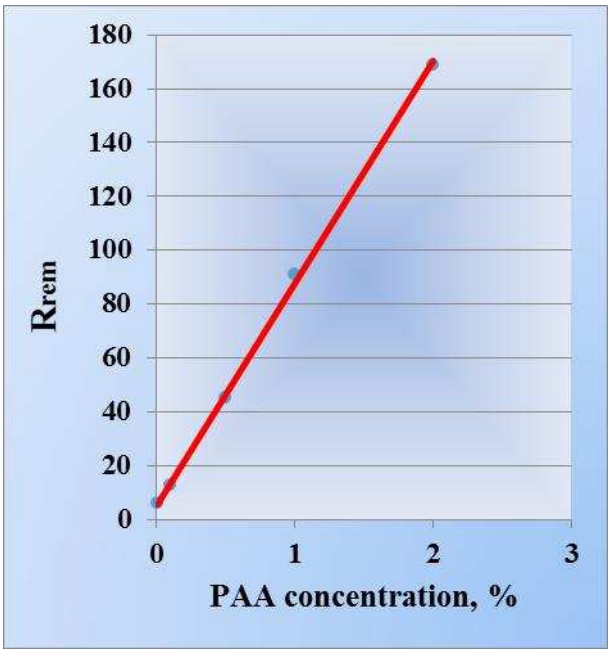


Figure 1. Remaining resistance factor and polymer concentration dependence graph

Mathematical statistics given below were used in order to achieve total dependence of remaining resistance factor on polymer compositions and medium permeability:

$$R_{rem} = 2{,}46(82{,}41C + 5{,}3623)^{0{,}9654}\, e^{-2{,}043 K_{bef}} \quad (5)$$

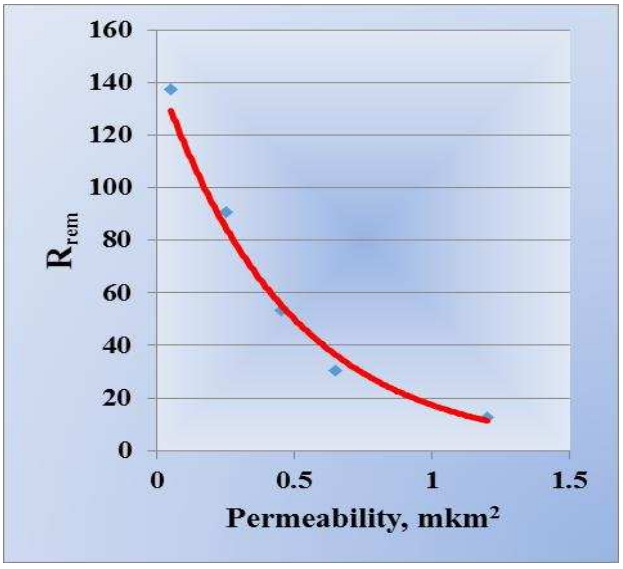


Figure 2. Remaining resistance factor and medium permeability dependence graph

Results achieved in formula (5) showed the similarity of estimated and the actual numbers of remaining resistance factor. Table 1 also reflected PAA fluid isolation ability from formula (2). As it is obvious from table 1, PAA fluid isolation ability is achieved by concentration and porous medium resistance. Based on polymer composition concentration, required numbers for porous medium resistance were set.

Below shown analytic formula refers to required concentration of polymer in the composition based on the highest number of isolation effect taken numbers of dependence of porous medium resistance:

$$C = \frac{0{,}47(1 - 2{,}043K_{pr} + 2{,}087K_{pr}^2)}{1 - 2{,}036K_{pr}} - 0{,}065 \quad (6)$$

Using the achieved results in the formula above, it is possible to calculate the maximum number of isolation coefficient and formation of rock permeability similar to polymer composition concentration.

Thus:

Based on the results achieved during experimental research, the dependence of remaining resistance factor on polymer composition concentration and permeability coefficient was built;

The dependence was achieved of the required polymer composition concentration providing high value of remaining resistance factor from absorber layer permeability allowing finding concentration.

Effect of the analysis of polymer compositions on the drilling fluid properties

Normally water based muds are used in the less absorber formation intervals with small permeability during drilling the wells. This is a normal practice and commonly used in other places and literature.

When oil well walls are not stable and formation has high permeability the requirement for chemical treatment of drilling fluids is necessary and technological parameters of drilling fluids are kept at the required level via the chemical compositions. Depending on the geological conditions, the required parameters of drilling fluids can be achieved by the regulation of chemical composition content. Based on the modeling of polymer composition properties, the values raise speed of the drilling fluids in the annular area provided by PAA and KMS composition concentration can be proved (Агамалиева, 2012). Depending on the geological conditions, following results can help to identify the concentration of polymer composition in the drilling fluids.

The effect of polymer composition on structure-mechanical properties of drilling fluid creates a great interest.

Bentonite oily based muds properties of structure-mechanical properties achieved in different concentration values of polymer compositions were measured and the dependence were built based on the results reflected in concentration values. Results are reflected in figure 3. As it is obvious, once chemical composition concentrations increase, viscosity and static friction tension also increases, water transfer property of fluids decreases. The same case is observed during chemical treatment of KMS polymer composition (Шарипов, 1995; Лушпеева и др., 2001).

Viscosity and static friction tension increase rate increases once fluid weight and composition concentration increase.

P.A.Rebinder explained the mechanism of structure-mechanical properties of water-based mud and it is obvious in the other articles as well (Агамалиева, 2012; Лушпеева и др., 2001; Шайхы-межденов, 2006).

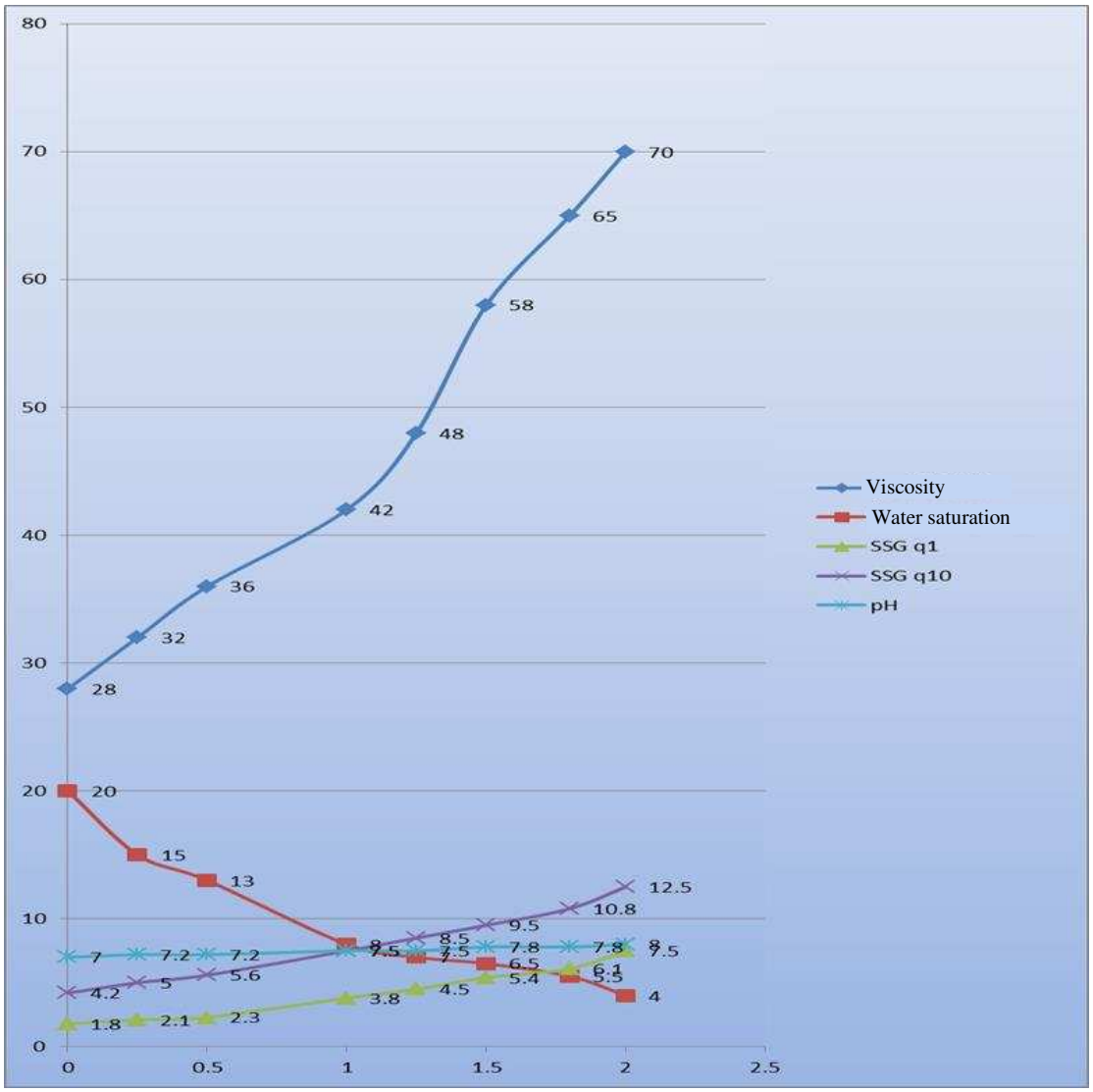


Figure 3. Dependence of polymer oily based mud structure-mechanical properties on polymer concentration

Conclusion

Based on the results achieved during experimental research, the dependence of remaining resistance factor on polymer composition concentration and permeability coefficient was built. The dependence was achieved of the required polymer composition concentration providing high value of remaining resistance factor from absorber layer permeability allowing finding concentration. Once chemical composition concentrations increase, viscosity and static friction tension also increases, water transfer property of fluids decreases. The same case is proved during chemical treatment of KMS polymer composition. Viscosity and static friction tension increase rate increases once fluid weight and composition concentration increase.

REFERENCES

АБАСОВ, М.Т., СТРЕКОВ, А.С., ЭФЕНДИЕВ, Г.М. 2009. Повышение эффективности ограничения водопритоков в нефтяных скважинах. Nafta-Press. Баку. 256 с.

АГАМАЛИЕВА, Ф.М. 2012. Разработка и регулирование составов буровых растворов и технология их применения при бурении глубоких скважин.. Дисс. на соиск. уч.степ.док. фил. Баку.

ГАЛЛЯМОВ, М.Н., РАХИМКУЛОВ, Р.Ш. 1978. Повышение эффективности эксплуатации нефтяных скважин на поздней стадии разработки месторождений. Недра. Москва. 207 с.

ЛУШПЕЕВА, О.А., КОШЕЛЕВ, В.Н., ВАХРУШЕВ, Л.П., БЕЛЕНКО, Е.В. 2001. О природе синергетического эффекта в полимер-глинистых буровых растворах. *Нефтяное хозяйство*, 3, 28-30.

РЕБИНДЕР, П.А. 1978. Поверхностные явления в дисперсных системах. Коллоидная химия. Избранные труды. Москва. 368 с.

ШАЙХЫМЕЖДЕНОВ, Ж.Г. 2006. Обеспечение устойчивости и целостности стенок ствола скважин при бурении в осложнённых условиях (на примере месторождений Западного Казахстана). Автореф. докт. дисс. Атырау. 291 с.

ШАРИПОВ, А.У. 1995. Проектирование и регулирование основных показателей бурения глубоких скважин. ВНИИОЭНГ. 280 с.

ЭФРОС, Д.А., ОНОПРИЕНКО, В.П. 1968, Моделирование линейного вытеснения нефти водой. *Тр. ВНИИ*, Гостоптехиздат, Москва, 12, 331-360.

SMITH, F.W. 1970. The behavior of partially hydrolyzed polyacrylamide in porous media. *Journal of Petroleum Technology*. 11, 22, 2,148-156.